THESIS APPROVAL

GRADUATE SCHOOL, KASETSART UNIVERSITY

Doctor of Philosophy (Chemistry)

DEGREE

Chemistry — **FIELD**

Chemistry — **DEPARTMENT**

TITLE: Structure, Reaction Mechanism and Dynamics of Hydrocarbons over Zeolites: Electronic Structure Theory Approaches

NAME: Mr. Bundet Boekfa

THIS THESIS HAS BEEN ACCEPTED BY

THESIS ADVISOR

(Professor Jumras Limtrakul, Dr.rer.nat.)

COMMITTEE MEMBER

(Assistant Professor Piboon Pantu, Ph.D.)

COMMITTEE MEMBER

(Associate Professor Supa Hannongbua, Dr.rer.nat.)

DEPARTMENT HEAD

(Associate Professor Noojaree Prasitpan, Ph.D.)

APPROVED BY THE GRADUATE SCHOOL ON _____

DEAN

(Associate Professor Gunjana Theeragool, D.Agr.)

THESIS

STRUCTURE, REACTION MECHANISM AND DYNAMICS OF HYDROCARBONS OVER ZEOLITES: ELCTRONIC STRUCTURE THEORY APPROACHES

BUNDET BOEKFA

A Thesis Submitted in Partial Fulfillment of
the Requirements for the Degree of
Doctor of Philosophy (Chemistry)
Graduate School, Kasetsart University
2009

Bundet Boekfa 2009: Structure, Reaction Mechanism and Dynamics of Hydrocarbons over Zeolites: Electronic Structure Theory Approaches. Doctor of Philosophy (Chemistry), Major Field: Chemistry, Department of Chemistry. Thesis Advisor: Professor Jumras Limtrakul, Ph.D. 99 pages.

The confinement effect of zeolite on the adsorption and reaction was studied with hybrid methodologies: ONIOM and embedded ONIOM (the ONIOM model embedded in the electrostatic potential field of periodic lattice). The interactions of saturated and unsaturated hydrocarbons over industrially important zeolites (H-MOR and H-FAU) were studied. The calculated adsorption energies of ethane, propane and n-butane in H-FAU and H-MOR with the ONIOM method are in good agreement with the experimental data. For the adsorption of alkenes in acidic zeolite, the adsorption energies for ethene, propene and 1-butene were predicted to be -9.4, -11.3 and -12.5 kcal/mol in H-FAU and -10.1, -13.8 and -17.4 kcal/mol for ethene, propene and 1-butene in H-MOR, respectively. These energies are in the range of the experimental data. For the polar molecule, acetone in H-FER, H-ZSM-5 and H-MCM-22 were calculated; the adsorption energies are -25.9, -26.3 and -25.1 kcal/mol for H-FER, H-ZSM-5 and H-MCM-22, respectively. The calculated adsorption energies of acetone compare well with the experimental data. For interaction with amino acid molecules, the adsorption of glycine and L-alanine on H-ZSM-5 were studied. The most stable adsorption structure involves the ion-pair interactions between the protonated amino acid molecule and the anionic zeolite with the computed adsorption energies of -31.3 and -34.8 kcal/mol for glycine and L-alanine, respectively. The other two adsorption complexes via hydrogen bond interaction through the carboxylic and the hydroxyl group of the amino acids are also found and have lower adsorption energies. The zwitterion form of glycine was found to be stable over Na-ZSM-5 with the adsorption energy of -24.8 kcal/mol. The framework effect on the reaction properties was studied via the tautomerization of acetone on H-FER, H-ZSM-5 and H-MCM-22. The activation energies are 30.0, 23.0 and 16.6 kcal/mol for H-FER, H-ZSM-5 and H-MCM-22, respectively. H-MCM-22 is found to be the most efficient catalyst for the reaction due to it having the smallest constrains influence on the transition structure. The confinement effect of the zeolite framework on the adsorption and reaction properties of hydrocarbon can be correctly described with the ONIOM model and lead to the differentiation of the adsorption and hydrocarbon activation process with different types of zeolites.

_____ _____ __ / __ / __

Student's signature Thesis Advisor's signature

ACKNOWLEDGEMENTS

First of all, it is with immense gratitude that I especially thank Professor Dr. Jumras Limtrakul for his confidence in me, kindness, suggestions, opportunities, direction and encouragement, and, forgiveness when I erred or was negligent. The time I spent in studying for my M.S. and Ph.D. was, without doubt, the most satisfying period of my life. My dual successes rewarded me with the sense of achievement that I had attained and, at the same time, rewarded my lecturers and advisors for the knowledge and ability that they had bestowed on me. Deep in my heart, I am proud and honored to be one of Professor Jumras's students. The academic knowledge and practical experience that I have gained help me to bravely walk forward with confidence in my career.

I would like to thank my advisory committee, Assistant Professor Piboon Pantu, for his kind help and suggestions, and Associate Professor Dr. Supa Hannongbua for her sincere and valuable suggestions. I would like also to thank Assistant Professor Yuthana Tantirungrotechai for his helpful suggestions.

I am grateful for kindness and sincerity shown me by Dr. Pipat Khongpracha for his good suggestions, Thana Maihom for his help, Boonruen Sunpetch for her help on laboratory problems, Phornpimon Maitarad for her suggestions, Saowapak Choomwattana for her always graceful assistance and sincere suggestions, and Porntip Boonsri for her suggestions, and all of my friends for their friendship. I would like also to thank Rattinan Meemanwit who gave me happiness, joy and always smiled.

This work was supported in part by grants from the National Science and Technology Development Agency (NANOTEC Center of Excellence), the Thailand Research Fund and the Kasetsart University Research and Development Institute (KURDI) , the Commission on Higher Education, Ministry of Education, under the Postgraduate Education and Research Programs in Petroleum and Petrochemicals, and Advanced Materials.

Finally, I would like to inscribe the glory of this thesis to my ever loving mom, who always believed in me and always gave me confidence to be brave, Tharinee Boekfa. Also, I would like to dedicate this thesis to the other members of my family; my father, Wattana Boekfa, and my nice brother, Arom Boekfa, and my cute sister, Nopparat Boekfa.

Bundet Boekfa

March 2009

TABLE OF CONTENTS

Page

TABLE OF CONTENTS i
LIST OF TABLES ii
LIST OF FIGURES iv
LIST OF ABBREVIATIONS ix
INTRODUCTION 1
LITERATURE REVIEW 8
METHODOLOGIES AND MODELS 16
Density Functional Theory (DFT) 16
Our own N-layered Integrated molecular Orbital and Molecular mechanics (ONIOM) 17
Basis set superposition error 19
Embedded Point Charges 19
Model 23
RESULTS AND DISCUSSION 32
Adsorption of Hydrocarbon on Various Zeolites 32
Interaction of Amino Acids with H-ZSM-5 Zeolites 55
Tautomerization of Acetone on Various Zeolites 66
CONCLUSIONS 79
LITERATURE CITED 81
CURRICULUM VITAE 98

LIST OF TABLES

Table		Page
1	The ONIOM(B3LYP/6-31G(d,p):UFF) optimized geometrical parameters and adsorption energies of ethane, propane and n-butane in H-MOR, and H-FAU	35
2	The distribution of adsorption energy of light alkanes and alkenes on H-FAU and H-MOR calculated at embedded ONIOM(MP2/6-31G(d,p):UFF)// ONIOM(B3LYP/6-31G(d,p):UFF) with BSSE correction	36
3	The ONIOM(B3LYP/6-31G(d,p):UFF) optimized geometrical parameters and adsorption energies of ethene, propene and 1-butene in H-MOR, and H-FAU	43
4	The ONIOM(B3LYP/6-31G(d,p):UFF) optimized geometrical parameters and adsorption energies of propene and 1-butene in H-FAU via the terminal alkyl group	44
5	Structural parameter for acetone/zeolite cluster complexes in various zeolites	51
6	The adsorption energies of acetone in the confined spaces of H-FER, H-ZSM-5 and H-MCM-22 (kcal/mol) where Quantum means ΔE(model, high), and UFF means ΔE(real, low) - ΔE(model, low)	51
7	The bond distance parameter of glycine/ ZSM-5 Zeolite, (Å)	59
8	The adsorption energies, ΔEads, of glycine/zeolite complexes, (kcal/mol)	60
9	The adsorption energies, ΔEads, of L-alanine/zeolite complexes, (kcal/mol)	63

LIST OF TABLES (Continued)

Table		Page
10	The reaction energies of acetone in the confined spaces of H-FER, H-ZSM-5 and H-MCM-22 (kcal/mol) where Quantum means ΔE(model, high), and UFF means ΔE(real, low) - ΔE(model, low) with B3LYP/6-31G(d,p):UFF	77
11	Structural parameter for adsorbate/zeolite cluster complexes along the reaction coordinate in various zeolites (distances in Å, and angles in degree)	78

LIST OF FIGURES

Table		Page
1	Various type zeolite pores and channel (a) FAU, (b) BEA, (c) MOR, (d) ZSM-5, (e) FER and (f) LTA.	2
2	The two-layer ONIOM extrapolation schemes.	18
3	The picture shows the zone of optimized charges (outer zone), non optimized charges (inner zone), zone without charges and quantum cluster.	21
4	Schematic diagram of the embedded ONIOM method.	22
5	The ONIOM model of 14T/120T cluster of H-FAU. (a) Side view shows the two supercages connected to the 14T quantum cluster, (b) Front view shows the 12-membered ring window connecting the two supercages. Atoms belonging to the 14T quantum region are drawn as spheres.	24
6	The ONIOM model of 14T/120T cluster of H-MOR. (a) Side view of the 12-membered ring straight channel, (b) Front view shows the 12-membered ring window of the straight channel. Atoms belonging to the 14T quantum region are drawn as spheres.	25
7	The ONIOM model of 12T/128T cluster of H-ZSM-5. (a) Side view of the 10-membered ring of intersection channel, (b) Front view shows the 10-membered ring window of the straight channel. Atoms belonging to the 12T quantum region are drawn as spheres	27
8	ONIOM (B3LYP/6-31G(d,p):UFF) optimized structures of 12T/112T H-FER, (a) 10T member ring channel, and (b) 8T member ring channel.(Ball-and-stick and line styles of illustrated atoms represent the quantum chemical and molecular mechanical calculations, respectively.)	29

LIST OF FIGURES (Continued)

Table		Page
9	ONIOM (B3LYP/6-31G(d,p):UFF) optimized structures of 12T/128T H-ZSM-5, (a) Side view of the 10-membered ring of intersection channel, (b) Front view shows the 10-membered ring window of the straight channel. (Ball-and-stick and line styles of illustrated atoms represent the quantum chemical and molecular mechanical calculations, respectively.)	30
10	ONIOM (B3LYP/6-31G(d,p):UFF) optimized structures of 14T/132T H-MCM-22, (a) Side view of the 10-membered ring channel, (b) View shows the 12-membered ring window of supercage. (Ball-and-stick and line styles of illustrated atoms represent the quantum chemical and molecular mechanical calculations, respectively.)	31
11	The optimized structures of the adsorption complexes of (a) ethane, (b) propane and, (c) n-butane on H-FAU. Atoms on the adsorbed molecules and the Brønsted acid site are drawn as spheres and the extended framework is omitted.	33
12	The optimized structures of the adsorption complexes of (a) ethane, (b) propane and, (c) n-butane on H-MOR. Atoms on the adsorbed molecules and the Brønsted acid site are drawn as spheres and the extended framework is omitted.	34
13	The optimized structures of the adsorption complexes of (a) ethene, (b) propene and, (c) 1-butene on H-FAU. Atoms on the adsorbed molecules and the Brønsted acid site are drawn as spheres and the extended framework is omitted.	40

LIST OF FIGURES (Continued)

Table		Page
14	The optimized structures of the adsorption complexes of (a) ethene, (b) propene and, (c) 1-butene on H-MOR. Atoms on the adsorbed molecules and the Brønsted acid site are drawn as spheres and the extended framework is omitted.	41
15	The optimized structures of the adsorption complexes of (a) propene and, (b) 1-butene on H-FAU via the terminal alkyl group. Atoms on the adsorbed molecules and the Brønsted acid site are drawn as spheres and the extended framework is omitted.	42
16	ONIOM (B3LYP/6-31G(d,p):UFF) optimized structures of the acetone adsorption on the 12T/112T model of H-FER: (a) the view along the straight channel and (b) focused on the Brønsted acid site. Selected optimized geometric parameters are given in Å. (Ball-and-stick and line styles of illustrated atoms represent the quantum chemical and molecular mechanical calculations, respectively.)	48
17	ONIOM (B3LYP/6-31G(d,p):UFF) optimized structures of the acetone adsorption on the 12T/128T model of H-ZSM-5: (a) Represent of ZSM-5 zeolite the view along the (a) straight channel (b) zigzag channel and (c) focused on the Brønsted acid site. Selected optimized geometric parameters are given in Å. (Ball-and-stick and line styles of illustrated atoms represent the quantum chemical and molecular mechanical calculations, respectively.)	49

LIST OF FIGURES (Continued)

Table		Page
18	ONIOM (B3LYP/6-31G(d,p):UFF) optimized structures of the acetone adsorption on the 14T/132T model of H-MCM-22: Represent of MCM-22 zeolite the view along the (a) straight channel (b) supercage and (c) focused on the Brønsted acid site. Selected optimized geometric parameters are given in Å. (Ball-and-stick and line styles of illustrated atoms represent the quantum chemical and molecular mechanical calculations, respectively.)	50
19	Glycine adsorb on H-ZSM-5 with (a,b) amino group, (c) carboxylic group and (d) hydroxyl of carboxylic group. (Distance in Å)	57
20	The zwitterion of glycine adsorb on Na-ZSM-5. (Distances in Å)	59
21	L-alanine adsorb on H-ZSM-5 with (a) amino group, (b) carboxylic group and (c) hydroxyl of carboxylic group. (Distances in Å)	63
22	Molecular structures and energy profile of the tautomerization of acetone in solvent-free environment calculated with B3LYP/6-31G(d,p) level of theory. Distance and energy are given in pm and kcal/mol.	67
23	Calculated with B3LYP/6-31G(d,p) level of theory, energy profile (energy in kcal/mol) of the tautomerization of acetone in solvent-assisted models (a) with one, (b) two and (c) three water molecules.	68
24	Molecular structures and energy profile of the tautomerization of acetone in H-FER (small-pore zeolite representative) of 12T/112T ONIOM model calculated with B3LYP/6-31G(d,p):UFF level of theory. Distances and energies are given in Å and kcal/mol.	74

LIST OF FIGURES (Continued)

Table		Page
25	Molecular structures and energy profile of the tautomerization of acetone in H-ZSM-5 (medium-pore zeolite representative) of 12T/128T ONIOM model calculated with B3LYP/6-31G(d,p):UFF level of theory. Distances and energies are given in Å and kcal/mol.	75
26	Molecular structures and energy profile of the tautomerization of acetone in H-MCM-22 (large-pore zeolite representative) of 14T/132T ONIOM model calculated with B3LYP/6-31G(d,p):UFF level of theory. Distances and energies are given in Å and kcal/mol.	76

LIST OF ABBREVIATIONS

AM1	=	Austin Model 1
B3LYP	=	Becke's three parameters hybrid functional using the Lee-Yang-Parr correlation functional
BEA	=	Beta zeolite
BSSE	=	Basis set superposition error
DFT	=	Density functional theory
ΔEa	=	Activation energy
FAU	=	Faujasite
FER	=	Ferrierite
FTIR	=	Fourier transform infrared spectroscopy
HF	=	Hartree-Fock
MFI	=	Mobil five zeolite
MM	=	Molecular mechanics
MNDO	=	Modified neglect of diatomic overlap
MOR	=	Mordenite
MP2	=	The second-order Møller-Plesset perturbation theory
ONIOM	=	Our own n-layered integrated molecular orbital and molecular mechanics
eONIOM	=	embedded ONIOM
PM3	=	Parameterized Model 3
QM	=	Quantum mechanics
QM/MM	=	Quantum mechanical/molecular mechanical
UFF	=	Universal force fields
ZSM-5	=	Zeolite socony mobil 5

STRUCTURE, REACTION MECHANISM AND DYNAMICS OF HYDROCARBONS OVER ZEOLITES: ELECTRONIC STRUCTURE THEORY APPROACHES

INTRODUCTION

Zeolite is one of the most important heterogeneous catalysts especially for the petrochemical industry. This material contains tetrahedral structure of aluminum (Al^{3+}) and silicon (Si^{4+}) atoms surrounding with four oxygen (O^{2-}) atoms. The substituted aluminum atoms make the negative charges on the oxygen framework and can be compensated with cations or metal cations or protons. This protonic form of zeolites is acidic. This type of acid form is called Brønsted acid site. The Brønsted acid site (Si-OH-Al) shows the high activity for chemical reactions, for example, hydrocracking, paraffin isomerization and dispropotionation (Hiroshige *et al.*, 1968; Lanewala *et al.*, 1969; Venuto *et al.*, 1994; Onyestyak *et al.*, 2002; Corma *et al.*, 2002; Peng *et al.*, 2005). The activities of these reactions not only depend on acidity of Brønsted acid site but also depend on the pore size character of zeolite. Zeolites can bear various pore sizes and channels (Fig 1). The diameters of zeolite pore sites are in the range of 3-12 Å.

The large pore zeolite, Faujasite (FAU) is widely used in fluid catalytic cracking and hydrocracking of heavy oil fractions (Hiroshige *et al.*, 1968; Sahoo et al, 2001; Corma *et al.*, 2002). The FAU has large cavities forming by connecting 10 sodalite cages through their hexagonal faces. The 12-membered ring pore (consisting of 12 tetrahedral Si atoms (12T)) channel has a diameter of 7.4 Å. This zeolite has a 3-dimensional pore structure. Other important 12 membered ring zeolites are BEA and MOR. Beta (BEA) zeolite is also a three-dimensional pore zeolite. BEA zeolite has cavities which are formed by interactions of two perpendicular 12 membered ring channels. It has pore dimension of 6.6 x 6.7 Å in diameter. BEA zeolite is used for cumene and ethylbenzene production (Tsai, *et al.*, 1991; Sridevi, et al, 2001). Mordenite (MOR), which is a two-dimensional zeolite, is a 12-membered ring zeolite with containing 8-membered ring site pockets. MOR has pore dimension of 6.5 x 7.0

Å in diameter. MOR zeolite is widely used for hydrocracking, hydroisomerization, dewaxing, transalkylation of aromatics, NOx decomposition and cumene synthesis (Shelef, 1995; Stöcker *et al.*, 2005).

Among medium pore zeolites, ZSM-5 is a very important catalyst for petrochemical processes such as hydrocracking, ethylbenezene and styrene production, xylene isomerization, methanol to gasoline (MTG), benzene alkylation, adsorption, toluene disproportionation and catalytic aromatisation (van Bokhoven *et al.*, 2004, Corma *et al.*, 2002, Yoda *et al.*, 2005, Stöcker *et al.*, 2005). The three dimensional structure of ZSM-5 contains a network of interconnected straight and zig-zag channels. The straight channel of this zeolite has a dimension of 5.4 × 5.6 Å and the sinusoidal channels has a dimension of 5.1 × 5.4 Å.

Zeolite A (LTA) is a small pore zeolite that is very important and has the largest of use in industry and market. Zeolite A has pore dimension only 4.1 Å. Zeolite A is used for ion exchange, molecular sieve and size-selective separation such as N_2/O_2/Ar and $H_2O/CH_3OH/C_2H_5OH$ (Chudasama *et al.*, 2005). Another important small pore zeolite is Ferrerite. Ferrerite (FER) is a two-dimensional zeolite with two channels whose dimensions are 4.2 x 5.4 Å and 3.5 x 4.8 Å. The two channels are perpendicular to each other. Due to the specific pore size of FER, it is use for n-butene skeletal isomerization (Stöcker *et al.*, 2005).

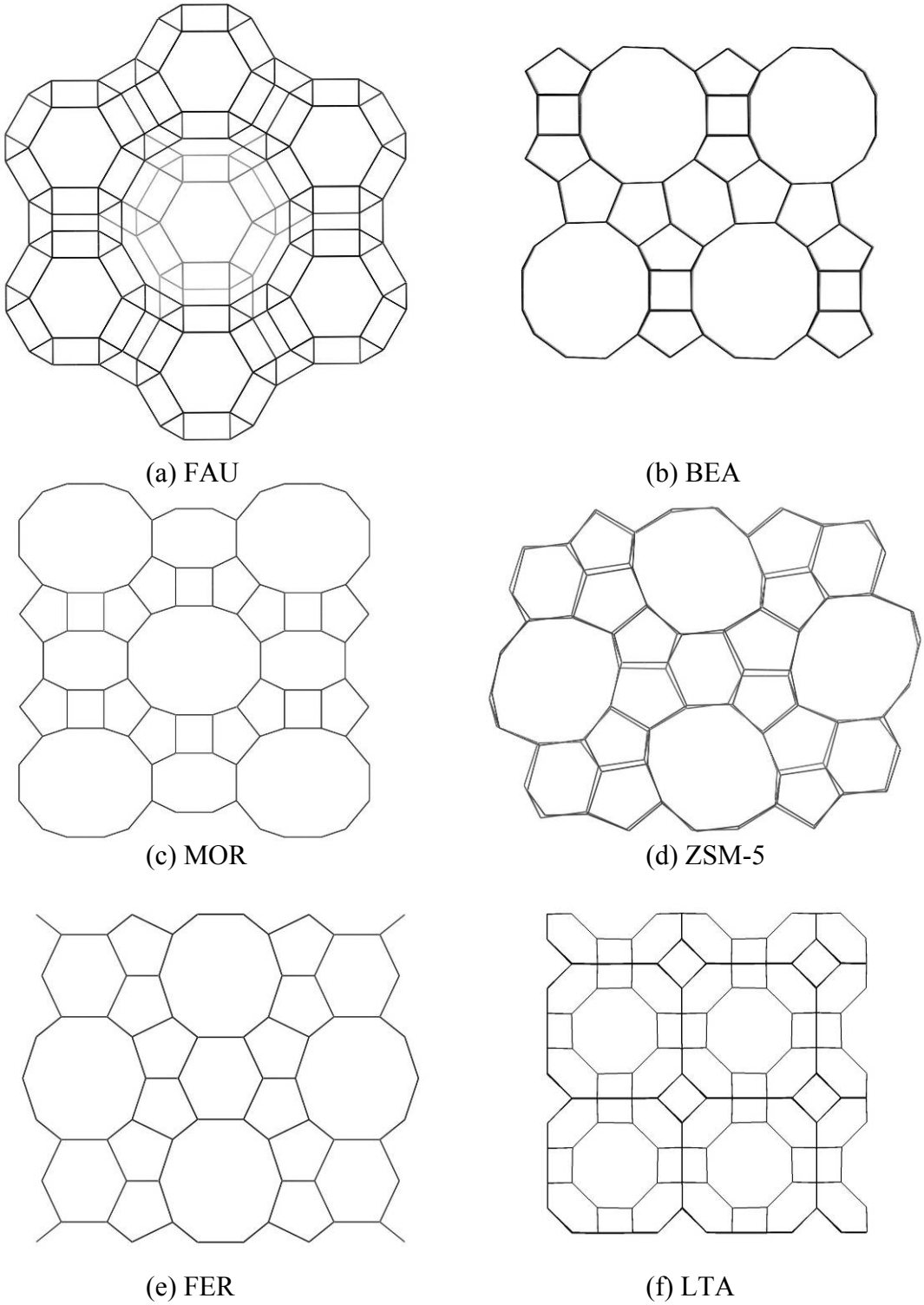

(a) FAU (b) BEA

(c) MOR (d) ZSM-5

(e) FER (f) LTA

Figure 1 Various type zeolite pores and channel (a) FAU, (b) BEA, (c) MOR, (d) ZSM-5 (e) FER and (f) LTA.

The zeolite pore size and geometry have been found to have significant effects on the adsorption and reaction of adsorbed molecules inside its nanostructured pores (Wei *et al.*, 1994; Derouane *et al.*, 2000; Boronat *et al.*, 2001; Bokhoven *et al.*, 2004). The pore size of zeolite is important to distinguish reactants and products by size and shape. The mechanism of molecular shape-selective catalysis can be summarized as reactant selectivity, product selectivity and restricted transition state-type selectivity (Stocker *et al.*, 2005). Reactant selectivity shows the catalysts acting as molecular sieves allowing suitable molecules to enter the crystal of catalysts. Product selectivity means the products that have distinct diffusivities may leave the microporous framework where as the bulky products may stay longer in the pore. Restricted transition state-type selectivity describes the transition state or intermediate of reaction which is limited from the shape and size of pore.

The confinement effect is opposite to molecular shape-selectivity. The confinement effect is longer range and attractive force such as van der Waals interaction (Derouane, 1998). This effect increases the physisorption energies and comparable the activation energies for chemical reactions. In zeolite, the confinement effect was proposed to explain the interactions between the zeolite framework and the adsorbed molecule. These interactions are mainly composed of dispersive van der Waals interactions. The confinement effects contribute to the remarkable sorption and catalytic properties of zeolites by stabilizing adsorbed molecules, intermediates, and reaction transition states. Derouane (Derouane, 2000) has reconsidered the confinement effect which arises from van der Waals interactions. For example, the heat of adsorptions of ammonia and several amines on zeolites MOR and MFI, are determined by chemical (heat of protonation) and physical (confinement represet up to 40% of the heat of adsorption). With confinement effect, the zeolite can be act as a solid solvent when the sizes of the sorbate and of the channels or cages are comparable.

To understand the confinement effect between zeolite and adsorbed molecule, the interaction and reaction of adsorbed molecules with the acid sites by theoretical calculation are become increasing important. The small quantum clusters representing the catalytic active site have been studied in the past. However, this has meant that the essential confinement effect from surrounding framework has been neglected. It is important, therefore, that the larger clusters which include such potentials should be taken into consideration. To facilitate this, large quantum clusters and periodic calculations have been specifically developed. Even though these calculations do provide accurate results, they are very expensive in terms of computational time and expense. The use of accurate periodic structure calculations are also computationally too expensive and impractical to perform when very large zeolites are concerned. The recent development of hybrid methods, such as the embedded cluster or combined quantum mechanics/molecular mechanics (QM/MM) (Brändle and Sauer, 1998, Greatbanks *et al.*, 1996, Limtrakul *et al.* 2000, Treesukol *et al.*, 2001, Khaliullin *et al.*, 2001, Hillier *et al.*, 1999) methods, as well as the more general ONIOM (Our-own-N-layer Integrated molecular Orbital + molecular Mechanics) method (Dapprich *et al.*,1999, Svensson *et al.*,1996) have brought a larger system within reach of obtaining accurate results at a more reasonable computational cost.

In this thesis, the interactions of saturated, unsaturated hydrocarbon, polar molecule and amino acid on various zeolites have been studied with ONIOM calculation. First, the adsorptions of linear alkanes and alkenes in different zeolites, (MOR, and FAU), are examined and compared to understand the adsorption process and to address the confinement effect in these nanostructured materials. The adsorption of alkanes in zeolite is simply physisorption. However, the adsorption of alkenes in acidic zeolites is complicated by the rapid reactions of oligomerization and isomerization at the Brønsted acid sites (Kondo *et al.*, 2003, Yoda *et al.*, 2005, Spoto *et al.*, 1994). The heat of adsorption of alkenes cannot be experimentally measured because of these reactions. The dominant adsorbed structure for alkenes adsorption in zeolites is a π-adsorption complex where the π-electron of the double bond carbons forms a hydrogen bonding with the Brønsted acidic proton of the zeolite (Spoto *et al.*, 1994). The other type of adsorption via interaction of the alkyl group of alkene and

the Brønsted acid of the zeolite has also been reported (Kondo *et al.*, 2003, Yoda *et al.*, 2005). It has also been proposed that the transition between these two adsorption structures may be important to the diffusion process of alkenes in microporous zeolites (Kondo *et al.*, 2003, Yoda *et al.*, 2005). The molecular details of adsorption of alkanes and alkenes which is nonpolar molecule on zeolites with different pore sizes have been completely studied in this thesis. For polar molecule, the acetone, which is important organic solvent, has been studied on various zeolites (FER, ZSM-5 and MCM-22). The acetone adsorption complex is in form of a hydrogen-bonded complex between the carbonyl group and the Brønsted acid site of zeolite. Sepa et al (Sepa *et al.*, 1996) found that the adsorption energy of acetone on H-ZSM-5 is 31.1 kcal/mol. Several theoretical studies on the adsorption of acetone in zeolite (Florien *et al.*, 1994, Kassab *et al.*, 1999) have provided useful information on the mechanism and energetic of reaction. However, most of previous studies did not include the effects of the zeolite framework. In this work, the interactions between acetone with different zeolites have been studied with the focus on the zeolite framework effect and the efficiency of the ONIOM method. To understand the effect of zeolite framework on biomolecule, the interactions of amino acids (glycine and L-alanine) adsorbed on the zeolite Brønsted acid site have been investigated. Glycine (NH_2CH_2COOH) is the simplest and smallest among the twenty most common amino acids found in proteins. Glycine is used as a basic adsorption model and is an important starting step for understanding interactions, structures and the reactivity of amino acids and peptides. To the best of our knowledge, the interaction of zeolites with amino acids adsorption has not been considered from a theoretical point of view. In this work, many type of adsorptions of glycine and L-alanine on zeolite have been performed to understand the fundamental of interactions of amino acids with zeolites.

The confinement effect of zeolite framework adsorption of hydrocarbons is clearly understood with ONIOM method. To understand the confinement effect on reaction, the tautomerization of acetone has been studied. This reaction is an important step before aldol condensation. The fundamental steps of the aldol condensation in acidic zeolites are proposed to be similar to which in the solutions (Fleogo *et al.*, 2000; Ernst *et al.*, 1991). The mechanism consists of the acid-catalyzed

tautomerization of acetone, the nucleophilic attack of the enol tautomer with the protonated carbonyl compound, and the aldol adduct dehydrogenation. Acetone is then transformed to α,β-unsaturated carbonyl compound. In the tautomerization, the acidity and the ionic strength of the reaction media may have crucial effects on the reactant activity. A number of theoretical studies on keto-enol tautomerization of acetaldehyde (Rodriguez-Santiago *et al.*, 2001) reported that the reaction proceeded through a high energy barrier (43.1-67.9 kcal/mol). In the solvent-assisted systems, the presence of solvent molecules in the transition state provides the hydrogen bonding network to lessen the geometry distortion of the transition state and thus reduces the energy barrier significantly. Previous calculations show that the acidity and bifunctional features of the H-ZSM-5 catalyst drastically reduce the barrier height for the tautomerization of acetaldehyde and acetone (Solans-Monfort *et al.*, 2002). Due to lack of confinement effect of zeolite framework, the adsorption energies of these two molecules are lower than experiment data and the reaction properties with different configuration of framework is still not studied. In this thesis, the tautomerization reaction of acetone on different pore size of zeolites has been studied to understand the confinement effect on the reaction properties. The 10T-membered and 12-membered ring of acidic zeolites (H-FER, H-ZSM-5 and H-MCM-22) have been studied.

In this thesis, the confinement effect of zeolite framework on the adsorption and reaction on acidic zeolite has been studied with ONIOM method. The effect of confinement on adsorptions of saturated, unsaturated hydrocarbon, polar molecule and amino acid are studied on various zeolites The confinement effect on reaction mechanism of tautomerization reaction of acetone is studied on three different pore sizes of zeolites.

LITERATURE REVIEW

Acidic zeolite is widely used as solid catalysts for many petroleum and chemical industries due to their high activity, stability and selectivity. The zeolite catalysts also offer the advantage of high selectivity toward the desired product due to the shape selective properties of their microcrystalline pore structures. The zeolite pore size has been found to have significant effects on the adsorption and reaction of adsorbed molecules inside its nanostructured pores (Wei *et al.*, 1994; Derouane *et al.*, 2000; Boronat *et al.*, 2001; Bokhoven *et al.*, 2004).

In 2000, Derouane *et al.*, studied interaction of ammonia on several zeolite such as MOR and MFI. The heats of adsorption of ammonia were measured and were determined by both chemical (heat of protonation) and physical (confinement factors). They reported the adsorption of ammonia and various zeolites: FER, MOR, MFI and FAU. The average heats of protonated, which are calculated form the different of heats of adsorption and confinement energies, are calculated to be 31.5 kcal/mol with a range of 2 kcal/mol for only high-silica zeolite (FER, MFI and MOR). The heat of protonation of several amnies adsorbes on MFI and MOR zeolite are measured in a range 35.9 ± 2 kcal/mol. Their results show the effect of confinement arising to the heat of adsorption up to 25-40% while the heats of protonation do not depend on type of zeolite. The confinement effects contribute to the remarkable sorption and catalytic properties of zeolites by stabilizing adsorbed molecules, intermediates, and reaction transition states. Their results shows that the confinement effects arising from van der Waals interactions.

The understanding and rational utilization of confinement effects will undoubtedly contribute to increasing the productivity, and selectivity (Corma *et al.*, 1997, Babitz *et al.*, 1999, Dubbeldam *et al.*, 2003, Maesen *et al.*, 2006). Recently, experimental investigations in molecular details of structures and adsorption dynamics and interaction energies of hydrocarbons in zeolites have been reported (Pieterse *et al.*, 2000, Yang *et al.*, 2001, Schuring *et al.*, 2001, Tielens *et al.*, 2003, Zecchina *et al.*, 2005, Kondo *et al.*, 2003, Yoda *et al.*, 2005). The adsorption of

alkanes in zeolite is simply physisorption. The linear correlations of interaction energy (heat of adsorption) and the number of carbon atoms of n-alkanes have been found in various zeolites (Derouane *et al.*, 1998). However, the adsorption of alkenes in acidic zeolites is complicated by the rapid reactions of oligomerization and isomerization at the Brønsted acid sites (Kondo *et al.*, 2003, Yoda *et al.*, 2005, Spoto *et al.*, 1994). The heat of adsorption of alkenes cannot be experimentally measured because of these reactions. The most stable adsorbed structure for alkenes adsorption in zeolites is a π-adsorption complex where the π-electron of the double bond carbons forms a hydrogen bonding with the Brønsted acidic proton of the zeolite (Spoto *et al.*, 1994). A less stable adsorption complex via interaction of the alkyl group of alkene and the Brønsted acid of the zeolite has also been reported (Kondo *et al.*, 2003, Yoda *et al.*, 2005). It has also been proposed that the transition between these two adsorption structures may be important to the diffusion process of alkenes in microporous zeolites (Kondo *et al.*, 2003, Yoda *et al.*, 2005). However, the molecular details of adsorption of alkanes and alkenes on zeolites with different pore sizes are still not completely understood. The quantum cluster calculations on small cluster were used to study the adsorption properties in the past. Several methods were applied on the adsorption on small quantum cluster.

The adsorption energies of ethylene on zeolite were calculated to be -4 to -7 kcal/mol (Kazansky *et al.*, 1999; Ugliengo *et al.*, 1996). The experimental investigations in molecular details of structures and adsorption dynamics and interaction energies of hydrocarbons in zeolites have been reported (Pieterse *et al.*, 2000, Yang *et al.*, 2001, Schuring *et al.*, 2001, Tielens *et al.*, 2003, Zecchina *et al.*, 2005, Kondo *et al.*, 2003, Yoda *et al.*, 2005). It was found that the pore size of zeolites and the geometries of adsorption sites had strong effects on the structures of the adsorption complexes and the adsorption energies. The adsorption of alkanes in zeolite is simply physisorption. The linear correlations of interaction energy (heat of adsorption) and the number of carbon atoms of n-alkanes have been found in various zeolites due to the electrostatic of the extended atoms (Derouane *et al.*, 2005).

In 2003, Wasinee (Wasinee and Limtrakul, 2003) used ONIOM to study the ethylene on H-ZSM-5. The ethylene on 3T bare cluster H-ZSM-5 gives the adsorption energy only -4.25 kcal/mol. The effect of zeolite framework is adding with ONIOM model 46T model and gives the adsorption energy up to -9.14 kcal/mol. The interaction energy of ethylene on H-ZSM-5 from ONIOM model agrees well with experimental estimate of -9 kcal/mol.

Increasing the size of probe molecule from ethylene to ethylbenzene, the adsorption of ethylene, benzene and ethylbenzene were studied over FAU zeolite with ONIOM method (Kasuriya *et al.*, 2003). The adsorption energies of ethylene, benzene and ethylbenzene over H-FAU were calculated to be -8.75, -15.17 and -21.08 kcal/mol, respectively. These energies are compared well with the experimental estimates of -9.1, -15.3 and -19.6 kcal/mol for ethylene, benzene and ethylbenzene, respectively. These results are compared with the bare quantum cluster and show the effect between the adsorbate and acidic zeolite both form Brønsted acid and lattice framework.

Not only the ONIOM method was applied on FAU zeolite, but the ONIOM method was also studied on MFI zeolite. The ONIOM approach has also been employed to study the interactions of ethylene and benzene over FAU and ZSM-5 zeolite (Karan and Limtrakul, 2003). The calculated interaction energies of ethylene are -16.94 and -14.27 kcal/mol for Li-ZSM-5 and Li-FAU zeolites, respectively. The binding energy of benzene are -28.78 and -19.46 for Li-ZSM-5 and Li-FAU zeolites, respectively. For the larger cation-exchanged Na-ZSM-5 and Na-FAU complexes, the calculated interaction energies are lower than complex over Li-Zeolite due to the conventional electrostatic tread. The calculated adsorption energy of ethylene over Na-FAU is -8.65 kcal/mol agrees well with experimental results (8.8-9.6 kcal/mol).

For the bigger molecular probe, the ONIOM method shows the performance for calculation. The aromatic compound on zeolite has been studied with ONIOM (Wongthong *et al.*, 2004). With the 3T bare cluster model, the interaction energy for benzene on H-FAU is -7.77 kcal/mol. Using ONIOM, the toluene over H-FAU is

calculated to be -19.44 kcal/mol agree well with experimental values of -20.39 kcal/mol.

In 2005, Ratana (Ratana *et al.*, 2005) studied the adsorption of benzene on various zeolite to study the effect of confinement effect. The interactions between benzene and H-BEA, H-ZSM-5 and H-FAU were studied with ONIOM approach. The adsorption energies after Basis Set Superposition Error (BSSE) of benzene on H-ZSM-5, H-BEA and H-FAU are -18.96, -16.34 and -15.18 kcal/mol, respectively. The calculated adsorption energy of benzene on H-FAU can be compared well with the experimental data of -15.31 kcal/mol.

Nevertheless, the ONIOM method can distinguish the adsorption of the same molecular weight number molecule with different configuration. The adsorption of ethene and four butene isomers on H-ZSM-5 have been studied using ONIOM approach (Supawadee *et al.*, 2006). The adsorption energy of ethene on H-ZSM-5 is calculated to be -8.17 kcal/mol, which is in good agreement with the experimental data of -9.0 kcal/mol. The trend for four butene isomers on H-ZSM-5 is as follows: 1-butene (-16.06) > cis-2-butene (-13.62) ≈ trans-2-butene (-13.25) > isobutene (-6.96). The steric repulsion between the methyl substituted around the C=C bond and zeolite framework make the less stable adsorption of isobutene. The Natural Bond Orbital (NBO) analysis shows the maximum charge transfer from the active site and largest stabilization energy in the case of isobutene. These results show the reason why isobutene is as product form the n-butene.

The ONIOM method is successful for study interaction of non-polar molecule. Next the ONIOM method was also applied to study polar molecule. The adsorptions of carbonyl compound over zeolite were also studied with ONIOM method (Boekfa *et al.*, 2004). The embedded ONIOM has been used and compares with the ONIOM method. The predicted adsorption energies of carbonyl compound over H-ZSM-5 with embedded ONIOM are -28.44 and -33.22 kcal/mol for acetaldehyde and acetone, respectively. The adsorption energy of acetone is calculated close with the experimental result of -31.1 kcal/mol.

The pyridine adsorption on H-FAU zeolite has studied with embedded ONIOM method (Jarun *et al.*, 2006). The embedded ONIOM includes the electrostatic effect of the infinite crystal lattice via point charge. These point charges were generated form the finite lattice of zeolite. Without embedded point charges, the adsorption energy of pyridine on H-FAU is -36.8 kcal/mol from ONIOM calculation. The interaction of pyridine on H-FAU with embedded ONIOM is -45.9 kcal/mol. This later energy is close to experiment of -47.6 kcal/mol. The data suggest that the embedded ONIOM scheme gives accurate result of the interaction of small organic molecule with zeolite.

Zeolites are also found to be potential for amino acid applications. For the adsorption application, the amino acids on the BEA and FAU zeolite were studied with HPLC (Krohn and Tsapatsis, 2005, Krohn and Tsapatsis, 2006). The various amino acids adsorption on ZSM-22, ZSM-5 and FAU were also studied with X-ray diffraction (Munsch *et al.*, 2001). The adsorption of amino acids is dominated by electrostatic interaction between their positively charged ammonium group and the negatively charged zeolite surface. The hydrophobic interactions of non-polar side chains of adsorbed amino acid molecules complement the ionic interactions. These two fundamental interactions allow the separation of amino acids from aqueous solution. Although experimental and theoretical studies on amino acid adsorption in zeolites have been reported (Yonsel *et al.*, 1993, Krohn and Tsapatsis, 2005, Krohn and Tsapatsis, 2006, Xu *et al.*, 2003, Munsch *et al.*, 2001) and a separation process of amino acids based on zeolites was claimed (Yonsel *et al.*, 1993),

In 2000, the peptide synthesis on zeolites were studied by Xing (Xing *et al.*, 2000). The microporous FAU zeolite (HY, HH_4Y, NaY) and mesoporous FAU zeolite (HDAY, HNH_4DAY) were selected to study. The α-chymotrypsin and thermolysin were immobilized in the microporous of zeolite and were active for peptide synthesis. The immobilization effect of FAU zeolite was better than DAY zeolite, suggesting that the FAU, which are more hydroxyl groups, is powerful

hydrogen bonds with enzyme molecules. This study was concluded that the zeolite pore and the activity are important for amino acid adsorption and reaction.

The theoretical studies have investigated the peptide bond formation on solid catalysts. Aquino (Aquino *et al.*, 2004) studied the amine bond formation for the reaction of acetic acid and methylamine on clay surface with VASP calculation. A series of catalysts of varying strength (Al^{3+}, $AlCl_3$, $Al(OH)_3$, $[Al(OH)_5]^{3+}$, H^+, H_3O^+, H_3O^+-H_2O, H_2O and $(H_2O)_2$) was investigated as Lewis or Brønsted acids. With catalysts, the activation barrier was reduced and the rate-determining step of the reaction is the N-C dative bond by proton transfer from nitrogen to oxygen.

In 2006, the peptide bond formation on silica surface was studied with ONIOM (Rimola *et al.*, 2006). The simulation was performed by the reaction of glycine and NH3. The glycine is unstable on the silica surface ($\Delta G \approx 6$ kcal/mol) and the catalysts reduce the activation energy ($\Delta G \approx 48$ kcal/mol) only 4 kcal/mol than that of the uncatalysts. However the activation energy is reduced ($\Delta G \approx 41$ kcal/mol) when a water molecule acts as a proton-transfer helper. In the same year, Rimola (Rimola *et al.*, 2006) calculated the interaction of glycine molecule on silica surface. In their work, the silica surface was simulated as 2D slab with periodic B3LYP simulation. They found that the glycine can interact with two forms: neutral form and zwitterions form. The silica surface shows the role of "solid solvent".

The adsorption of acetaldehyde on zeolite was studied by infrared spectroscopy (Carlos *et al.*, 1992). Acetaldehyde vapor was exposed to thin film zeolite at various pressures. The band at 3600 cm^{-1}, assigned to the hydroxyl group of zeolite was vanished and the shift to lower frequency of carbonyl peak showed that the primary interaction between acetaldehyde and H-ZSM-5 is proton transfer. The "ion-pair" structure of acetone on zeolite was found by Kubelkova (Kubelkova, 1991). The carbonyl bond in ketone is perturbed far more by the bridging hydroxyl of active site of zeolite cause the formation of a protonated ketone. The proton transfer of acetone was studied by Florián and Kubelkova (1994). They studied both FTIR and *ab initio* HF/3-21G. The spectra of stretching of the hydroxyl group of zeolite at

3611 cm^{-1} decreases while the bands at 2995-2770 and 2435-2370 cm^{-1} arise. This mean the adsorption of acetone and H-ZSM-5 is strong hydrogen bond.

The ^{13}C NMR has also been used to study the condensation of acetaldehyde and acetone (Biaglow *et al.*, 1995). This experimental indicated the adsorptions of acetone and acetaldehyde with H-ZSM-5 are hydrogen bond at low coverage. At room temperature acetone adsorbed on H-ZSM-5 with hydrogen bond and can be transformed to mesityl oxide at higher temperature and coverage. Xu *et al.* (1994) also studied the adsorption of acetone using ^{13}C MAS NMR, the structure of the adsorption of acetone on H-ZSM-5 would involve strong hydrogen bonding. The proton transfer can observe on H-ZSM-5 to mesityl oxide which is product of aldol condensation of acetone, in the ^{13}C chemical shift. However, they observed an odd peak at 85 ppm, which disappeared when mesityl oxide formed. It possible the acetone can form alkoxide intermediate. Furthermore the ^{1}H MAS NMR (Böhlmann *et al.*, 2002; Xu *et al.*, 2003) indicated the acetone on H-ZSM-5 was a strong interaction. In ^{1}H MAS NMR result showed that the enol formed as an intermediate.

Dumitriu *et al.* (2001) studied the aldol condensation of lower aldehydes on H-ZSM-5. The surface properties of zeolite was investigated by temperature-programmed reduction, X-ray photoelectron spectroscopy, temperature-programmed desorption of ammonia, Fourier transform infrared spectroscopy and microcalorimetry. Vapor phase aldol condensation of acetaldehyde on H-ZSM-5 has been carried out, and it has been observed that the structure features of the catalysts do play an important role in controlling conversion and selectivity. Moreover, the increase of the aluminium content in the H-ZSM-5 samples has a strong influence on the catalytic selectivity to aldol products.

The condensation reaction of acetone on H-ZSM-5 has been studied by FTIR (Panov and Fripiat, 1998). The acetone produces 4-methyl-2-pentanone (methyl isobutyl ketone, MIBK) which widely used as a solvent in the manufacture of important chemicals such as inks and lacquers. MIBK has been produced from acetone in a three-step process. First, acetone is converted to diacetone alcohol

(DDA) by base- and acid-catalyzed aldol condensation reaction. Next, DAA is dehydrated on an acid catalyst to mesityl oxide (MO). The C=C bond of the MO is hydrogenated on a metal such as Pt to product MIBK (Cosimo *et al.*, 2002).

For the adsorption, the heat of adsorption of acetone is experimentally and theroitically studied. The heat of adsorption for acetone on H-ZSM-5 was measured by Sepa *et al.* (1996) to be 31.1 ± 1.0 kcal/mol. The theoretical study of carbonyls on clusters zeolite was under taken by Sepa (1996) and Kassab (1999). They simulate the zeolite by a small cluster consisting of a few atom surrounding the zeolite hydroxyl bond and low level of calculation. The predicted adsorption energies were lower than experimental report.

Concerning keto-enol isomerization of carbonyl compound, the tautomerization of acetaldehyde and acetone was studied via the concerted mechanism (Chen-Chang *et al.*, 1996; Rodriguez-Santiogo *et al.*, 2001). The activation energy of acetone was calculated to be 75.0 kcal/mol with MP2/6-31G(d) (Chen-Chang *et al.*, 1996). The activation energies of acetaldehyde were calculated to be 76.1 kcal/mol and 67.9 kcal/mol with MP2/6-31G(d) and B3LYP/6-31G(d), respectively (Chen-Chang *et al.*, 1996; Rodriguez-Santiogo *et al.*, 2001). For acetaldehyde the activation energy can be reduce to 40.6 kcal/mol with water molecule.

In recent theoretical studies (Monfort *et al.*, 2002) concerning the keto-enol isomerization of acetaldehyde on H-ZSM-5 using 63T ONIOM2. The interactions of acetaldehyde with the H-ZSM-5 are -12.9, -13.7, -7.4, and -9.3 kcal/mol for the 3T, 5T, 63T ONIOM2(B3LYP:AM1) and 63T ONIOM2 (B3LYP:PM3), respectively. In this study the acetaldehyde form a hydrogen bond complex. However, at B3LYP:AM1 level the proton of the zeolite is completely transferred to acetaldehyde. In their study, the keto-enol isomerisation of acetaldehyde on H-ZSM-5 is concerted mechanism and the reaction is endothermic reaction.

METHODOLOGIES AND MODELS

METHODOLOGIES

In this thesis, the zeolite and their adsorption complexes were calculated with ONIOM models (Dapprich *et al.*,1999, Svensson *et al.*,1996). The small active region was treated with quantum calculation, while the rest of the model was approximated by less computationally method. The density functional theory with B3LYP/6-31G(d,p) level of theory was used for the quantum calculation to represent the active site of zeolite. The extended framework connecting the quantum region was treated with the universal force field (UFF) to represent the van der Waals contributions from the interactions of adsorbed molecules with the zeolite pore structures.

To represent the long range interactions of the infinite zeolite lattice, The Madelung potential from the zeolite lattice beyond the quantum cluster was used via the set of optimized point charges using Matlab program as the code. These point charges were applied for the quantum region calculation. The combined between point charge and the ONIOM 2 layer model is called "embedded ONIOM2" approach (Lomratsiri , *et al.,* 2006; Injan, *et al.,* 2005). The Density functional theory, ONIOM, BSSE and embedded point charge are discussed in brief:

1. Density Functional Theory (DFT)

Density Functional Theory (DFT) (Hohenberg and Kohn, 1964; Chalasinski, 2000) is one of the most useful techniques for computational chemistry because it takes several advantages such as less computational cost and demand, less time consuming, and provide the agreement result with the experimental value. The energy part of DFT is a functional of the electron density, E[ρ], which is itself of a functional of position, ρ(r). The exact ground state energy of an n-electrons molecule is

$$E[\rho] = T[\rho] + V_{ext}[\rho] + E_{xc}[\rho] \qquad (1)$$

Where T[ρ] is the total kinetic energy

V_{ext}[ρ] is the potential energy

E_{xc}[ρ] is the exchange-correlation energy

The major problem of DFT is not known the exact E_{xc} term. There are many way to approximate the E_{xc} term such as local-density approximation (LDA), which give the functional depend on the electron density, Generalized Gradient Approximation (GGA), which include the gradient of the electron density as well as the electron density, and hybrid functional.

The hybrid functional is widely used. One of the most popular functions is B3LYP. In this thesis, we use the B3LYP for quantum calculation. The B3LYP is combined with the HF exchange term, Becke exchange term and the LYP correlation term:

$$E_{XC}^{B3LYP}[\rho] = \alpha E_X^{HF}[\rho] + (1-\alpha)E_X^B[\rho] + bE_c^{LYP}[\rho] \qquad (2)$$

2. Our own N-layered Integrated molecular Orbital and Molecular mechanics (ONIOM)

The ONIOM approach has been developed by Morokuma (Svenssen *et al.*, 1996). The basic idea is partition the system to the two or three layer and treaded the high quantum calculation only the small layer. The ONIOM2 approach, the calculation of energies can be simplified by the active site treated by high-Level quantum mechanical approach while the extended framework is a less expensive level. The total energy of the whole system can be expressed within the framework of the ONIOM methodology by:

$$E_{ONIOM\,2} = E_{Low}^{REAL} + \left(E_{High}^{Cluster} - E_{Low}^{Cluster}\right) \quad (3)$$

Where the superscript Real means the whole system and the superscript Cluster means the active region. Subscripts High and Low mean high- and low- level methodologies.

An important feature for combination method is the treatment at the boundary region between different levels of calculation. With ONIOM the covalent bond at the boundary region have to cut to generate the inner cluster and have to be saturated, usually with hydrogen atoms to avoid a dangling bond.

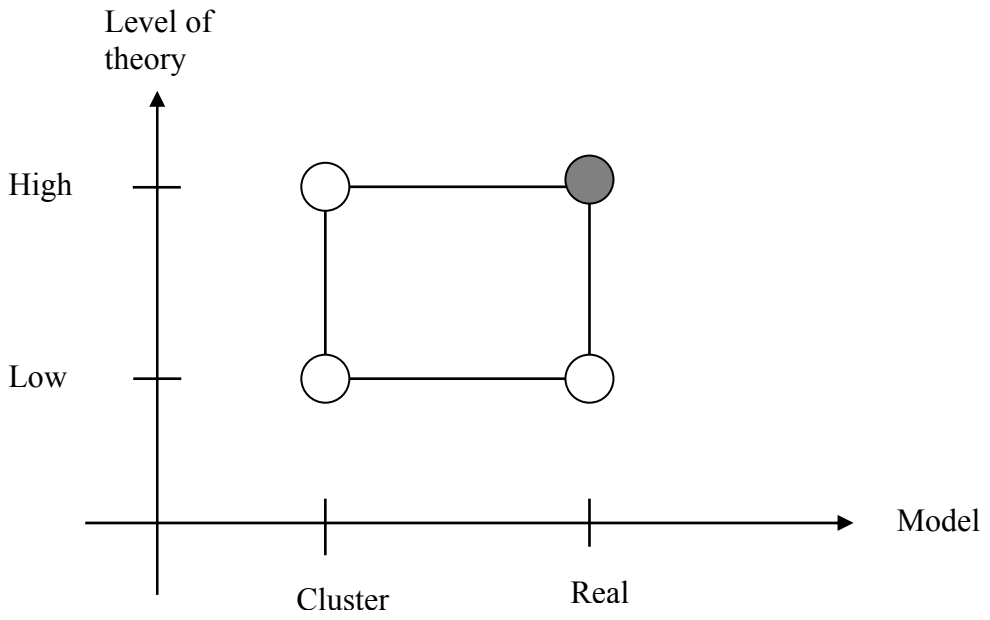

Figure 2 The two-layer ONIOM extrapolation schemes.

3. Basis set superposition error

In quantum chemical calculation, the basis set superposition error (BSSE) (Boys and Berbnardi, 1970) can be occurred when we calculated the interaction energy of two or more molecules with finite basis set. The error is come from the different of the basis set in each isolated energy. The BSSE has been calculated with counterpoise procedure. The Counterpoise (CP) defines as

$$\Delta E_{CP} = E(Zeo)^{*}_{Zeo,Hydrocarbon} + E(Hydrocarbon)^{*}_{Zeo,Hydrocarbon} - E(Zeo)^{*}_{Zeo} + E(Hydrocarbon)^{*}_{Hydrocarbon} \quad (4)$$

where, $E(a)^{*}_{b}$ is the basis set b for a

The BSSE correction energy is given as

$$E_{BSSE} = E_{adsorption} - \Delta E_{CP} \quad (5)$$

4. Embedded Point Charges

The set point charges to represent the long range electrostatic potential of zeolite are generated from the zeolite lattice (Vollmer *et al.*, 1999). These charges are fitted with the electrostatic potential from the quantum region. There are two types of point charges in the inner zone and outer zone.

In the inner zone, the charges are not optimized and have values one-half the formal charges of the zeolite atoms (Si = +2 and O = -1). The point charges in the inner zone should be a shell thickness 5-10 Å and a few hundred of point charges. In the outer zone, the charge is fixed charge. These charges are optimized by the Ewald summation method. The point charges in the outer layer can define by equation 6.

$$Q' = Q_{outer} + \Delta Q \quad (6)$$

ΔQ is the vector of derivative and derived in the following way. The electrostatic potential from the infinite crystal is calculated at the grid points using the Ewald summation method. Then electrostatic potential form the zeolite cluster and the point charge in both zones are deducted as follows:

$$V_{outside} = V_{ewald} - V_{cluster} - V_{inner/outer} \quad (7)$$

Then ΔQ reproduces $V_{outside}$ by solving the matrix of equations:

$$A \bullet \Delta Q = V_{outside} \quad (8)$$

$V_{outside}$ is set of column matrix with rows of the grid point numbers. A is the distance matrix with the number of rows from the grid point numbers and columns from the charges in the outer zone. This number can be defined as $A_{ij} = 1/|R_i - R_j|$. R is the position of grid i and j.

The point charges in the inner zone and the optimized charges in the outer zone which along to the crystal zeolite position are used to the quantum calculation region. The flowchart of point charges are shown in Figure 3. These charges are included using a further layer with the ONIOM model. We call it “embedded ONIOM” and the schematic diagram is shown in Figure 4.

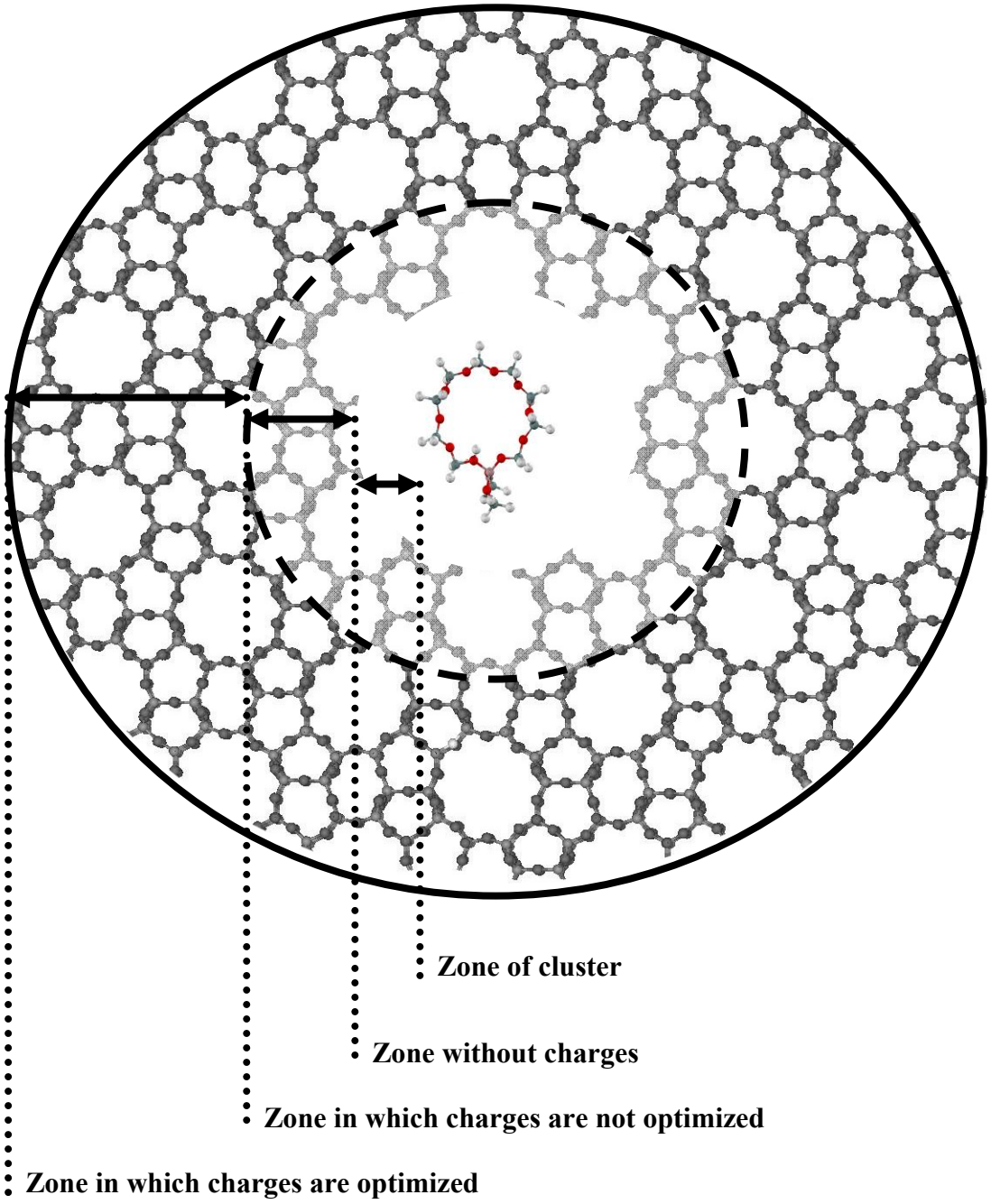

Figure 3 The picture shows the zone of optimized charges (outer zone), non optimized charges (inner zone), zone without charges and quantum cluster.

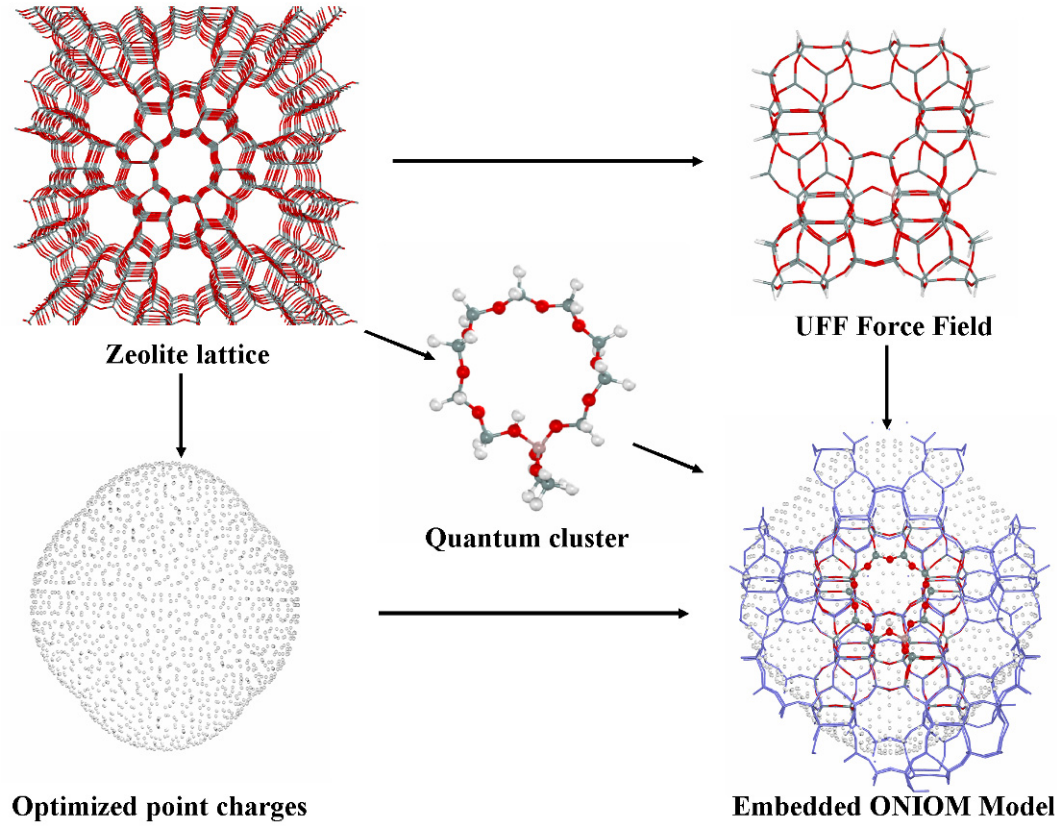

Figure 4 Schematic diagram of the embedded ONIOM method.

1. Adsorption of Hydrocarbon on Various Zeolites

The ONIOM approach was employed to model the different types of zeolites and their complexes with unsaturated and saturated hydrocarbons. For computational efficiency, only the small active region was treated with the density functional theory method, while the contribution of interactions from the rest of the model was approximated by a less computationally demanding method. The structure of MOR and FAU were obtained from their crystal structures (Alberti *et al.*, 1986, Olson *et al.*, 1969). The FAU 14T quantum cluster was the 12-membered-ring window of 7.4 Å in diameter with one substituted aluminum atom (T2 position) and two terminal silyl groups. The attached 120T extended cluster was modeled with the UFF force field to represent the two connecting supercages (Figure 5). Similarly, the MOR 14T quantum cluster (T1 position) was modeled to the 12-membered-ring (MR) window of the straight channel of 6.5 x 7.0 Å. The 120T extended cluster was modeled to cover an ample portion of the straight channel with the crossed 8 MR windows (2.8 x 5.7 Å) opening to the side pockets (Figure 6).

The B3LYP/6-31G(d,p) level of theory was applied for the 14T quantum cluster, which was considered to represent the active site of the zeolites. The 120T extended framework connecting the quantum region was treated with the universal force field (UFF) (Rappe *et al.*, 1992) to represent the van der Waals contributions from the interactions of adsorbed molecules with the zeolite pore structures. This force field has been previously reported to provide a good description of the short-range van der Waals interactions between the sorbate molecules and the zeolitic wall (Kasuriya *et al.*, 2003., Namuangruk *et al.*, 2005).

All structure optimization was performed at the B3LYP/6-31G(d,p):UFF level of theory. In order to obtain more reliable interaction energies, the single point energy calculations at MP2/6-31G(d,p):UFF//B3LYP/6-31G(d,p):UFF and the basis set superposition errors (BSSE) corrections were carried out.

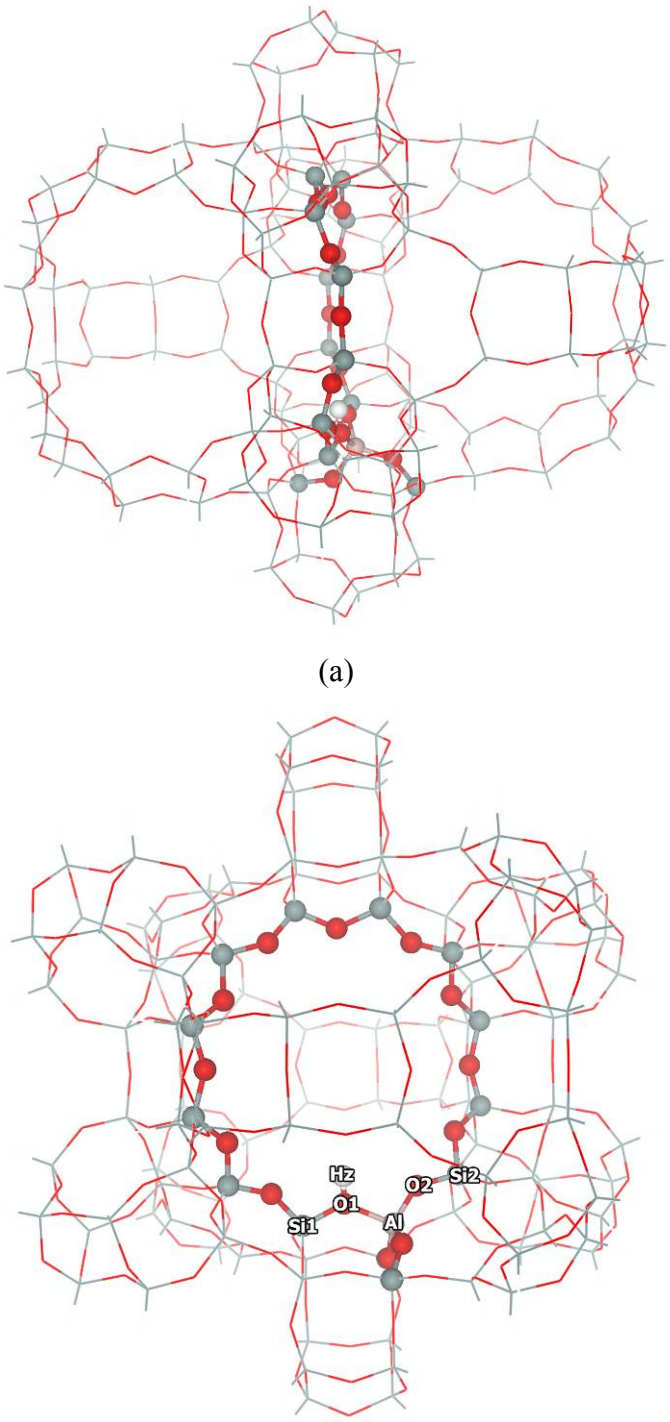

(a)

(b)

Figure 5 The ONIOM model of 14T/120T cluster of H-FAU. (a) Side view shows the two supercages connected to the 14T quantum cluster, (b) Front view shows the 12-membered ring window connecting the two supercages. Atoms belonging to the 14T quantum region are drawn as spheres.

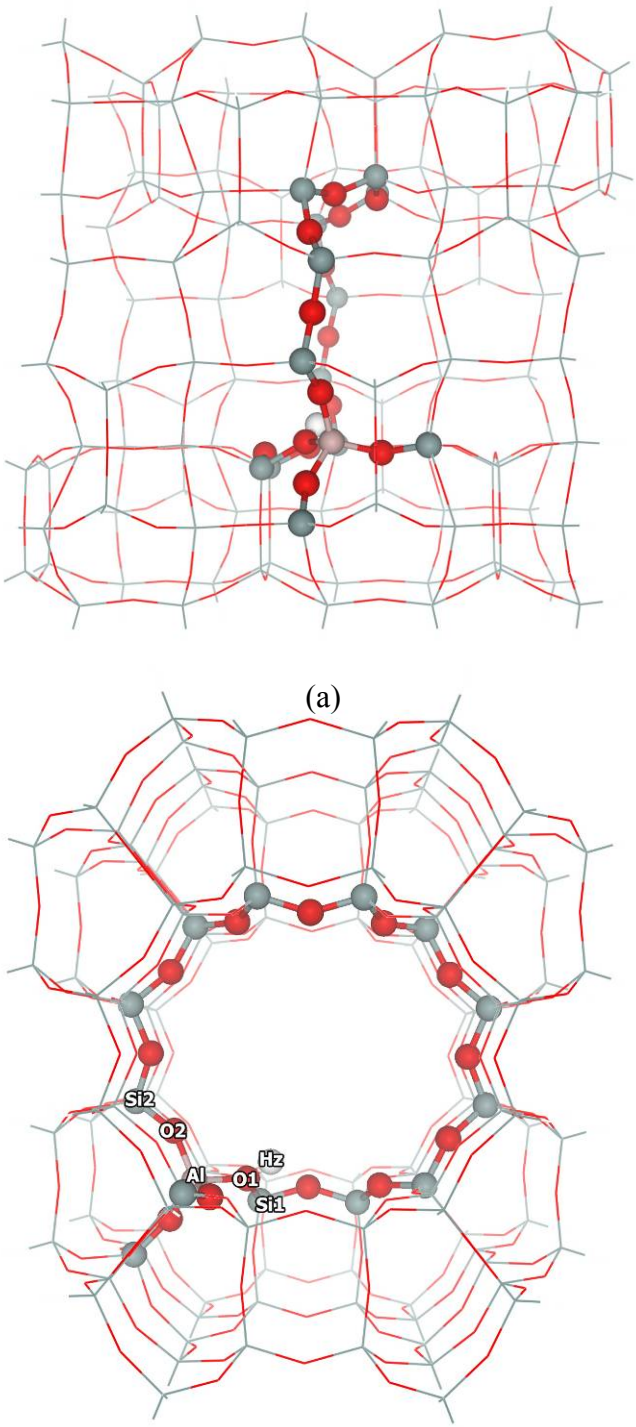

Figure 6 The ONIOM model of 14T/120T cluster of H-MOR. (a) Side view of the 12-membered ring straight channel, (b) Front view shows the 12-membered ring window of the straight channel. Atoms belonging to the 14T quantum region are drawn as spheres.

2. Interaction of Amino Acids with H-ZSM-5 Zeolite

The 128T cluster model of the nanocavity of ZSM-5 zeolite which covers the intersection of the straight and zigzag pore channels was taken from the lattice structure of ZSM-5 zeolite (H. Van Koningsveld, *et al.,* 1987). The cluster model was subdivided into two sub-regions according to the ONIOM method. The 12T cluster model, covering the 10-membered-ring window of the zigzag channel of the zeolite, was treated at the 6-31G(d,p) level of theory. The rest of the 128T extended cluster was treated with the universal force field (UFF) to represent the confinement effect (E.G. Derouane, *et al.,* 1988, C.M. Zicovich-Wilson, *et al.,* 1994) of the nanocavity which is mainly composed of dispersive van der Waals interactions. This force field has been previously reported to provide a good description of the short-range van der Waals interactions between the sorbate molecules and the zeolitic wall (J. Lomratsiri, *et al.,* 2006, S. Namuangruk, *et al.,* 2004, S. Kasuriya, *et al.,* 2003, K. Bobuatong, *et al.,* 2003, W. Panjan, *et al.,* 2003, N. Injan, *et al.,* 2005) since it explicitly considers the van der Waals interactions. In order to derive the full description of the interactions of animo amino acids in nanopores of zeolites, it is necessary to take into account the long range interactions of the infinite zeolitic lattice. The Madelung potential from the zeolite lattice beyond the 12T quantum cluster was introduced by using the "embedded ONIOM2" approach which has previously been successfully employed (N. Injan, *et al.,* 2005). A set of optimized point charges was generated from the infinite zeolite lattice to represent the Madelung potential beyond the 12T quantum cluster.

All structure optimizations were performed at the ONIOM (B3LYP/6-31G(d,p):UFF) level of theory. The Brønsted acid 5T cluster and the interacting probe molecule were allowed to relax while the rest was fixed along to the crystallographic coordinate. In order to achieve more reliable adsorption energies, the single point energy calculations at MP2/6-31G(d,p):UFF//B3LYP/6-31G(d,p):UFF and the counterpoise corrections for the basis set superposition errors (BSSE) were carried out.

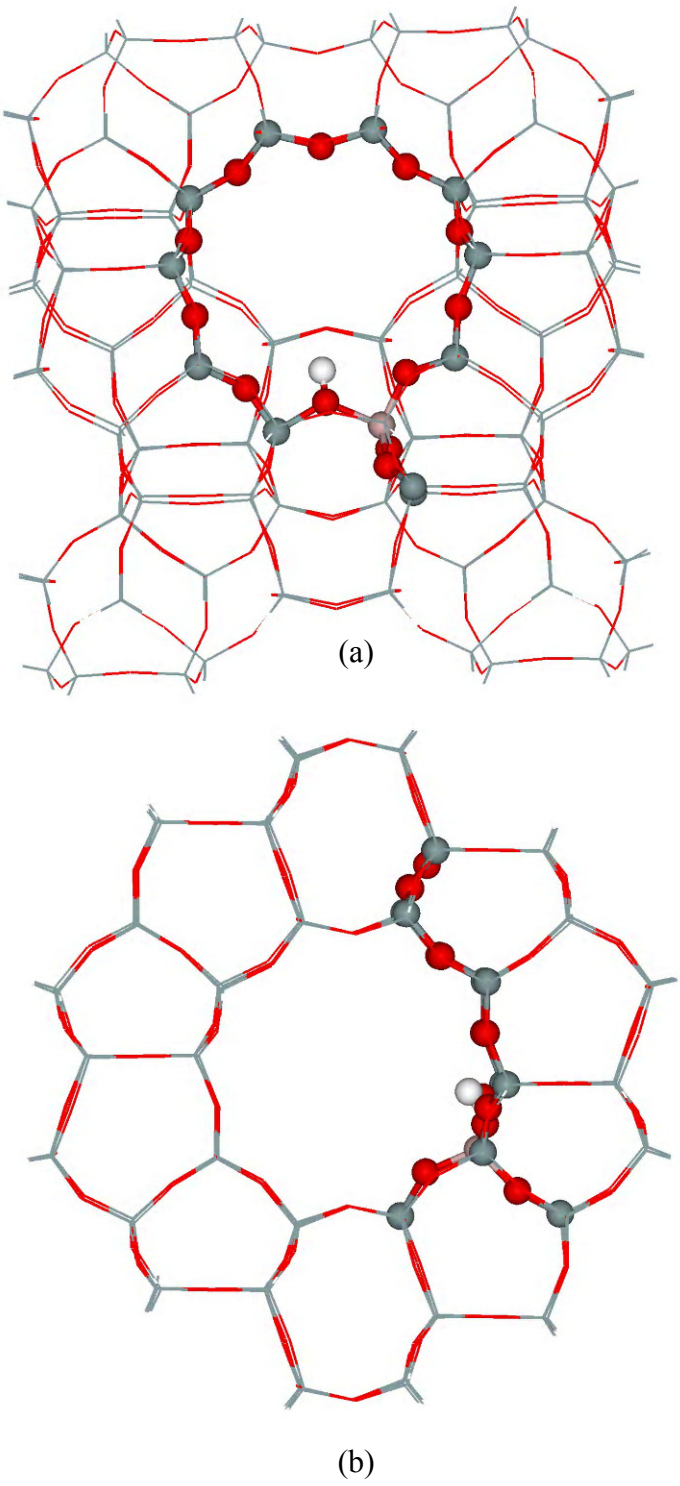

Figure 7 The ONIOM model of 12T/128T cluster of H-ZSM-5. (a) Side view of the 10-membered ring of intersection channel, (b) Front view shows the 10-membered ring window of the straight channel. Atoms belonging to the 12T quantum region are drawn as spheres.

3. Tautomerization of Acetone on H-FER, H-ZSM-5 and H-MCM-22

A variety of models were employed to model the H-FER, H-ZSM-5 and H-MCM-22 zeolites. Ferrerite (FER) is a two-dimensional zeolite (Morris *et al.*, 1994). The pore site of FER contains 10-membered ring which is perpendicular with 8-membered ring. The cluster model of FER zeolite is represented by 112T cluster model, as shown in Figure 8. The quantum region for H-FER is in the 10T straight channel over the 8T and 6T member channel. One silicon atom at the T2 site is replaced with an aluminium atom to represent Brønsted acid site. The 128T of ZSM-5 covers the channel intersection cavity, the straight pore channel and the zigzag channel (van Koningsveld *et al.*, 1987). The quantum region for H-ZSM-5 is in the 10T at the intersection between straight channel and zigzag channel. A silicon atom was substituted with an aluminum atom at the most favorable position (T12). The framework is extended from the center of intersect cavity about 9 Å. The 132T of MCM-22 includes the main gateway of 12-membered channels (Kennedy *et al.*, 1994). The model covers 10T straight channel and 12T supercage. The quantum region is modeled at the 12T supercage. The substituted aluminum atom is located at T4 site (Zhou *et al.*, 2006; Hongyuan *et al.*, 2007).

All calculations were performed with the Gaussian03 code. The ONIOM methodology, consists of two layers of the model, was applied to all calculations. B3LYP level of theory was utilized in the inner layer of the model composed of the active site and adsorbate molecules. During geometry optimizations, only 5T active region of ≡SiOHAl$(OSi)_2$OSi≡ and reacting molecules are allowed to relax while the rest of the structure is kept fixed along the crystallographic data. The outer layer of the environmental structure was treated with the universal force field (UFF). We chose UFF since it is previously reported to include the van der Waals force which is significant in describing the confinement effect.

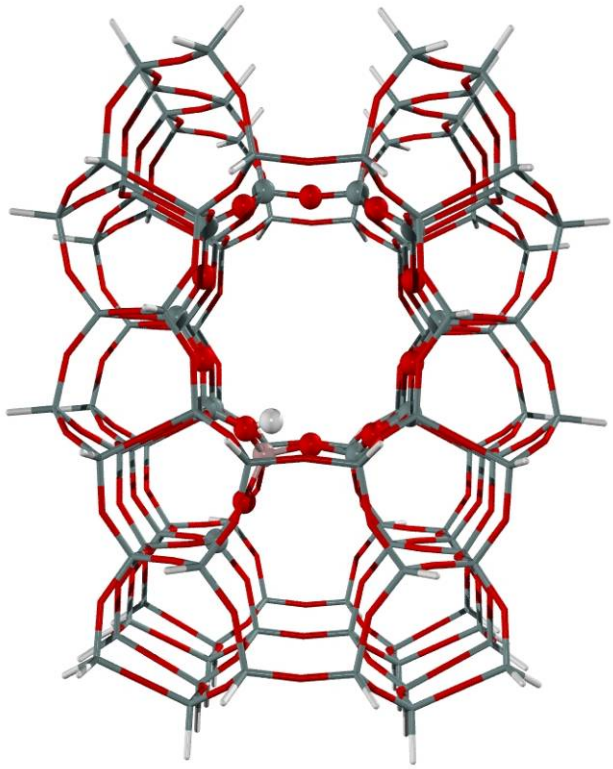

(a)

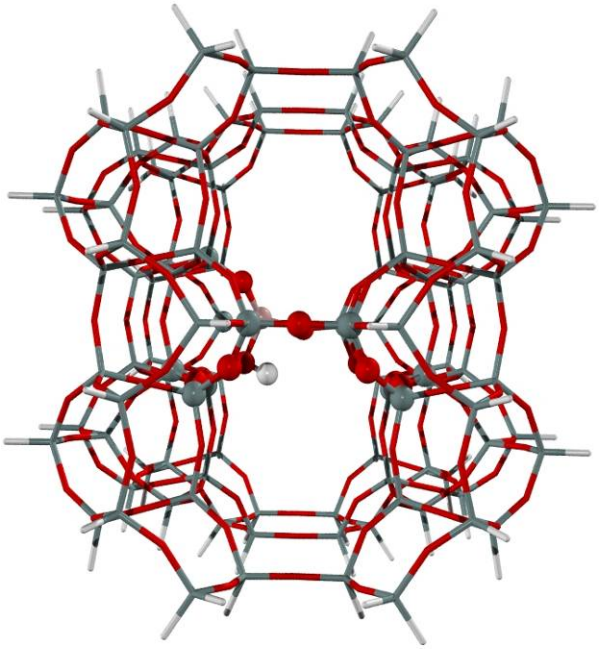

(b)

Figure 8 ONIOM (B3LYP/6-31G(d,p):UFF) optimized structures of 12T/112T H-FER, (a) 10T member ring channel, and (b) 8T member ring channel.(Ball-and-stick and line styles of illustrated atoms represent the quantum chemical and molecular mechanical calculations, respectively.)

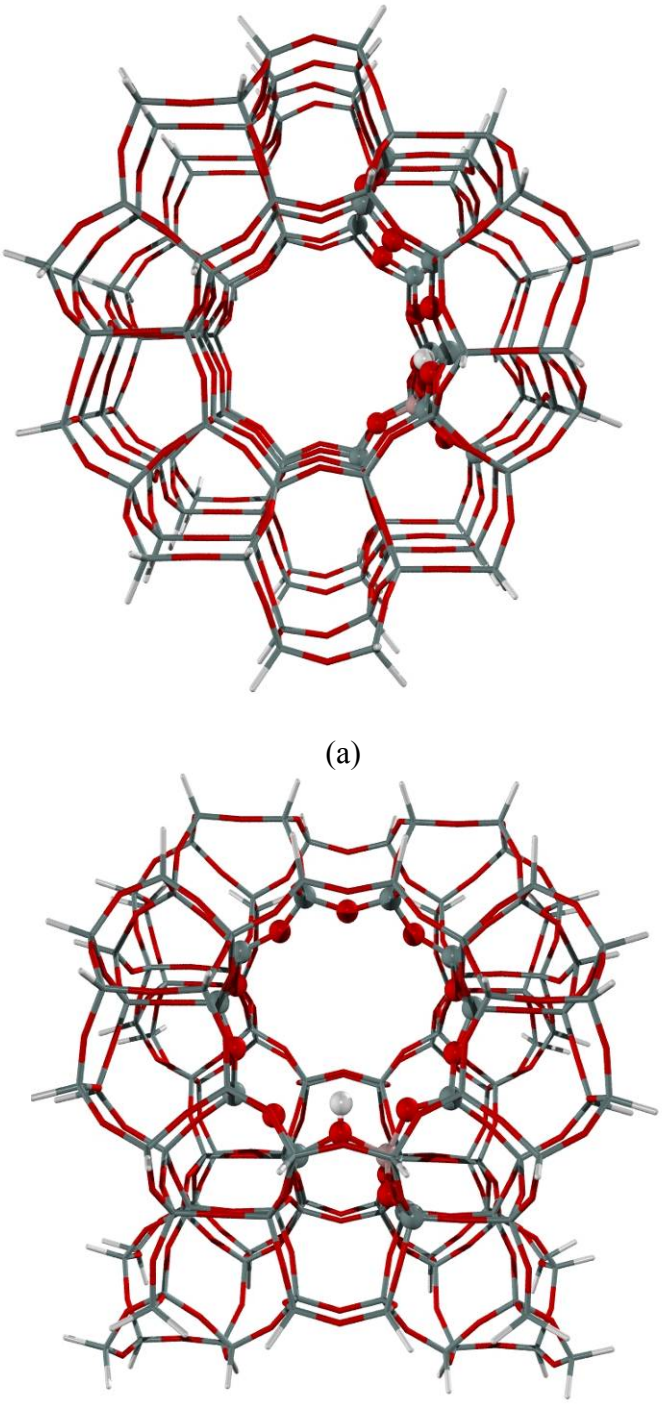

(a)

(b)

Figure 9 ONIOM (B3LYP/6-31G(d,p):UFF) optimized structures of 12T/128T H-ZSM-5, (a) Side view of the 10-membered ring of intersection channel, (b) Front view shows the 10-membered ring window of the straight channel. (Ball-and-stick and line styles of illustrated atoms represent the quantum chemical and molecular mechanical calculations, respectively.)

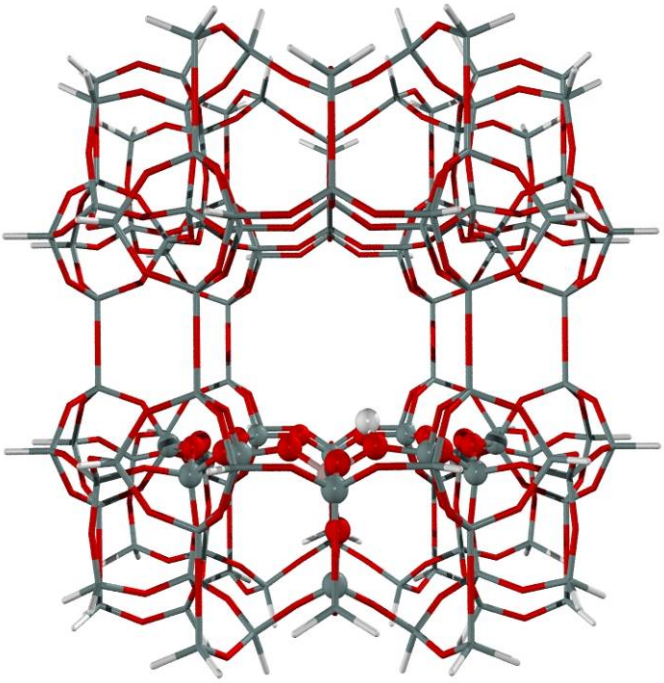

(a)

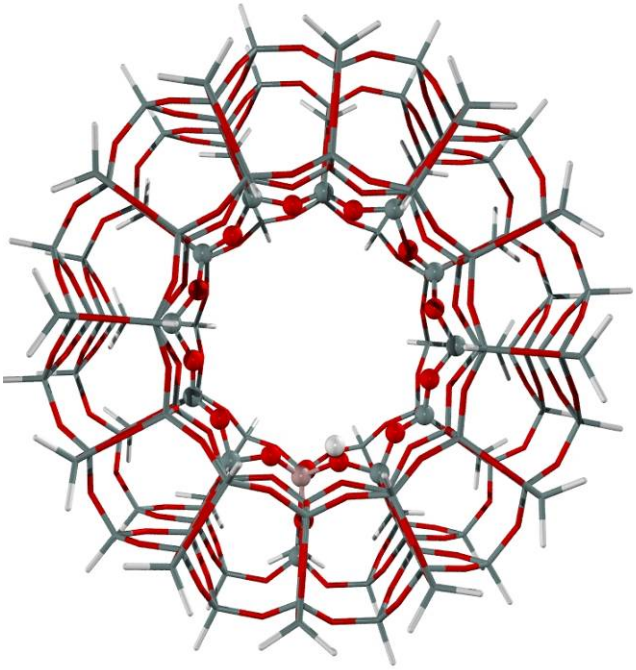

(b)

Figure 10 ONIOM (B3LYP/6-31G(d,p):UFF) optimized structures of 14T/132T H-MCM-22, (a) Side view of the 10-membered ring channel, (b) View shows the 12-membered ring window of supercage. (Ball-and-stick and line styles of illustrated atoms represent the quantum chemical and molecular mechanical calculations, respectively.)

RESULTS AND DISCUSSION

1. Adsorption of Hydrocarbon on Various Zeolites

1.1. Adsorption of light alkanes in H-FAU, and H-MOR zeolites

The adsorptions of light alkanes in H-FAU and H-MOR have been studied with ONIOM models. The models are subdivided into two parts. The inner part (catalytic center) is a fourteen-tetrahedral (14T) quantum cluster representing the active site. The second part is the 120T extended framework modeled by the Universal Force Field to account for the confinement effect of the surrounded zeolitic pore. The H-FAU model consists of a 14T quantum cluster which is the 12-membered-ring window of 7.4 Å in diameter with one substituted aluminum atom and two terminal silyl groups. The attached 120T extended cluster is modeled with the UFF force field to represent the two connecting supercages. The H-MOR 14T quantum cluster covers the 12-membered-ring (MR) window of the straight channel of 6.5 x 7.0 Å. The 120T extended cluster is modeled to cover an ample portion of the straight channel.

The optimized structures of adsorption complexes of alkanes on H-FAU, and H-MOR zeolites are illustrated in Figures 11-12, respectively. Selected geometrical parameters of the complexes and their corresponding adsorption energies are listed in Table 1.

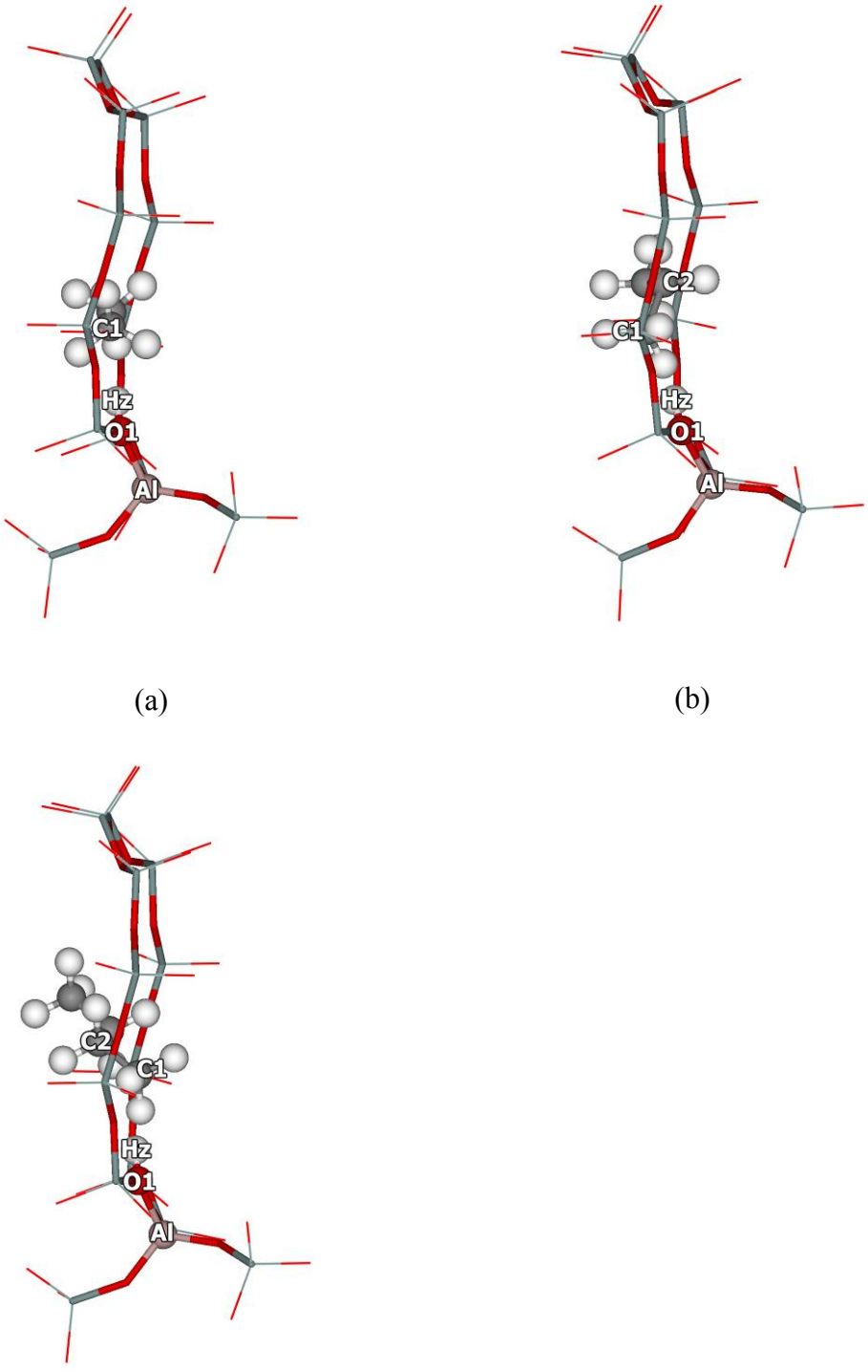

(a) (b)

(c)

Figure 11 The optimized structures of the adsorption complexes of (a) ethane, (b) propane and, (c) n-butane on H-FAU. Atoms on the adsorbed molecules and the Brønsted acid site are drawn as spheres and the extended framework is omitted.

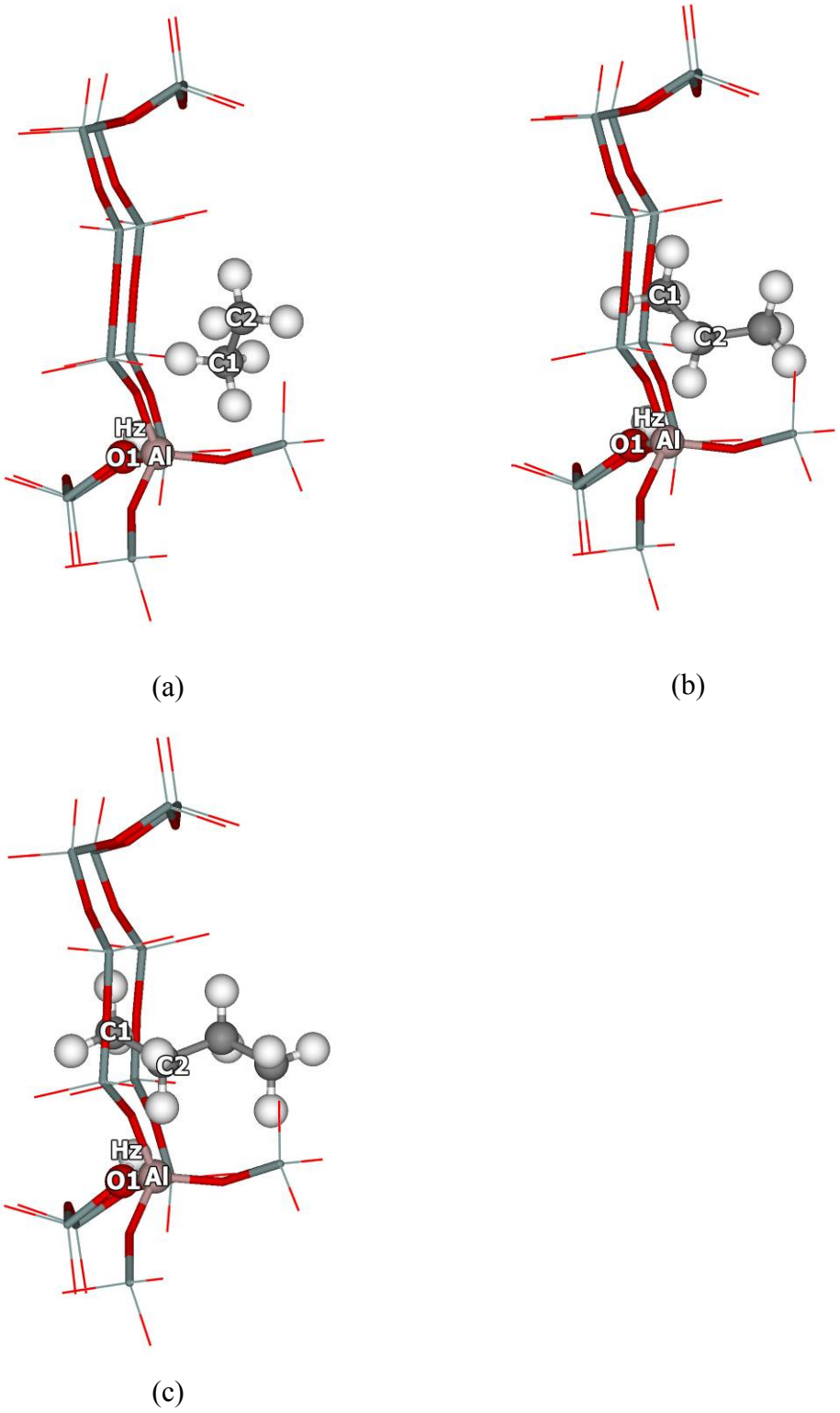

Figure 12 The optimized structures of the adsorption complexes of (a) ethane, (b) propane and, (c) n-butane on H-MOR. Atoms on the adsorbed molecules and the Brønsted acid site are drawn as spheres and the extended framework is omitted.

Table 1 The ONIOM(B3LYP/6-31G(d,p):UFF) optimized geometrical parameters and adsorption energies of ethane, propane and n-butane in H-MOR, and H-FAU

Parameters	H-MOR				H-FAU			
	Isolated	Ethane	Propane	n-Butane	Isolated	Ethane	Propane[(d)]	n-Butane[(d)]
Geometry								
Distance (Å)								
C1-C2[(a)]	1.53	1.53	1.53	1.53	1.53	1.53	1.54(1.53)	1.53(1.53)
C1 - - Hz		2.84	3.56	3.58		2.32	2.33(3.33)	2.37(3.49)
C2 - - Hz		3.68	2.56	2.67		3.57	3.70(2.35)	3.60(2.37)
O1-Hz	0.97	0.97	0.97	0.97	0.97	0.97	0.98(0.98)	0.98(0.98)
Al-O1	1.80	1.80	1.80	1.80	1.95	1.94	1.94(1.94)	1.94(1.94)
Si1-O1	1.68	1.68	1.68	1.68	1.71	1.70	1.70(1.70)	1.70(1.70)
Angle (degree)								
O2-Al-O1	104.8	104.7	104.7	104.6	99.0	99.5	99.6(99.7)	99.5(99.8)
Si1-O1-Al	127.3	127.1	127.2	127.1	129.4	129.5	129.3(129.3)	129.3(129.3)
Energy (kcal/mol)								
B3LYP:UFF		-7.7	-9.8	-12.3		-4.6	-6.2(-5.4)	-7.3(-6.1)
MP2:UFF [(b)]		-8.2	-10.6	-13.5		-4.3	-5.8(-5.5)	-7.1(-6.4)
Experiment [(c)]		-8.0	-9.8	-11.9		-5.1	-6.4	-8.1

[(a)] The C1-C2 distances of ethane, propane and n-butane are 1.53 Å from the B3LYP/6-31G(d,p) calculations.

[(b)] Single point energy calculation at ONIOM(MP2/6-31G(d,p):UFF//B3LYP/6-31G(d,p):UFF) with the BSSE correction

[(c)] From ref. 13-15

[(d)] Two adsorption structures were found. The parameters for the less stable adsorbed structure are in parenthesis.

Table 2 The distribution of adsorption energy of light alkanes and alkenes on H-FAU and H-MOR calculated at embedded ONIOM(MP2/6-31G(d,p):UFF)// ONIOM(B3LYP/6-31G(d,p):UFF) with BSSE correction

	H-FAU			**H-MOR**		
	14T QM[(a)]	120T UFF[(b)]	Total	14T QM[(a)]	120T UFF[(b)]	Total
Ethane	-2.6	-1.7	-4.3	-2.0	-6.2	-8.2
Propane	-3.3	-2.5	-5.8	-3.2	-7.4	-10.6
n-Butane	-3.6	-3.5	-7.1	-3.6	-9.9	-13.5
Ethene	-7.3	-1.7	-9.0	-5.8	-4.2	-10.0
Propene	-8.4	-2.5	-10.9	-6.8	-6.8	-13.5
1-Butene	-8.9	-3.2	-12.1	-7.2	-9.9	-17.1

(a) interaction energy from the 14T quantum cluster calculated at MP2/6-31G (d,p) with the BSSE correction

(b) interaction energy from the 120T extended framework modeled with the UFF

The adsorption of alkanes in the microporous of zeolite occurs via weak interactions between the alkyl group and the Brønsted acid of the zeolite. Since the interactions are weak, there are only minute structural changes of the zeolite framework and the adsorbate upon the adsorption. The acidic OH bond distance is almost the same as in the isolated zeolite. The ethane adsorbs on the Brønsted acid by having an alkyl end of the molecule pointing to the acid site of the faujasite zeolite. The distance between the carbon atom of the adsorbed ethane and the zeolite proton (C1--Hz) is 2.32 Å. The adsorption energy is calculated to be -4.3 kcal/mol which agrees well with the experimentally measured value of -5.1 kcal/mol (Stach *et al.*, 1986). For propane and n-butane, two modes of adsorption are found, one via the terminal methyl (C1) and another via the internal methylene carbon (C2). In faujasite, it is found that the adsorption via the terminal methyl (C1) is slightly more stable with the C1--Hz distances of 2.33 and 2.37 Å for the adsorbed propane and n-butane, respectively. The energy differences between these two configurations are within 1 kcal/mol. The adsorption energies are calculated to be -5.8, and -7.1 kcal/mol, for propane and n-butane adsorption in H-FAU, respectively. The computed adsorption energies are in good agreement with the experimentally measured heats of adsorption of -6.4 and -8.1 kcal/mol for propane and n-butane, respectively (Eder *et al.*, 1997).

In mordenite zeolite, the adsorption energies of these light alkanes are significantly larger since the pore confinement is more pronounced. The channel of H-FAU is 7.4 Å in diameter and, moreover, has two large supercages connected to it. While, the straight channel of H-MOR is elliptical with a dimension of 6.5x7.0 Å. The adsorption energies are calculated to be -8.2, -10.6, and -13.5 kcal/mol, for ethane, propane and n-butane adsorption, respectively. The computed adsorption energies are also in good agreement with the measured heats of adsorption of -8.0, -9.8, -11.9 kcal/mol for ethane, propane and n-butane adsorption in H-MOR, respectively (Eder *et al.*, 1997; Mayorga *et al.*, 1972).

In the ONIOM model, the interaction energies can be broken down to see the contribution of each layer. In this modeling scheme, the inner layer is calculated at the MP2 level of theory to represent the interaction between the adsorbate and the Brønsted acid of the zeolite. The extended framework is modeled at a low level of theory by the UFF force field to represent the van der Waals interactions between the adsorbate and the zeolite pore wall. From the energy distribution (Table 2), one can see that the interaction of these light alkane molecules with the acid site of the zeolite is only a few kcal/mol, indicating that there is no strong interaction between the adsorbed alkanes and the acid site. The differences in the adsorption energies of these zeolites mainly arise from the low level contribution representing pore confinement. The van der Waals interactions contribute about 40% and 70% of the adsorption energies in H-FAU, and, H-MOR, respectively. It can be noticed that the van der Waals interactions increase with the sizes of the adsorbed molecules and have larger values in the smaller pore H-MOR than in the H-FAU. In H-MOR, the van der Waals interaction is clearly more important than the interaction with the acid site.

The computed adsorption energies that are in good agreement with the experimental measurements clearly demonstrate that the ONIOM model used in this work can represent interactions between the adsorbate molecules and the zeolites very well. The combination of the MP2 method at the active region embedded in the extended structure modeled by the UFF methods works well in representing electron correlation, and van der Waals interactions in the zeolite system.

1.2. Adsorption of light alkenes in H-FAU, H-MOR zeolites

The adsorptions of alkenes on H-FAU, and H-MOR zeolites have been studied with ONIOM model. Selected geometrical parameters of the complexes and their corresponding adsorption energies are listed in Table 3. Alkene molecules are found to adsorb on the Brønsted acid of zeolites via the π-electrons of the double bond carbons as the most stable adsorption structure (Spoto *et al.*, 1994). The changes in the structural parameters upon the adsorption are small. However, the changes are in accordance with Gutmann's rules (Gutmann, 1978), i.e., a lengthening of the O-H and C=C bonds and shortening of the Si-O and Al-O bonds. For all zeolites, the acidic O-H bond distance is slightly elongated by 0.01-0.03 Å and the C-C bond distance of ethene is slightly elongated by about 0.01 Å upon adsorption on H-FAU and H-MOR. The π-adsorption complexes of ethene on H-FAU and H-MOR have symmetrical structures with almost equal distances between C1--Hz and C2--Hz.

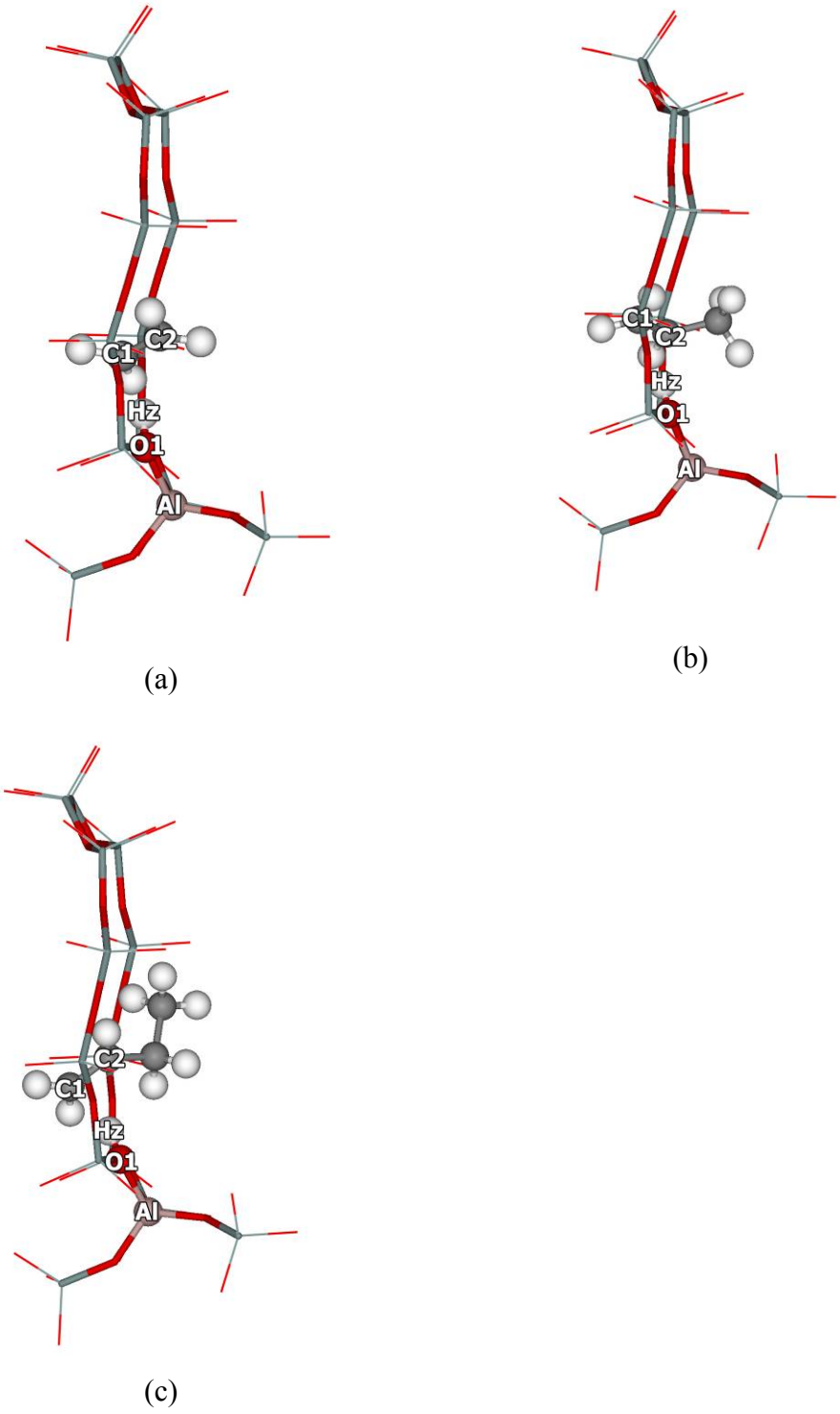

Figure 13 The optimized structures of the adsorption complexes of (a) ethene, (b) propene and, (c) 1-butene on H-FAU. Atoms on the adsorbed molecules and the Brønsted acid site are drawn as spheres and the extended framework is omitted.

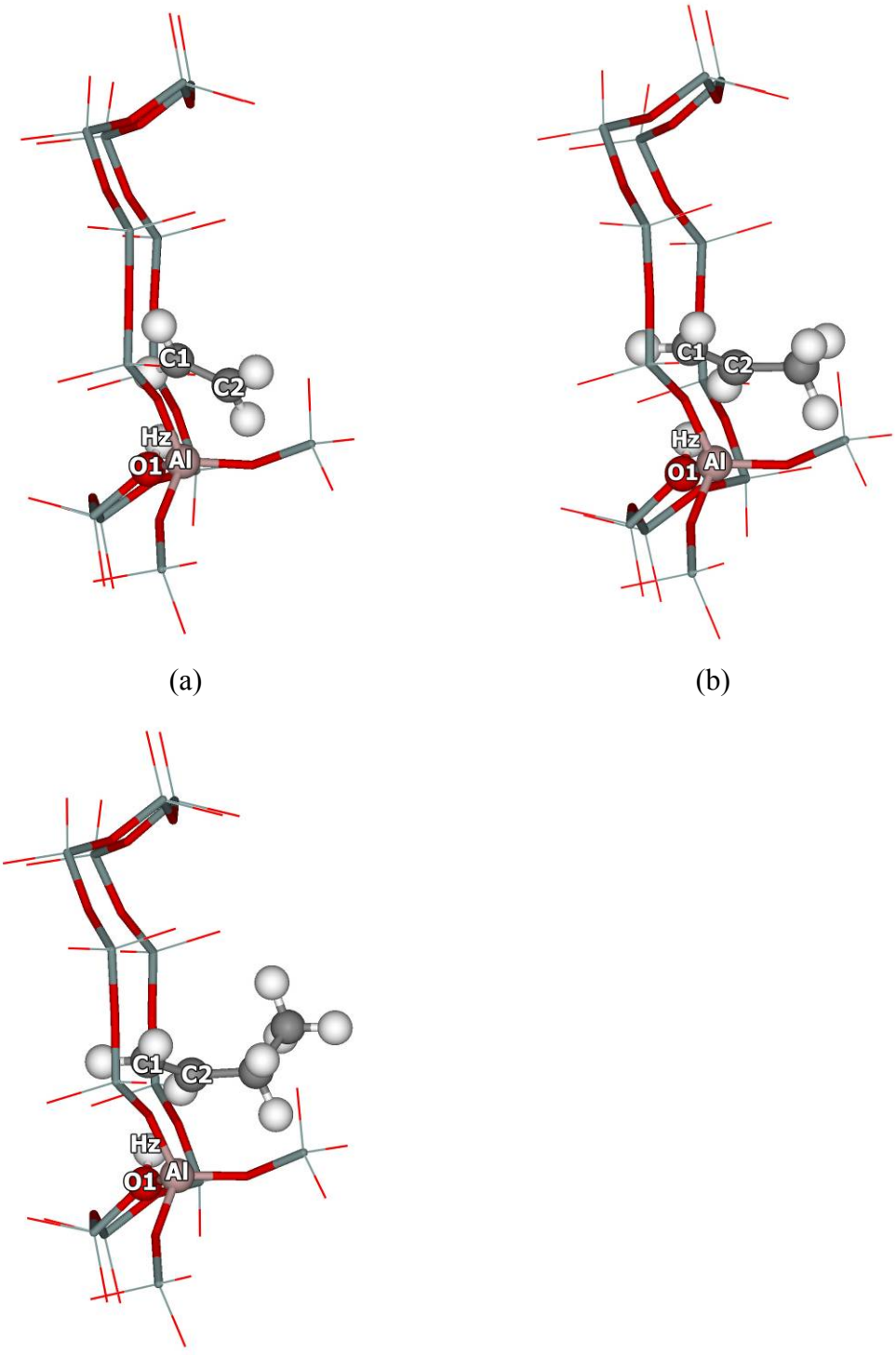

Figure 14 The optimized structures of the adsorption complexes of (a) ethene, (b) propene and, (c) 1-butene on H-MOR. Atoms on the adsorbed molecules and the Brønsted acid site are drawn as spheres and the extended framework is omitted.

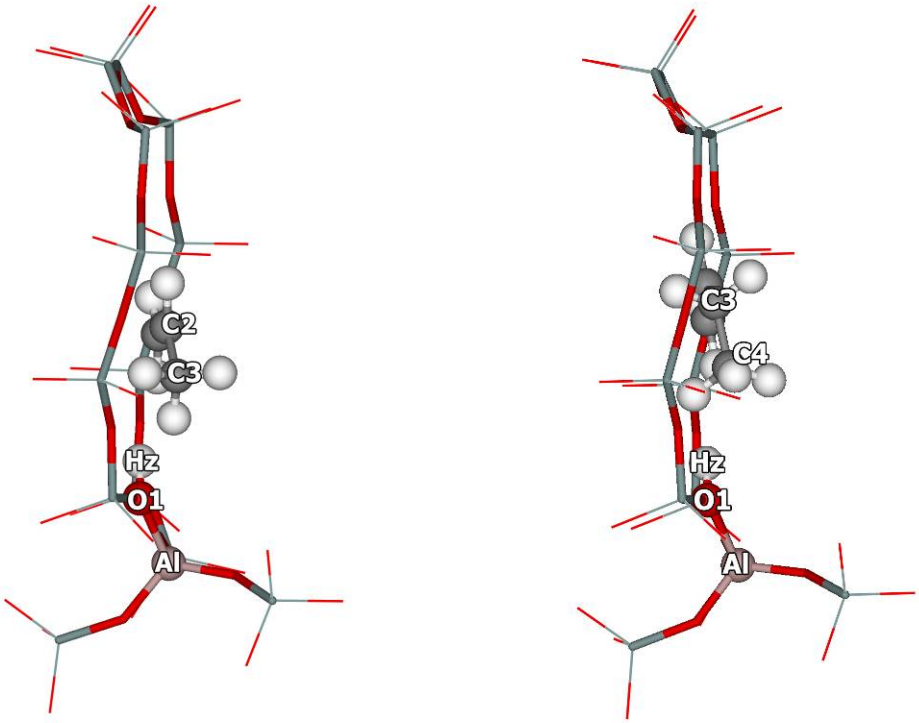

(a) (b)

Figure 15 The optimized structures of the adsorption complexes of (a) propene and, (b) 1-butene on H-FAU via the terminal alkyl group. Atoms on the adsorbed molecules and the Brønsted acid site are drawn as spheres and the extended framework is omitted.

Table 3 The ONIOM(B3LYP/6-31G(d,p):UFF) optimized geometrical parameters and adsorption energies of ethene, propene and 1-butene in H-MOR, and H-FAU

Parameters	H-MOR				H-FAU			
	Isolated	Ethene	Propene	1-Butene	Isolated	Ethene	Propene	1-Butene
Geometry								
Distance (Å)								
C1-C2[(a)]	1.33	1.34	1.34	1.34	1.33	1.34	1.34	1.34
C1 - - Hz		2.22	2.10	2.10		2.16	2.07	2.04
C2 - - Hz		2.23	2.30	2.35		2.17	2.26	2.22
O1-Hz	0.98	0.99	1.00	1.00	0.97	1.00	1.00	1.00
Al-O1	1.80	1.79	1.79	1.79	1.95	1.93	1.93	1.93
Si1-O1	1.68	1.67	1.67	1.67	1.71	1.70	1.70	1.70
Angle (degree)								
O2-Al-O1	104.8	105.1	104.6	104.6	99.0	100.3	100.4	100.2
Si1-O1-Al	127.3	127.3	127.2	127.1	129.4	129.2	128.9	129.3
Energy (kcal/mol)								
B3LYP:UFF		-11.4	-14.5	-17.7		-10.9	-12.3	-13.2
MP2:UFF [(b)]		-10.0	-13.5	-17.1		-9.0	-10.9	-12.1
Experiment		-	-	-		-9.1	-	-

(a) The C1-C2 distance of ethene, propene and 1-butene are 1.33 Å from the B3LYP/6-31G(d,p) calculations.

(b) Single point energy calculation at ONIOM(MP2/6-31G(d,p):UFF//B3LYP/6-31G(d,p):UFF) with the BSSE correction

Table 4 The ONIOM(B3LYP/6-31G(d,p):UFF) optimized geometrical parameters and adsorption energies of propene and 1-butene in H-FAU via the terminal alkyl group

Parameters	H-FAU		
	Isolated	Propene	1-Butene
Geometry			
Distance (Å)			
C1-C2 [(a)]	1.33	1.33	1.33
C - - Hz [(b)]		2.40	2.41
O1-Hz	0.97	0.98	0.98
Al-O1	1.95	1.95	1.95
Si1-O1	1.71	1.70	1.71
Angle (degree)			
O2-Al-O1	99.0	99.7	99.8
Si1-O1-Al	129.4	129.3	129.1
Energy (kcal/mol)			
B3LYP:UFF		-5.7	-6.6
MP2:UFF [(c)]		-5.6	-6.6

(a) The C1-C2 distance of propene and 1-butene are 1.33 Å from the B3LYP/6-31G(d,p) calculations

(b) Distance from the terminal carbon (C3, C4 for propene and 1-butene, respectively) to the Brønsted acid proton

(c) Single point energy calculation at ONIOM(MP2/6-31G(d,p):UFF//B3LYP/6-31G(d,p):UFF) with the BSSE correction

The calculated adsorption energy of ethene on H-FAU is -9.0 kcal/mol which is in excellent agreement with the experimental estimate of −9.1 kcal/mol (Cant *et al.*, 1972). The adsorption energy of ethene on H-MOR is -10.0 kcal/mol. The more exothermic adsorption energy in H-MOR is clearly due to the stronger confinement effect of the smaller pore dimension.

For larger unsaturated hydrocarbons, propene and 1-butene, the hydrogen bond complexes between the π-electrons of the double bond carbons and the acidic proton are not symmetrical. For instance, the C1--Hz and C2--Hz distances are 2.07 and 2.26 Å for propene adsorption on H-FAU. The more steric C2 carbon atom is located farther away from the zeolite framework. The predicted adsorption energies are -10.9, and -12.1 kcal/mol for propene and 1-butene adsorption on H-FAU, respectively and are -13.5, and -17.1 kcal/mol for propene and 1-butene adsorption on H-MOR, respectively. The adsorption energies in H-MOR are larger than in H-FAU by 1.0, 2.6, and 5.0 kcal/mol for the adsorption of ethene, propene, and 1-butene, respectively. These numbers demonstrate that the confinement effect is more pronounced when the size of the adsorbed molecule becomes larger.

A less stable adsorbed configuration was also considered. The optimized geometries of alkyl adsorption complexes of propene and 1-butene on H-FAU are presented in Figure 14 and selected geometrical parameters and adsorption energies are listed in Table 4. In this adsorption configuration, the alkene molecules interact with the Brønsted acid of zeolites via the terminal alkyl group. The adsorption structures are similar to the adsorbed structures of the corresponding alkanes. The adsorption distances (C4--Hz) are 2.40 and 2.41 Å for adsorption of propene, and 1-butene, respectively which are slightly longer than the adsorption distances of propane and butane on H-FAU by 0.07, and 0.04 Å, respectively. The alkyl interactions with the acid site are much weaker than that of the π-adsorption complex. The adsorption energies are calculated to be –5.6, and –6.6 kcal/mol for adsorption of propene, and 1-butene, respectively, which are comparable to those of the corresponding alkane adsorption. Due to the weak alkyl interaction with the Brønsted acid of zeolites, this adsorption configuration will not contribute significantly to the

adsorption energies of alkenes in the zeolites. However, this adsorption configuration may play a role in the diffusion of alkenes through the microporous of zeolite in which the molecules proceed through a series of adsorption and desorption on various sites along the zeolite pore channels (Kondo *et al.*, 2003; Yoda *et al.*, 2005).

The contributions of each layer in the computed ONIOM2 models are listed in Table 2. The π-electrons interactions with the Brønsted acid of the zeolites are stronger than the alkyl interactions. The interaction energies are in the range of 5.8-8.9 kcal/mol which are almost three fold higher than the alkyl interactions. Whereas, the van der Waals interactions are about the same for the adsorption of alkenes and alkanes with the same carbon number. The van der Waals interactions contribute about 20% and 50% of the adsorption energies of the alkenes in H-FAU, and, H-MOR, respectively.

There is no experimental data for adsorption energies of alkenes on proton forms of zeolites which is due to the facile reactions of isomerization and oligomeization of alkenes over acidic zeolites (Kondo *et al.*, 2003; Yoda *et al.*, 2005; Spoto *et al.*, 1994). The only available adsoption energy is for small ethene in H-FAU zeolite. Our predicted value of -9.0 kcal/mol is in excellent agreement with the experimental estimate of −9.1 kcal/mol obtained by Cant and Hall (Cant *et al.*, 1972), indicating that this ONIOM model can accurately compute the π-electron interaction with Brønsted acid of the zeolites. Moreover, the model has demonstrated its accuracy in describing the confinement effect of the zeolites by giving adsorption energies of alkanes that are in good agreement the experimental measurements. Therefore, our predicted adsorption energies of propene and 1-butene should be reasonable estimates. These results suggest that this embedded ONIOM scheme provides a practical method for investigating the adsorption of unsaturated and saturated hydrocarbons on zeolites.

1.3 Adsorption of acetone in H-FER, H-ZSM-5 and H-MCM-22 zeolites

In previous section, the confinement effect of various zeolite structures on adsorbed nonpolar molecules has been studied. In this section, the adsorption and interactions of a polar molecule, acetone, will be described on various zeolites. H-FER, H-ZSM-5 and H-MCM-22 are chosen as representatives of zeolites with different channels. For medium pore zeolites whose acid sites are in a 10-membered ring, such as H-ZSM-5 and H-FER, a 12T quantum cluster is used to model the active sites. A 14T quantum cluster is used to represent the active site of H-MCM-22 in a 12-membered ring. The surrounding frameworks are included into the models by using the ONIOM scheme to cover a sufficient portion of the zeolite cavity i.e. 112T, 128T and 132T for H-FER, H-ZSM-5 and H-MCM-22, respectively.

1.3.1 Structure of various zeolites

H-FER has a two-dimensional pore structure with a main straight channel (10-membered ring, 4.2 x 5.4 Å in diameter) and a smaller channel (8-membered ring, 3.5 x 4.8 Å in diameter) [see fig 16]. These two channels are perpendicular to each others and intersect to form site pockets. FER has four different T-sites. T1 site is located at a six membered ring in the site pocket. T2, T3 and T4 sites are located in the 10T straight channel. T2 and T4 sites are specifically located at the intersection of the 8T site pocket with the main channel. The most favorable site is T2 site which has highest the Al substituted population (Bordiga *et al.*, 2000; Simperler *et al.*, 2004). Hydrogen is added at an oxygen atom next to the substituted Al atom to form the Brønsted acid site. The O-H bond is point into the middle of 8T membered ring making a small angle (30.3^0) with the direction of 10T straight channel.

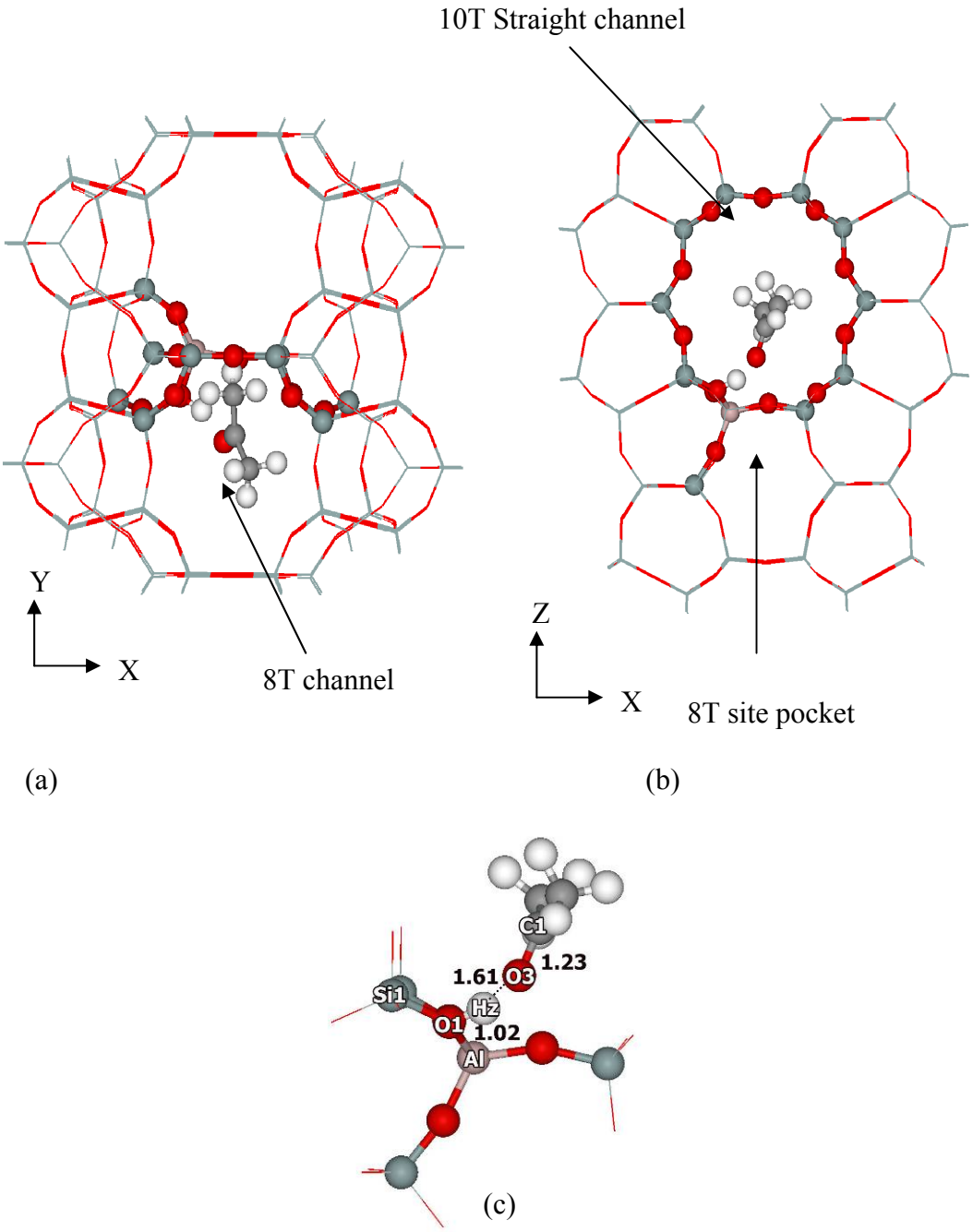

Figure 16 ONIOM (B3LYP/6-31G(d,p):UFF) optimized structures of the acetone adsorption on the 12T/112T model of H-FER: Represent FER zeolite view at the (a) 8T channel and (b) 10T straight channel and (c) focused on the Brønsted acid site. Selected optimized geometric parameters are given in Å. (Ball-and-stick and line styles of illustrated atoms represent the quantum chemical and molecular mechanical calculations, respectively.)

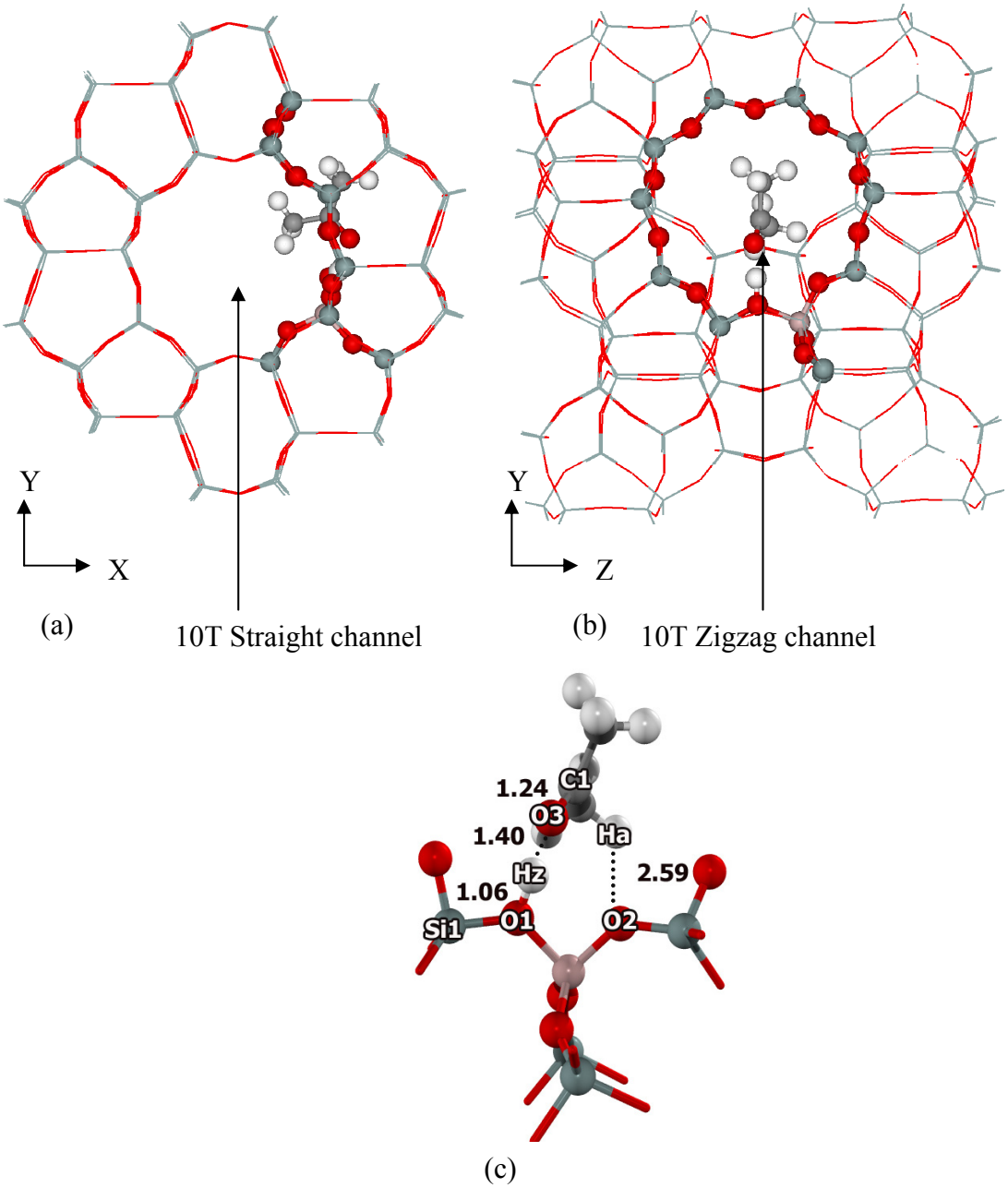

Figure 17 ONIOM (B3LYP/6-31G(d,p):UFF) optimized structures of the acetone adsorption on the 12T/128T model of H-ZSM-5: (a) Represent of ZSM-5 zeolite the view along the (a) straight channel (b) zigzag channel and (c) focused on the Brønsted acid site. Selected optimized geometric parameters are given in Å. (Ball-and-stick and line styles of illustrated atoms represent the quantum chemical and molecular mechanical calculations, respectively.)

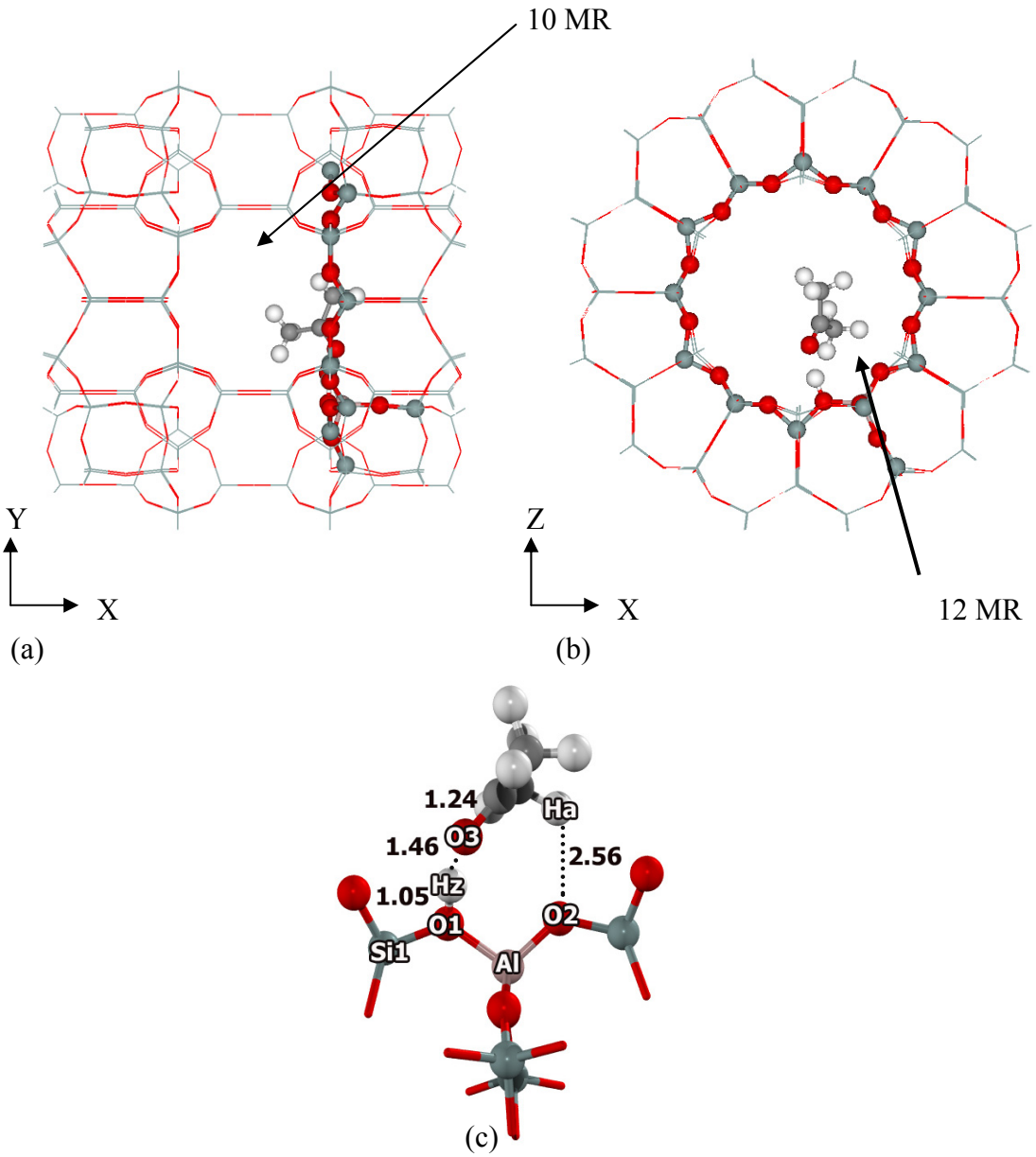

Figure 18 ONIOM (B3LYP/6-31G(d,p):UFF) optimized structures of the acetone adsorption on the 14T/132T model of H-MCM-22: Represent of MCM-22 zeolite the view along the (a) straight channel (b) supercage and (c) focused on the Brønsted acid site. Selected optimized geometric parameters are given in Å. (Ball-and-stick and line styles of illustrated atoms represent the quantum chemical and molecular mechanical calculations, respectively.)

Table 5 Structural parameter for acetone/zeolite cluster complexes in various zeolites

Parameters	H-FER		H-ZSM-5		H-MCM-22	
	Bare	**AD**	**Bare**	**AD**	**Bare**	**AD**
Distance						
Si1-O1	1.67	1.66	1.66	1.64	1.71	1.68
Si2-O2	1.61	1.60	1.58	1.57	1.62	1.61
O1-Al	1.88	1.84	1.79	1.76	1.81	1.78
O2-Al	1.67	1.67	1.66	1.66	1.66	1.67
Al - - Hz	2.25	2.37	2.34	2.42	2.42	2.36
O1-Hz	0.98	1.02	0.97	1.06	0.97	1.05
Hz - - O3		1.61		1.40		1.46
O1 - - O3		2.59		2.46		2.50
O3-C1	1.22	1.23	1.22	1.24	1.22	1.24
C1-C2	1.52	1.51	1.52	1.50	1.52	1.50
C2-Ha	1.09	1.09	1.09	1.10	1.09	1.10
Ha - - O2		2.80		2.59		2.56
O1-O2	2.54	2.58	2.44	2.47	2.73	2.73
C1 - - O1		3.42		3.25		3.35
C1 - - O2		3.91		3.26		3.32
Angle						
Al-O1-Si1	143.7	142.3	128.8	129.9	129.7	126.2
Al-O2-Si2	151.8	155.4	129.5	132.4	125.4	126.9
O1-Hz-O3		158.8		179.1		166.9
O1-Al-O2	91.2	94.5	89.8	92.6	103.5	104.6

Table 6 The adsorption energies of acetone in the confined spaces of H-FER, H-ZSM-5 and H-MCM-22 (kcal/mol) where Quantum means ΔE(model, high), and UFF means ΔE(real, low) - ΔE(model, low)

Zeolite	Methods	Quantum	UFF	Total
H-FER	B3LYP/6-31G(d,p):UFF	-18.1	-7.8	-25.9
H-ZSM-5	B3LYP/6-31G(d,p):UFF	-18.5	-7.8	-26.3
H-MCM-22	B3LYP/6-31G(d,p):UFF	-21.6	-3.5	-25.1

H-MFI is a three-dimensional pore zeolite. The main straight channel (10-membered ring, 5.4 x 5.6 Å in diameter) intersects with the zigzag channel (10-membered ring, 5.1 x 5.4 Å in diameter) [see fig 17]. At the intersection there is a large cavity of about 9 Å. The MFI structure has 12 different T sties. The Al atom is most favorably substituted at T12 (Brand *et al.*, 1993; Simperler *et al.*, 2004). The O-H bond of H-MFI points into the middle of the zigzag channel.

MCM-22 is a three-dimensional pore zeolite. The main straight channel (10 membered ring) has a dimension of 4.0 x 5.5 Å. The main channel opens to the supercage (7.1 x 7.1 x 18.4 Å). In this study, we consider the Brønsted acid site located in the large cavity of the supercage. The Al atom is placed at the T4 position (Zhou *et al.*, 2006; Hongyuan *et al.*, 2007). The acidic O-H points to the middle of the 12T member ring of supercage.

1.3.2 Acetone adsorption structures on various zeolites

The optimized structures of acetone adsorption on three different zeolites are shown in figure 16-18. Selected geometric parameters are presented in table 5. In the H-FER, an acetone molecule adsorbs on the Brønsted acid site at the intersection of the 10T main channel and the 8T site pocket. The acetone molecule resides in the 10T straight channel whose diameter is 4.2 x 5.4 Å. The acetone molecule forms hydrogen bonding between its carbonyl oxygen (O3) and the Brønsted acidic proton (Hz). The Brønsted O1-Hz bond distance is increased slightly from 0.98 Å to 1.02 Å and the ketone C1-O3 double bond is increased slightly from 1.22 Å to 1.23 Å. The O1-Hz-O3 bond angle, used to describe the hydrogen bond, is 158.8 degree which is far from 180 degree. The deviation from linear of the hydrogen bond angle is a result of the poor alignment of the Brønsted acid site which does not directly point to the main channel where the adsorbed acetone molecule is located. The other weak interaction between terminal hydrogen, Ha, of acetone and the adjacent oxygen, O2, in the zeolite framework is also with distance of Ha-O2 to be 2.79 Å. The adsorption energy is calculated to be -25.8 kcal/mol.

In H-ZSM-5 zeolite, an acetone molecule is adsorbed on the Brønsted acid site at the intersection cavity. The acetone molecule forms strong hydrogen bond interaction with the acid site. The Brønsted O1-Hz bond distance is increased significantly from 0.97 Å to 1.06 Å and the carbonyl C1-O3 double bond is slightly increased from 1.22 Å to 1.24 Å. The O1-Hz-O3 bond angle is 174.3 degree closely to linear. The closer to linear angle indicates a stronger hydrogen bond than in the case of H-FER. The adsorption energy is calculated to be -26.3 kcal/mol.

In the largest pore cavity of H-MCM-22, an acetone molecule adsorbs on the Brønsted acid site on the 12T membered ring of the super cage. The O1-Hz bond of Brønsted acid increases from 0.97 Å to 1.05 Å and the carbonyl O3-C1 bond distance increases from 1.22 Å to 1.24 Å. The O1-Hz-O3 bond angle is measured to be 166.9 degree. In addition, it was found that the neighboring oxygen is also interacted with the adsorbed acetone molecule. The O2···Ha bond distance is about 2.56 Å. The adsorption energy is calculated to be -25.1 kcal/mol.

The adsorption energies can be broken down into 2 parts (inner part and outer part) as shown in table 6. The interaction energies from inner part model 12T quantum with B3LYP method are -18.07 and -18.51 kcal/mol for H-FER and H-ZSM-5. For H-MCM-22, the interaction energy is -21.55 kcal/mol with 14T quantum cluster. For the interaction in H-FER and H-ZSM-5, the single point only 5T Brønsted acid site was taken to distinguish the different of adsorption properties. The interaction energies of acetone on 5T Brønsted acid site are -13.83 and -16.67 kcal/mol for H-FER and H-ZSM-5, respectively. The effect from the window 7T member ring of H-FER, which is about 4.24 kcal/mol, is higher than H-ZSM-5, is about 1.84 kcal/mol, because of the small pore of H-FER (4.2 x 5.4 Å). For H-MCM-22, the adsorption energy of acetone on 5T Brønsted acid is 18.14 kcal/mol. Due to the acidic of H-MCM-22 is more than H-ZSM-5 supported from the adsorption energies of pyridine on H-ZSM-5 and H-MCM-22 are 46.7 and 55.0 kcal/mol (Parrillo *et al.*, 1994; Maloni *et al.*, 2001), the adsorption energy of H-MCM-22 on 5T Brønsted acid is higher than H-ZSM-5. The trend for interaction energy inner part 12T quantum cluster (B3LYP) is H-FER ≈ H-ZSM-5 < H-MCM-22. However,

including the framework effect, the results are different. Because of the large pore of H-MCM-22, the interaction energy from the outer part is the lowest. The energies are -7.78, -7.82 and -3.54 kcal/mol for H-FER, H-ZSM-5 and H-MCM-22, respectively. The energies from the framework of H-FER (4.2 x 5.4 Å) and H-ZSM-5 (5.4 x 5.6 Å) are similar due to the framework closes to the probe molecule than H-MCM-22 (7.1 x 7.1 Å). The total calculated adsorption energies are -25.85, -26.33 and -25.09 kcal/mol for H-FER, H-ZSM-5 and H-MCM-22, respectively. When break down the energy, the inner part quantum cluster can treat about 69.9, 70.3 and 85.9 % for H-FER, H-ZSM-5 and H-MCM-22, respectively. The outer part frameworks treat about 30.1, 29.7 and 14.1% for H-FER, H-ZSM-5 and H-MCM-22, respectively. The energy from the framework for the small and medium pore is about 30 % while in the large pore the energy is only 14 %. The framework effect is essential to describe the confinement effect from the different confined spaces of zeolite

For the adsorption energy in the H-ZSM-5 system, the ONIOM method gives -26.33 kcal/mol while the energy is measured to be -31.1 kcal/mol from the experiment (Sepa *et al.*, 1996). Previous work, the small quantum gave the adsorption energies in the range 10-20 kcal/mol (Florian et al, 1994; Sepa *et al.*, 1996; Kassab *et al.*, 1999). From our calculation, the adsorption energy of acetone on Brønsted acid 5T quantum of H-ZSM-5 is only -16.67 kcal/mol. With the 10T member window, the adsorption energy is -18.51 kcal/mol. These two adsorption energy is lower than experiment due to the lack of framework effect. Only ONIOM calculation gives the adsorption energy agrees well with experiment data. However the B3LYP does not include the dispersion force, the adsorption energy of acetone on H-ZSM-5 is slightly lower than experiment about 4.8 kcal/mol. To improve the adsorption energy, the calculation with MP2 method at high basis set level will give the energy correct but it takes large computational cost.

2. Interaction of Amino Acids with H-ZSM-5 Zeolite

2.1 Structures of glycine adsorption complexes

Since amino acids contain both basic amino and acidic carboxyl groups, the net charge of the molecule is pH dependent. At low pH, the amino group is protonated and the molecule carries a positive charge, at high pH, the carboxylic group is dissociated and the molecule has a negative charge. At pH equal to the isoelectric point, the amino acid presents in the zwitterion form where the molecule contains a protonated amino cation and a carboxylate anion but the net charge of the molecule is zero. Glycine has an isoelectric point of 5.97. In a near neutral solution, glycine predominantly presents as zwitterions. Therefore, in this study, we consider adsorption of glycine in both neutral and zwitterion forms in ZSM-5 zeolite.

Figure 19 illustrates the optimized structures of glycine adsorbed via, (a,b) the amino group, (c) the carboxylic group and (d) the hydroxyl of carboxylic group on H-ZSM-5 and the selected geometry parameters are presented in Table 7. The interaction energies and the adsorption energies are calculated relative to the gaseous amino acid and bare zeolite cluster with the single point energy correction at the ONIOM (MP2/6-31G (d, p): UFF) and the counterpoise BSSE corrections (Table 8). Glycine is adsorbed in its most stable conformation via the interactions of its amino group with the zeolite Brønsted acid (Figures 19a and 19b). Upon adsorption, the amino group is protonated as indicated by the break of the acidic O1-Hz bond and the formation of the N-Hz bond (1.05 Å). The N-Hz bond and the other two N-H bonds have virtually equal distances, which indicate the complete proton transfer of the Brønsted acid of the zeolite to the adsorbed glycine. The adsorption complex is in a form of ion-pair adduct. Figures 19a and 19b illustrate that both the amino and the carboxylic groups of glycine are interacting with the zeolite. Two hetero-hydrogen bonds (N-H---O) between the amino group and the zeolite framework and one homo-hydrogen bond (O-H---O) between the carboxylic group and the zeolite framework are formed. The N-Hz---O1 and N-H4---O2 hydrogen bond distances are computed to be 2.74 and 2.69 Å, respectively and the O4-H1---O5 hydrogen bond distance is 2.61

Å. The hydroxyl (O4-H1) of carboxylic group of glycine is lengthened from 0.97 to 1.01 Å. The adsorption energy of this is calculated to be -31.3 kcal/mol.

The second conformation of the adsorbed glycine is the complex where the glycine carboxylic group interacts with the zeolite Brønsted acid (Fig. 19c). The adsorption complex forms a cyclic double hydrogen bonded structure where the carbonyl oxygen of the carboxylic group interacts with the Brønsted acid of the zeolite and the hydroxyl group of the carboxylic group interacts with the nearby oxygen framework. Two homo-hydrogen bonds are formed: The carbonyl C=O acts as a hydrogen bond acceptor and the zeolite Brønsted acid is a hydrogen bond donor. The zeolite Brønsted O1-Hz is lengthened by 0.08 Å and the carbonyl C=O double bond is lengthened by 0.03 Å. The corresponding hydrogen bond distance is 2.50 Å (O1-Hz---O3). In another hydrogen bond, the O4-H1 hydroxyl acts as a hydrogen bond donor and the zeolite oxygen framework is an acceptor. The acidic hydroxyl group of glycine, O4-H1, is lengthened by 0.03 Å. The corresponding hydrogen bond distance is 2.76 Å (O4-H1---O2). The overall adsorption energy of this adsorbed conformation is -25.4 kcal/mol.

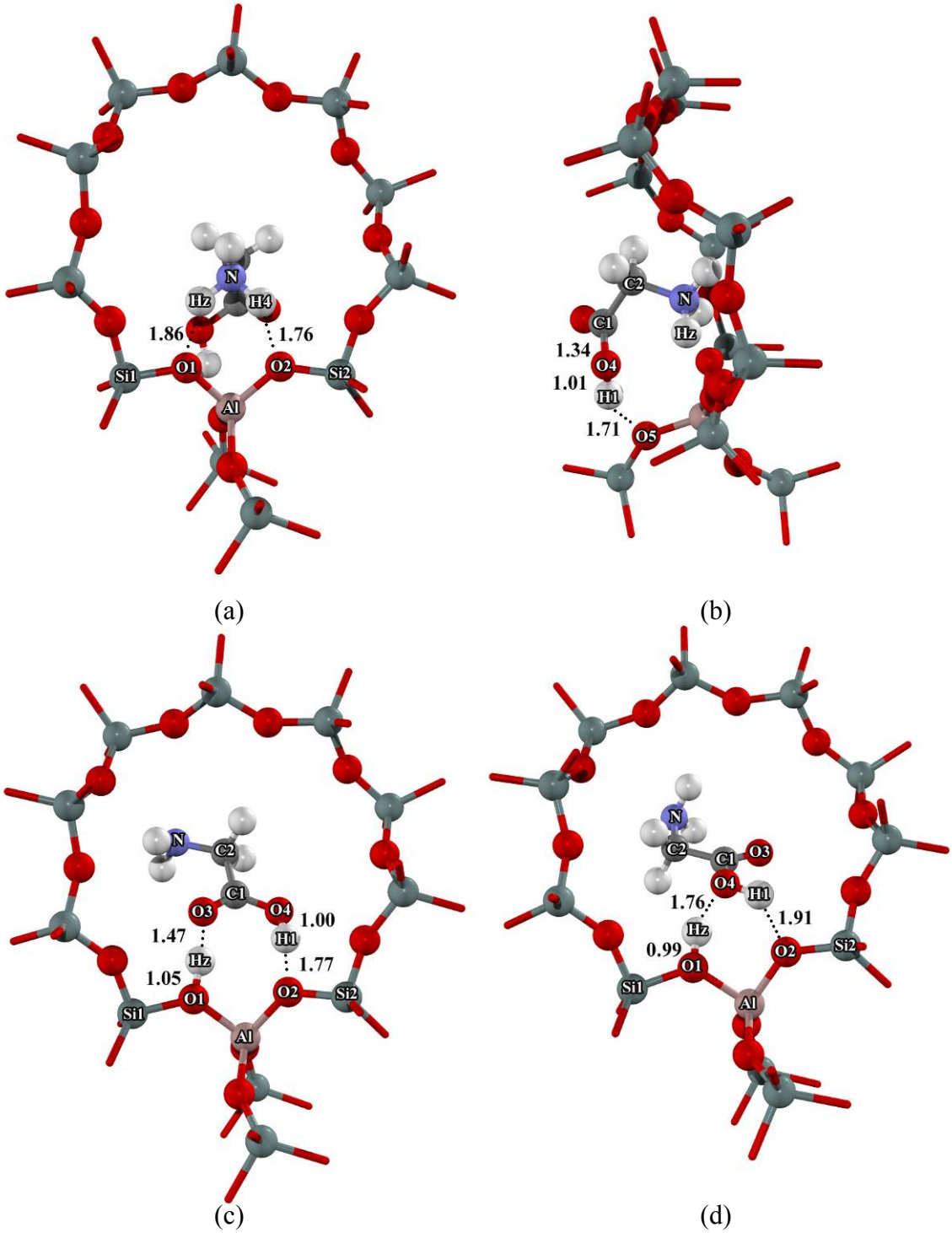

Figure 19 Glycine adsorb on H-ZSM-5 with (a,b) amino group, (c) carboxylic group and (d) hydroxyl of carboxylic group. (Distances in Å)

The glycine molecule can also adsorb via interactions of its hydroxyl (-OH) of the carboxylic group and the zeolite acid site (Fig. 19d). The adsorption complex consists of two hydrogen bonds. The hydrogen bond distances are 2.70 Å (O1-Hz---O4) and 2.67 (O4-H1---O2). The acidic proton of zeolite, O1-Hz, is slightly elongated by about 0.02 Å. The rather long hydrogen bond distance and the small increase of the Brønsted O1-Hz bond distance indicate that the interaction of the Brønsted acid of zeolite with the glycine hydroxyl group is not as strong as the interaction with the glycine carbonyl oxygen. The adsorption energy of this complex is calculated to be -20.7 kcal/mol.

The adsorption of the glycine zwitterion on the acid site of zeolite is also considered as one of the possible adsorption structures. However, when the glycine zwitterion interacts with the zeolite acid site, it is readily protonated. The optimized structure of the adsorbed zwitterion on the Brønsted acid of zeolite could not be found. On the other hand, the glycine zwitterion is found to be stably adsorbed on Na-ZSM-5. Similarly, Krohn and Tsapatsis (Krohn *et al.*, 2005) have reported the adsorption of phenylalanine on beta zeolite where the ion-pair adsorption complex (between the protonated phenylalanine and the anionic zeolite) was observed as a major adsorption species up to a pH of approximately 8.5-9. At pH>9 where the cationic phenylalanine was not present, the adsorption was primarily in a form of zwitterion.

The optimized structure of the adsorption complex of the glycine zwitterion on Na-ZSM-5 is shown in the Fig 20. The adsorbed glycine zwitterion has its carboxylate anion interacting with the sodium cation and its cationic amino group interacting with the oxygen atom on the zeolite framework. The distance between the carboxylate oxygen (O3) and the sodium cation is 2.17 Å. The cationic amino group forms a hydrogen bond with the oxygen atom (O5) on the framework (N-H4--O5= 2.81 Å). The adsorption energy is calculated to be -24.8 kcal/mol. It is noted that in this study all computed adsorption energies are relative to the gaseous neutral amino acid. Since, the glycine zwitterion is not stable in the gas phase (no minimum on the potential surface) (Jensen *et al.,* 1995).

The presence of solvent molecules is essential in stabilizing the zwitterions. In aqueous solution, the glycine zwitterion solvated by water molecules is more stable than the solvated neutral form by 7-9 kcal/mol (Aikens *et al.*, 2006). The theoretical calculation of glycine adsorption on hydroxyl groups at the silica surface also reported that adsorbed zwitterions were found at the high loading condition where adsorbed glycine molecules can interact with each other and, thus, intrastrand hydrogen bond cooperatively stabilized the zwitterions (Rimola *et al.*, 2006), whereas adsorbed zwitterions were not found at the low loading condition on isolated hydroxyl groups. In this work, cooperative interactions with the sodium cation and the anionic zeolite framework can stabilize the glycine zwitterion on Na-ZSM-5. This finding suggests that the zeolite framework has an important role as a "solid solvent molecule."

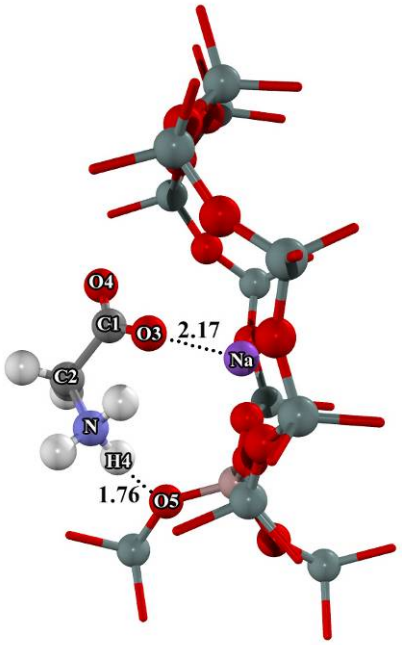

Figure 20 The zwitterion of glycine adsorb on Na-ZSM-5. (Distances in Å)

Table 7 The bond distance parameter of glycine/ ZSM-5 Zeolite, (Å)

	H-ZSM-5				Na- ZSM-5	
	BARE	**amino group**	**carboxylic group**	**hydroxyl group**	**BARE**	**zwitterion**
Al-O1	1.79	1.69	1.76	1.78	1.70	1.69
Al-O2	1.66	1.70	1.68	1.67	1.71	1.69
O1-Hz	0.97	1.86	1.05	0.99		
O1-O3			2.50			3.59
O1-Na					2.16	2.31
O2-Na					2.20	2.30
Na-O3						2.17
O3-C1	1.21	1.21	1.24	1.21	1.21	1.29
C1-O4	1.35	1.34	1.31	1.37	1.35	1.22
C1-C2	1.52	1.53	1.52	1.52	1.52	1.57
C2-N	1.45	1.50	1.45	1.45	1.45	1.50
N-H4	1.02	1.05	1.02	1.02	1.02	1.05
N-H5	1.02	1.02	1.02	1.02	1.02	1.02
H1-O4	0.97	1.01	1.00	0.99		
N-H1						1.06
O2-H4		1.76				
O2-H1			1.77	1.91		
Hz-O3			1.47			
Hz-O4				1.76		
Hz-N		1.05				
O5-H1		1.71				
O5-O4		2.61				
O5-H4						1.76
Hydrogen Bond Distance						
N-Hz - - O1		2.74				
N-H4 - - O2		2.69				
O4-H1 - - O5		2.61				
O1-Hz - - O3			2.50			
O2-H1 - - O4			2.76	2.67		
O1-Hz - - O4				2.70		
N-H4 - - O5						2.81

Table 8 The adsorption energies, ΔEads, of glycine/zeolite complexes, (kcal/mol)

	H-ZSM-5			Na-ZSM-5
	Amino group	**Carboxylic group**	**Hydroxyl group**	**Zwitterion**
Quantum (MP2+BSSE)	-23.7	-17.8	-13.4	-15.4
UFF	-5.6	-6.7	-7.0	-9.4
Lattice Charge	-2.0	-0.9	-0.3	-0.046
ΔE_{ads}	**-31.3**	**-25.4**	**-20.7**	**-24.8**

2.2 Energetics of glycine adsorption complexes

The adsorption energies of the four adsorption structures of glycine considered in this study are summarized in Table 8. The adsorption energy obtained from the ONIOM calculations can be partitioned into: (i) the interaction energy of the adsorbate and the zeolite acid site at the quantum region (MP2+BSSE), (ii) the van der Waals interaction energy between the adsorbate and the extended framework of the zeolite which is modeled by the UFF force field, and (iii) the long-range electrostatic interaction of the infinite lattice which is modeled by a set of optimized charges.

In all cases, the interaction with the zeolite acid site at the quantum region is the biggest contribution to the overall adsorption energy, especially, in the ion-pair complex of the protonated glycine cation and the anionic zeolite cluster, this interaction amounted to 23.7 kcal/mol of the total adsorption energy of 31.3 kcal/mol (76% contribution). The influence of the confinement of the zeolite pore ranges from 5.6 to 9.4 kcal/mol, accounting for 18-38% of the overall adsorption energies, depending on the mode of interactions. The contribution from the long-range electrostatic interaction with the infinite lattice accounts for less than 10% of the overall interactions. This relatively low interaction arises from the optimized point

charges including only the lattice points which are rather far away from the adsorption site while the electrostatic interactions of the lattice points near the adsorption site are already included in the quantum region. Nonetheless, the long-range electrostatic interaction contributes some non-negligible interaction (-2.0 kcal/mol) to the ion-pair adsorption complex where the adsorbed molecule contains a net positive charge.

2.3 Adsorption of L-Alanine on H-ZSM-5

Adsorption of a larger amino acid, L-alanine, is also considered to ascertain the effect of confinement of the zeolite pores. It is generally expected that with the increased size of adsorbates the confinement effect should be more pronounced. L-alanine is an amino acid that has a similar structure to glycine but with a methyl substituent and has an isoelectric point close to that of glycine. The three optimized structures of adsorbed L-alanine on H-ZSM-5 zeolite are shown in Figure 21 and interaction energies and adsorption energies are tabulated in Table9. Geometries of the three adsorption complexes of L-alanine are similar to their corresponding glycine adsorption. The same trend of the relative stability of adsorption complexes is also observed. The ion-pair complex of protonated L-alanine and the anionic zeolite has the highest adsorption energy of -34.8 kcal/mol. The adsorption complexes via the carbonyl and the hydroxyl groups have the adsorption energies of -30.0 and -23.9 kcal/mol, respectively.

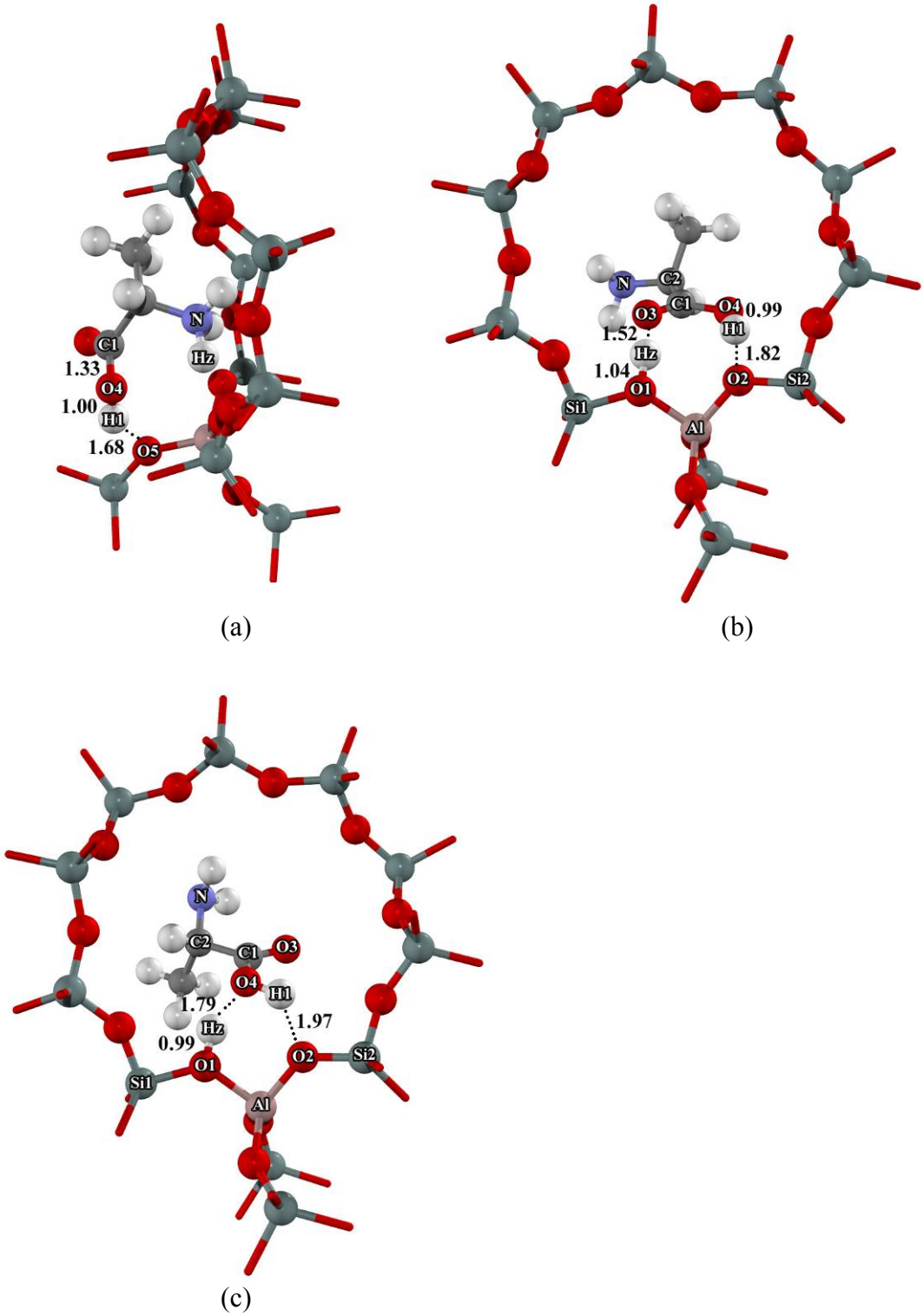

Figure 21 L-alanine adsorb on H-ZSM-5 with (a) amino group, (b) carboxylic group and (c) hydroxyl of carboxylic group. (Distances in Å)

Table 9 The adsorption energies, ΔEads, of L-alanine/zeolite complexes, (kcal/mol)

	H-ZSM-5		
	Amino group	**carboxylic group**	**hydroxyl group**
Quantum (MP2+BSSE)	-24.1	-15.8	-11.2
UFF	-8.5	-13.9	-12.4
Lattice Charge	-2.2	-0.3	-0.3
ΔE_{ads}	**-34.8**	**-30.0**	**-23.9**

The adsorption energies of L-alanine are significantly higher than those of glycine. The increased adsorption energy is mainly due to the increase of the van der Waals interactions between the pore walls and the adsorbed molecules. For the adsorption of protonated L-alanine, the interaction energy derived from the quantum region is slightly more than that of the protonated glycine adsorption. The increase in the ion-pair interaction is reflected in the slightly shorter intermolecular distances. The hydrogen bond, N-Hz--O1, is 2.69 Å and the O4-H1--O5 is 2.59 Å, which are shorter than N-Hz--O1 distance of 2.74 Å and O4-H1--O5 distance of 2.69 Å in the adsorption complex of glycine. However, the N-H4--O2 hydrogen bond distance of 2.80 Å is slightly longer than the corresponding distance of 2.69 in the adsorption complex of glycine. While the interaction energy in the quantum region is increased by only 0.4 kcal/mol, the van der Waals interaction is increased by 2.9 kcal/mol or from -5.6 to -8.5 kcal/mol as the molecular sizes of the adsorbates increase from glycine to L-alanine. The van der Waals interaction contributes about one third of the overall adsorption energy of this ion-pair interaction.

For the other two adsorption complexes via hydrogen bonds, the interactions in the quantum region decrease as the molecular sizes increase. For the adsorption of L-alanine via the carboxylic group, the interaction energy with the zeolite acid site is -15.8 kcal/mol, which is less than the value of -17.8 and that for the glycine adsorption. Similarly, for adsorption of L-alanine via the hydroxyl group, the MP2 interaction energy is -11.2 kcal/mol, which is less than the value of -13.4 kcal/mol for the glycine adsorption. The lower interactions result in the longer intermolecular

distances and the less perturbance of the O-H Brønsted acid bond distance. The distance between the carbonyl oxygen atom and the Brønsted proton (O3-Hz) is longer in the adsorption of L-alanine (1.52 vs. 1.47 Å), while, the O-H Brønsted acid bond distance is shorter in the adsorption of L-alanine (1.04 vs. 1.05 Å). Similarly, for the adsorption via the hydroxylic group, the O4-Hz distances are 1.79 and 1.76 Å and the O-H Brønsted acid bond distances are 0.99 and 0.99 Å for adsorption of L-alanine and glycine, respectively. The decreased interaction in the quantum region is compensated by the increase of the van der Waals interactions by nearly twofold, from -6.7 to -13.9 kcal/mol and from -7.0 to -12.4 kcal/mol for the adsorption via the carboxylic group and the hydroxyl group of glycine and L-alanine, respectively. These results are attributed to the confinement effect of zeolite as proposed by Derouane that the adsorbed molecules in zeolites tend to optimize their van tder Waals interactions with the zeolite walls. The bulkier L-alanine has its adsorption complexes that optimize for the van der Waals interactions with the zeolite pore walls at the expense of decreasing the hydrogen bonding interactions. For the two hydrogen bonded complexes (via the carboxylic group and the hydroxyl group) of L-alanine, the van der Waals interactions account for about half of the overall adsorption energy.

3. Tautomerization of Acetone on Various Zeolites

To understand the confinement effect on the reaction, the tautomerization reaction of acetone has been studied on various zeolites by using the ONIOM method. The tautomerization of acetone in uncatalyzed systems and zeolite-catalyzed systems have been studied. Effects of three different zeolites (H-FER, H-ZSM-5 and H-MCM-22) pore structures and local Brønsted acid structure will be discussed.

3.1 Tautomerization of Acetone on Uncatalyzed Systems

For gas phase uncatalyzed system, the tautomerization of acetone is considered to occur via the concerted mechanism similar to the reports in literature of acetone tautomerization (Cucinotta *et al.*, 2006; Zakharov *et al.*, 2008). Figure 21 shows the potential energy diagram and the geometries of the acetone, the transition state, and the reaction product. The transition state shows that the reaction involves the C2-H1 bond breaking and the O1-H1 bond forming. The structure is confirmed with the normal mode analysis. The vibration mode of the corresponding imaginary frequency at -2147.5 cm^{-1} shows the proton movement from the methyl carbon (C1) to the oxygen atom of carbonyl group. The C2-H1 bond distance increases from 1.09 to 1.50 Å. The double bond C1-O1 increases from 1.22 to 1.29 Å while the single bond C1-C2 decreases from 1.52 to 1.42 Å. The O1-C1-C2 angle is changed from 121.7 to 108.7 degree. The reaction proceeds through a high activation barrier of 68.4 kcal/mol similar to previous work (Lee *et al.*, 1997; Cucinotta *et al.*, 2006; Zakharov *et al.*, 2008). The product is enol form of acetone. The C1-O1 is changed from double bond to single bond with distance 1.37 Å and the C1-C2 is changed from single bond to double bond with distance 1.34 Å. The forming O1-H1 bond is 0.97 Å. The reaction is endothermic by 14.2 kcal/mol. This value agrees well with the differential in heat of formation of keto form and enol from of acetone (13.9 kcal/mol) (Homles *et al.*, 1982).

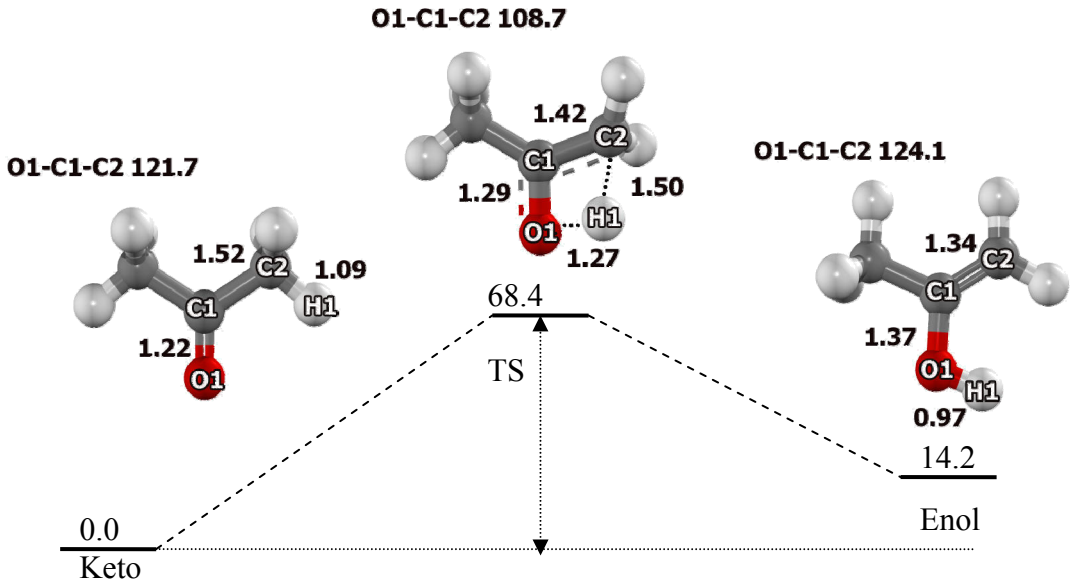

Figure 21 Molecular structures and energy profile of the tautomerization of acetone in uncatalyzed gas phase environment calculated with B3LYP/6-31G(d,p) level of theory. Distances and energies are given in Å and kcal/mol.

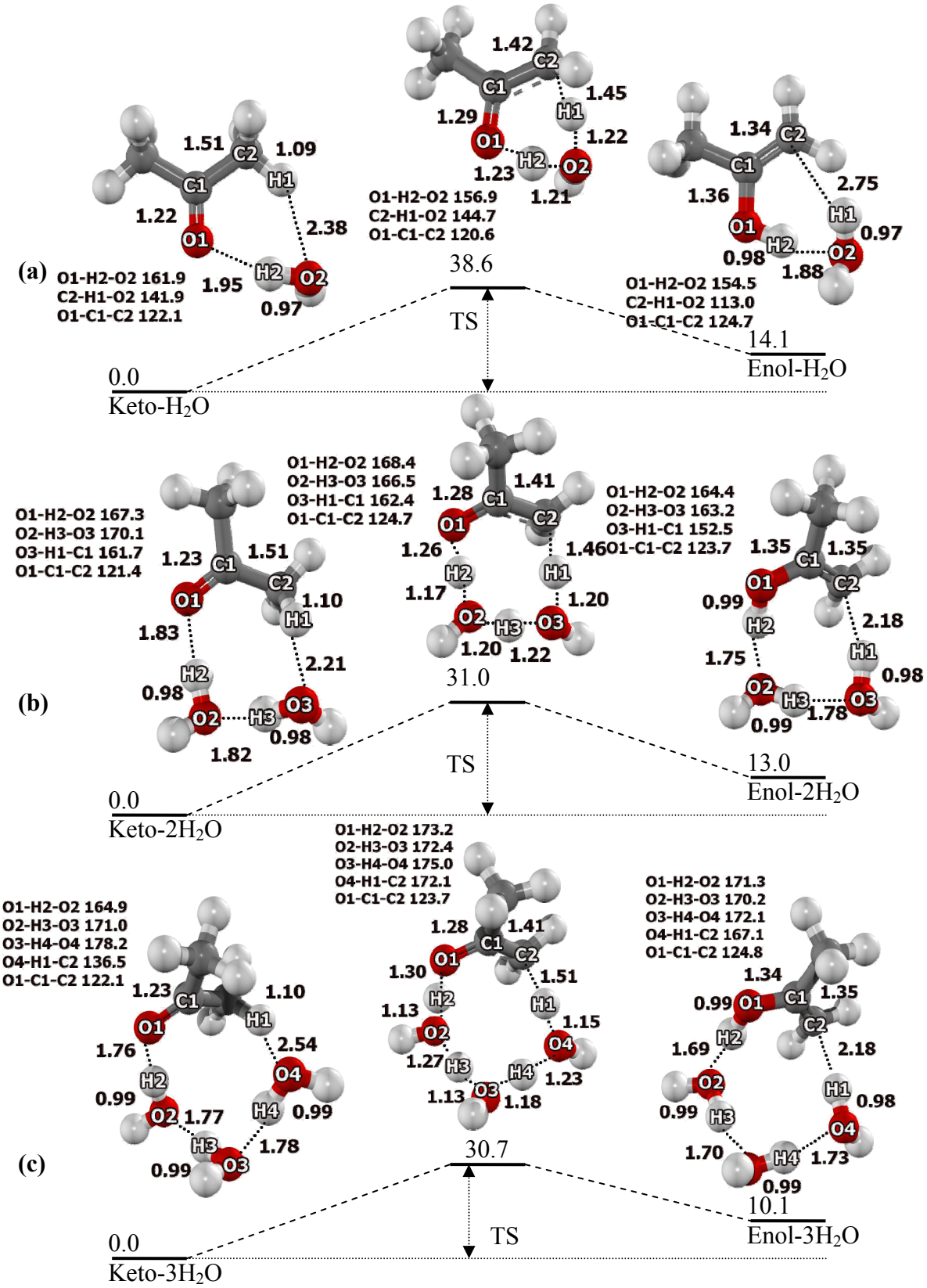

Figure 22 Calculated with B3LYP/6-31G(d,p) level of theory, energy profile (energies in kcal/mol) of the tautomerization of acetone in water-assisted models (a) with one, (b) two and (c) three water molecules.

In solvent-assisted systems, the solvent molecule reduces the energy barrier by providing the hydrogen bonding network (Lee *et al.*, 1997; Cucinotta *et al.*, 2006; Zakharov *et al.*, 2008). With the addition of a water molecule to the system, the acetone interacts with the water molecule via 2 hydrogen bonds: O1-H2-O2 and C2-H1-O2 bond (Fig 22a). The O1-H2 hydrogen bond distance is about 1.95 Å and the H1-O2 hydrogen bond distance is about 2.38 Å. Two protons are transferred through hydrogen bonding, the proton of water molecule (H2) moves to carbonyl oxygen atom of acetone molecule while the proton of methyl group of acetone (H1) moves to the oxygen atom of the water molecule. The transition state is confirmed with the imaginary frequency at -1631.4 cm^{-1} which corresponds to the breaking of two intramolecular bonds of the O2-H2 and the C2-H1 and forming of two intermolecular bonds of the H1···O2 and the H2···O1. The O1-C1-C2 bond angle is changed from 122.1 to 120.6 degree. The hydrated enol is a product of this reaction. This transformation is the proton exchange between acetone and water which leads to the enol formation.

The activation energy of this reaction is found to be 38.6 kcal/mol. As the proton transfer is facilitated with the water molecule, the barrier is much smaller than the barrier in the gas phase uncatalyzed-system (68.4 kcal/mol). The reaction is calculated to be 14.1 kcal/mol endothermic. The activation energy with water molecule decreases from the gas phase about 29.8 kcal/mol. The decreasing of activation energy because the water molecule relaxes the transition state structure evidence from the O1-C1-C2 bond angle.

Effects on the activation barrier with more than one water molecule have been studied; the number of assisting water molecules is scaled up to 2 and 3 molecules. The reactant, transition state and product of acetone in 2 and 3 water molecules are shown in figures 22b and 22c. The proton transfer proceeds through the hydrogen bond network. Comparing to the gas phase uncatalyzed and the one water molecule assistant models, the activation energies of keto-enol isomerization associated with two and three water molecules are further reduced to 31.0 and 30.7 kcal/mol, respectively. It is evidenced that the transition structure of acetone in 2 or 3 water

molecules give the O1-C1-C2 bond angle similar (123.7 degree) and in between the angle of reactant and their product. Another thing is the angle of hydrogen bond transfer (O - - H - - O) are closely to liner when the water molecule assistant more than one. These factors stabilize transition structure and reduce the activation barrier to be about 31 kcal/mol.

3.2 Tautomerization of acetone on H-FER, H-ZSM-5 and H-MCM-22

The tautomerization reactions of acetone have been studied on H-FER, H-ZSM-5 and H-MCM-22 zeolite. The tautomerization reaction of acetone on the Brønsted acid site of zeolite gives the enol product that is adsorbed on the acid site. Due to the tautomerization reaction is an important step before aldol condensation reaction, studying the effect of zeolite framework on this reaction is important to understand the effect of zeolite framework on mechanism. An acetone molecule is first adsorbed on the active site of H-zeolite with a strong hydrogen bonding as discuss in previous section. The reaction mechanism is considered to be concerted similar to the uncatalyzed and solvent assisted system. By the proton exchange between the adsorbate and the zeolite framework, the enol compound is produced. As the result, product is adsorbed on H-zeolite with the interaction between π bond of C1-C2 and the Brønsted acid site (H1). Figures 23-25 present the energy profiles for the acetone tautomerization on H-FER, H-ZSM-5 and H-MCM-22. The geometric parameters of the intermediates and transition state are listed in table 10.

In FER zeolite (Fig 23), the tautomerization reaction of acetone is occurred in the 10T straight channel. First, the acetone molecule is held with two hydrogen bonding between the zeolite proton and the acetone (O1-Hz - - O3) and the proton of acetone and oxygen of zeolite (C2-Ha - - O2). The reaction is preceded via the concerted step of the proton exchange between the zeolite and the adsorbate. Similar to the other endothermic reaction (Solans-Monfort *et al.*, 2002), the geometry of transition state is closer to the product than to the reactant. The alcohol (Hz-O3) is nearly formed whereas the hydrogen atom of methyl group of acetone (Ha) is nearly closed to the in the oxygen atom of zeolite (O2). The Hz-O1 bond distance increases

from 1.02 Å to 1.64 Å and the C2-Ha bond distance increases from 1.09 Å to 1.52 Å. The C1-C2 single bond is changing to the double bond formation. The distance is changed from 1.51 Å to 1.39 Å. The transition state structure corresponds with the imaginary frequency at -977.6 cm^{-1}. The vibration shows the proton of Brønsted acid site (Hz) is moving from oxygen of zeolite (O1) to oxygen of acetone (O3), the proton at methyl group of acetone (Ha) is moving from methyl group (C1) to oxygen of zeolite (O2), and the single bond of acetone (C1-C2) is contracting to the double bond. For the zeolite, the similar distances of O1-Al and O2-Al are formed to 1.72 and 1.78 Å. The activation energy is 30.0 kcal/mol. For enol product, the enol form of acetone interacts with the zeolite via two hydrogen bonds: the hydroxyl group of enol (O3-Hz) and the oxygen of zeolite (O1), and the π bond of enol (C1=C2) and the proton of Brønsted acid site (Ha). The distance between hydrogen of hydroxyl group (Hz) and oxygen of zeolite (O1) is about 1.85 Å. The distances between carbon of double bond and the proton of Brønsted acid site are 2.34 and 2.81 Å for C1 - - Ha and C2 - - Ha, respectively. The relative energy is 0.5 kcal/mol. The reaction energy is 26.3 kcal/mol.

In ZSM-5 zeolite (Fig 24), the reaction mechanism is occurred similar with previous zeolite but different in the structure of complexes. Due to the high acidic of H-ZSM-5, the acetone is adsorbed slightly better than H-FER as discussed in the previous section. The concerted mechanism of a proton exchange is proposed as same as mentioned earlier. The O1-Hz bond is breaking, the C1-Ha is breaking and the C1-C2 is contracting in the transition structure correspond with the imaginary at -853.6 cm^{-1}. The O1-Hz distance is increased from 1.06 Å to 1.62 Å whereas the C2-Ha distance is increased from 1.09 Å to 1.51 Å. The computed activation energy is 23.0 kcal/mol. The enol is the product of this reaction. Two hydrogen bonds is found between hydroxyl group of enol and oxygen of zeolite (O3-Hz - - O1) with distance 1.75 Å, and the π bond of enol (C1=C2) and the proton of Brønsted acid site (Ha) with distance 1.93 Å and 2.49 Å for C2 - - Ha and C1 - - Ha, respectively. The relative energy for enol in H-ZSM-5 is -4.7 kcal/mol and the reaction energy is 21.7 kcal/mol.

In MCM-22 (Fig 25), the reaction is similar with both previous zeolites. However, the large-pore of MCM-22 gives the different of structure in transition structure and product. At transition state, the vibration mode at -998.9 cm^{-1} shows the moving of proton of Brønsted acid site (Hz) to the carbonyl group (O3) with distance 1.78 Å while the proton of acetone (Ha) is moving to the oxygen of zeolite (O2) with distance 1.77 Å. The contract of C1-C2 bond is found from 1.50 Å of adsorption complex to 1.39 Å of transition state structure. The activation energy is 16.6 kcal/mol. The product is enol which interacts with the Brønsted acid via two hydrogen bond. The interaction between hydroxyl group of enol and oxygen of zeolite is measured via Hz - - O1 bond distance to be 1.94 Å. The another bond is via π bond and Brønsted acid site with distances of 1.77 Å and 2.26 Å for Ha - - C2 and Ha - - C1 distances, respectively. It is evidence that the distance between C atom of enol and Ha atom of zeolite is shortest compared with other zeolites and agree well with the strongest relative energy is -9.4 kcal/mol and the lowest reaction energy is 15.7 kcal/mol.

Due to the acidic of zeolite and the framework effect, the energy barrier of tautomerization of acetone in zeolite is found to be 30.0 – 16.6 kcal/mol reduced from the uncatalyzed gasphase reaction (68.4 kcal/mol) and water assistant system (38.6 – 30.7 kcal/mol). The activation barriers are 30.0, 23.0 and 16.6 kcal/mol for H-FER, H-ZSM-5 and H-MCM-22. The activity order is H-FER < H-ZSM-5 < H-MCM-22. The reaction energy shows the stability of the product and are calculated to be 26.3, 21.7, 15.7 kcal/mol for H-FER, H-ZSM-5 and H-MCM-22, respectively. Due to the endothermic reaction, the transition state is related to the product complex. The reaction has small activation energy when the product is stable. The stability of transition state corresponds with the stability of product from these three zeolites.

The break-down energies are shown in table 10. The activation energies from quantum cluster are 27.4, 25.0 and 17.1 kcal/mol for H-FER, H-ZSM-5 and H-MCM-22, respectively. The reaction order is H-FER< H-ZSM-5 < H-MCM-22 and correspond with the ONIOM calculation. The framework impact the transition state about 2.6, -2.0 and -0.5 kcal/mol for H-FER, H-ZSM-5 and H-MCM-22, respectively.

In the small pore of H-FER, the framework impact the transition state higher than H-ZSM-5. Whereas the larger pore of H-MCM-22 has slightly effect on the activation energy.

As a result, the tautomerization reaction was studied on various with ONIOM scheme. In all cases, the reaction is endothermic. When compared with the gas phase uncatalysed system and water system, the reaction activity is enhanced in the zeolite environment because of Brønsted acid and the framework effect. In zeolite, the reaction is a concerted mechanism with a proton exchange. The catalytic efficiency trend is predicted to be H-FER < H-ZSM-5 < H-MCM-22. The larger pore of H-MCM-22 can catalyze the tautomerization reaction more effectively than H-FER and H-ZSM-5 Zeolite.

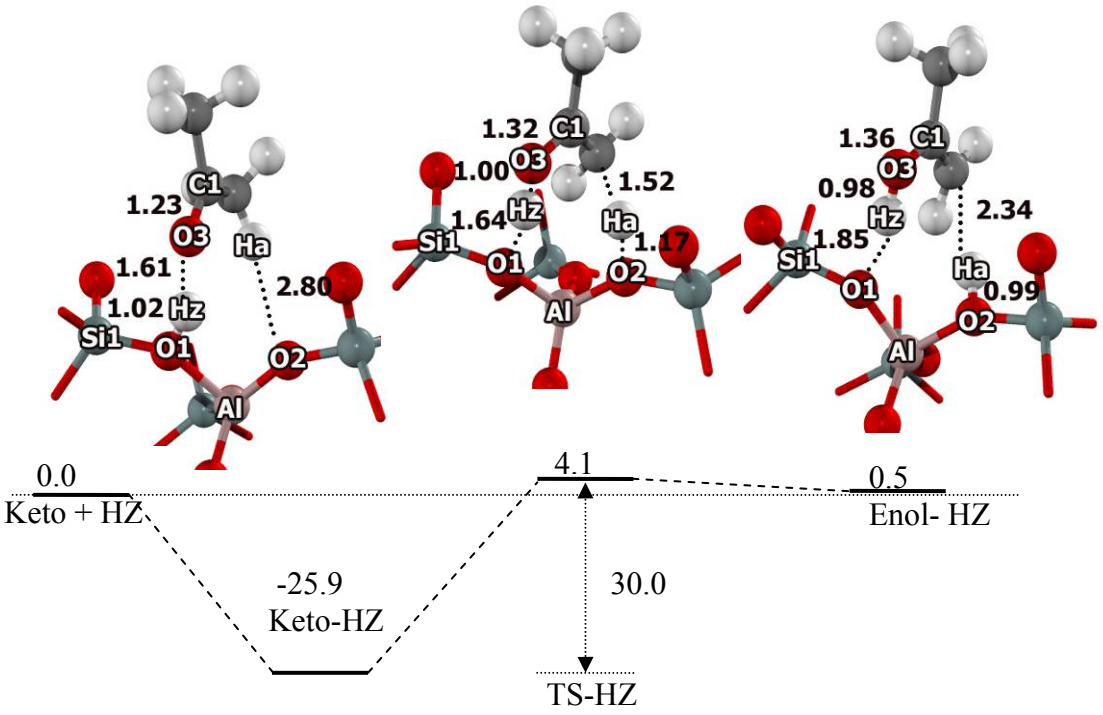

Figure 23 Molecular structures and energy profile of the tautomerization of acetone in H-FER (small-pore zeolite representative) of 12T/112T ONIOM model calculated with B3LYP/6-31G(d,p):UFF level of theory. Distances and energies are given in Å and kcal/mol.

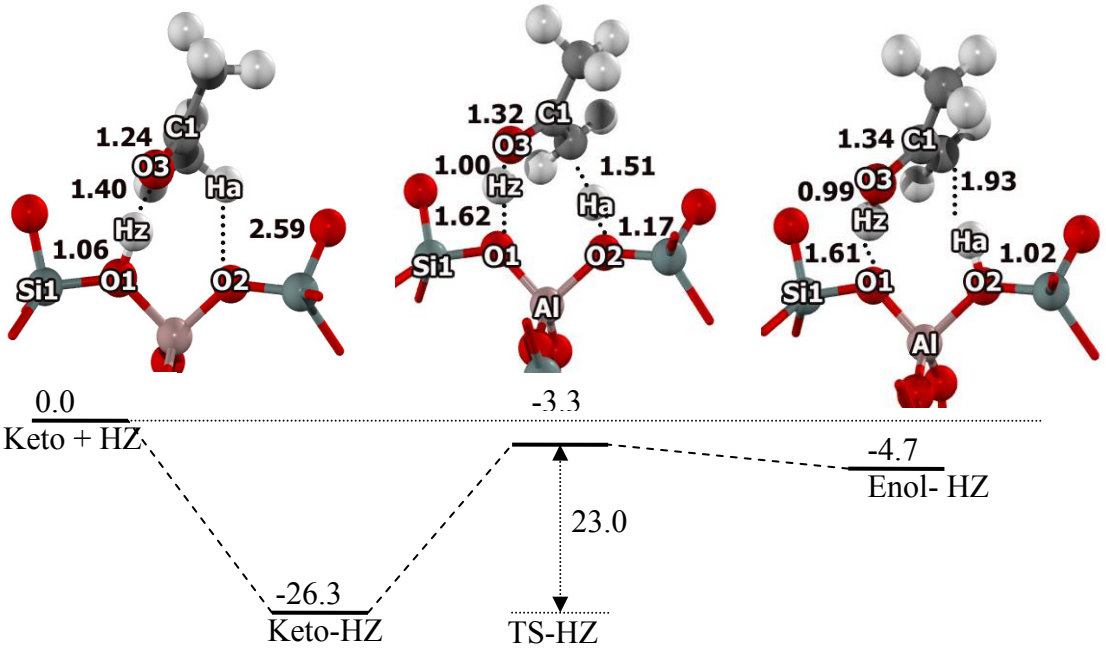

Figure 24 Molecular structures and energy profile of the tautomerization of acetone in H-ZSM-5 (medium-pore zeolite representative) of 12T/128T ONIOM model calculated with B3LYP/6-31G(d,p):UFF level of theory. Distances and energies are given in Å and kcal/mol.

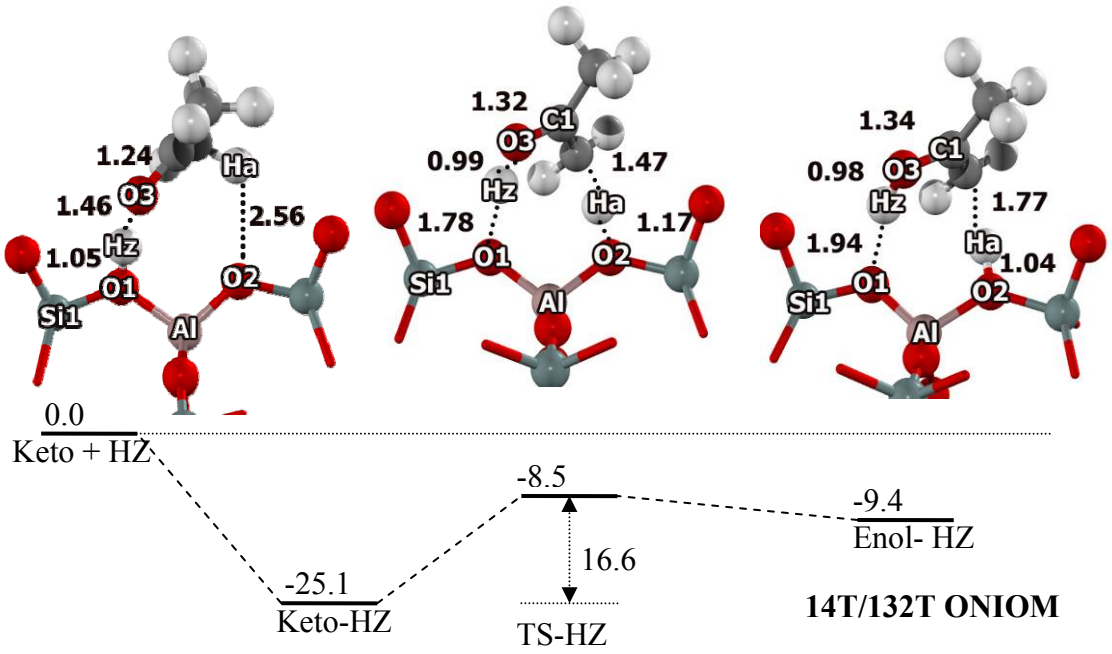

Figure 25 Molecular structures and energy profile of the tautomerization of acetone in H-MCM-22 (large-pore zeolite representative) of 14T/132T ONIOM model calculated with B3LYP/6-31G(d,p):UFF level of theory. Distances and energies are given in Å and kcal/mol.

Table 10 The reaction energies of acetone in the confined spaces of H-FER, H-ZSM-5 and H-MCM-22 zeolite (kcal/mol) where Quantum means ΔE(model, high), and UFF means ΔE(real, low) - ΔE(model, low) with B3LYP/6-31G(d,p):UFF

Zeolite		Quantum	UFF	Total
H-FER	Reactant	-18.1	-7.8	-25.9
	Transition State	9.3	-5.2	4.1
	Product	8.3	-7.8	0.5
	Activation Energy	27.4	2.6	30.0
	Reaction Energy	26.3	-0.01	26.3
H-ZSM-5	Reactant	-18.5	-7.8	-26.3
	Transition State	6.5	-9.8	-3.3
	Product	5.5	-10.2	-4.7
	Activation Energy	25.0	-2.0	23.0
	Reaction Energy	24.1	-2.4	21.7
H-MCM-22	Reactant	-21.6	-3.5	-25.1
	Transition State	-4.4	-4.0	-8.5
	Product	-5.1	-4.3	-9.4
	Activation Energy	17.1	-0.5	16.6
	Reaction Energy	16.5	-0.8	15.7

Table 11 Structural parameters for adsorbate/zeolite cluster complexes along the reaction coordinate in various zeolites (distances in Å, and angles in degree)

	H-FER				H-ZSM-5				H-MCM-22			
Parameters	**Bare**	**AD**	**TS**	**PR**	**Bare**	**AD**	**TS**	**PR**	**Bare**	**AD**	**TS**	**PR**
Distance												
Si1-O1	1.67	1.66	1.61	1.61	1.66	1.64	1.60	1.61	1.71	1.68	1.63	1.63
Si2-O2	1.61	1.60	1.66	1.70	1.58	1.57	1.62	1.64	1.62	1.61	1.66	1.69
O1-Al	1.88	1.84	1.72	1.70	1.79	1.76	1.68	1.67	1.81	1.78	1.70	1.68
O2-Al	1.67	1.67	1.78	1.84	1.66	1.66	1.75	1.78	1.66	1.67	1.75	1.78
Al - - Hz	2.25	2.37	2.84	3.10	2.34	2.42	2.88	2.99	2.42	2.36	2.95	3.08
O1-Hz	0.98	1.02	1.64	1.85	0.97	1.06	1.62	1.75	0.97	1.05	1.78	1.94
Hz - - O3		1.61	1.00	0.98		1.40	1.00	0.99		1.46	1.00	0.98
O1 - - O3		2.59	2.61	2.81		2.46	2.61	2.72		2.50	2.71	2.82
O3-C1	1.22	1.23	1.32	1.36	1.22	1.24	1.32	1.34	1.22	1.24	1.32	1.34
C1-C2	1.52	1.51	1.39	1.35	1.52	1.50	1.39	1.36	1.52	1.50	1.39	1.36
C2-Ha	1.09	1.09	1.52	2.34	1.09	1.10	1.51	1.93	1.09	1.10	1.47	1.77
C1-Ha		2.15	2.27	2.81		2.87	2.20	2.49		2.95	2.07	2.26
Ha - - O2		2.80	1.17	0.99		2.59	1.17	1.02		2.56	1.17	1.04
Angle												
Al-O1-Si1	143.7	142.3	142.9	140.4	128.8	129.9	126.9	125.2	129.7	126.2	125.7	125.5
Al-O2-Si2	151.8	155.4	150.4	151.5	129.5	132.4	129.1	123.1	125.4	126.9	127.3	127.3
O1-Hz-O3		158.8	162.9	164.9		179.1	167.9	167.3		166.9	154.7	147.6
C2-Ha-O2		144.3	164.6	172.1		114.0	171.8	174.4		115.8	168.4	166.0
O1-C1-C2	121.7	122.1	123.4	124.9	121.7	122.9	123.0	124.0	121.7	122.5	122.5	123.8

CONCLUSIONS

The adsorptions of hydrocarbons in various zeolites were studied by using hybrid methods: ONIOM and e-ONIOM approaches. The effect of the long range interactions is also included via optimized point charges added to the ONIOM, embedded ONIOM. For saturated hydrocarbon, the ONIOM2 calculations gave accurate adsorption energies for the adsorption of ethane, propane and n-butane in H-FAU and H-MOR that were in good agreement with the experimental measurements. The adsorption energies were calculated to be -8.2, -10.6, -12.3 kcal/mol for ethane, propane, and n-butane in H-MOR, respectively and -4.3, -5.8, -7.1 kcal/mol for ethane, propane, and n-butane in H-FAU, respectively. For adsorption of unsaturated hydrocarbon in acidic zeolite, which is not possible to experimentally measure, the adsorption energies were predicted to be –9.0, –10.9, –12.1 kcal/mol for ethene, propene, and 1-butene in H-FAU, respectively and –10.0, –13.5, –17.1 kcal/mol for ethene, propene, and 1-butene in H-MOR, respectively. For the polar molecule, the adsorption energy of acetone on zeolites are computed to be -25.9, -26.3 and -25.0 kcal/mol for H-FER, H-ZSM-5 and H-MCM-2, respectively. The calculated adsorption energies of acetone compare well with the experimental data which is reported; acetone on H-ZSM-5 to be -31.3 kcal/mol. For interaction with the amino acid molecule, the adsorption of glycine and L-alanine on H-ZSM-5 zeolite has been theoretically studied. The most stable adsorption complex is the ion-pair interaction between the protonated amino acid and the anionic zeolite with adsorption energy -31.3 kcal/mol. Two adsorption complexes via hydrogen bond interaction through the carboxylic and the hydroxyl group of the amino acids are also found and have lower adsorption energies. The adsorption energies are -25.4 and -20.7 kcal/mol for carboxylic and hydroxyl group of the glycine interaction, respectively. L-alanine has higher adsorption energy than glycine, mainly due to the confinement effect of the zeolite walls which is stronger for the larger adsorbed molecule. For the adsorption of glycine, the van der Waals interactions account for approximately 20-30%. For the adsorption of the larger molecule, L-alanine, the van der Waals interactions increase to as much as 50%. The long-range electrostatic interactions account for less than 10% of the overall adsorption energies. Nevertheless, it has non-negligible

contributions when the adsorbed molecule carries a net charge. The zwitterion form of glycine is not observed in the acidic H-ZSM-5 zeolite due to the rapid acid-base reaction but it can be observed in the Na-ZSM-5. The glycine zwitterion is stabilized by the interactions with the sodium cation and the oxygen atom on the zeolite framework. Our findings demonstrate that the zwitterion of amino acid is stabilized by cooperatively building up hydrogen bonding within the zeolitic framework, which is in line with those found in solvent molecules and/or in counter ions.

The confinement effect on the reaction properties has been studied on the reaction mechanism of acetone tautomerization on different pore sizes of zeolites represented with H-FER, H-ZSM-5 and H-MCM-22 with the ONIOM method. The tautomerization of acetone is theoretically investigated on the noncatalyzed gas-phase, water-assisted and zeolite environments. The activation energy is predicted to be 68.4 kcal/mol for the noncatalyzed gas-phase reaction; the barrier is then reduced to be in the range of 30.7 to 38.6 kcal/mol by the presence of water-assisted molecules. The activation energies for the zeolite-catalyzed reaction are 30.0, 23.0 and 16.6 kcal/mol for H-FER, H-ZSM-5 and H-MCM-2, respectively. H-MCM-22 is found to be the most efficient catalyst for the reaction due to it having the smallest constraining influence on the transition structure. The confinement effect of zeolite on the adsorption and reaction of hydrocarbon can be correctly described via the ONIOM model. The quantum cluster calculation can accurately compute interactions of the adsorbate with the acid site but cannot cover the van der Waals interactions with the zeolite walls. The extended zeolitic framework that was modeled by the UFF force field was found to be essential for describing the confinement effect of the zeolite and led to the differentiation of different types of zeolites.

LITERATURE CITED

Aikens, C.M. and M.S. Gordon. 2006. Incremental salvation of nonionized and zwitterionic glycine. **J. Am. Chem. Soc.** 128(39): 12835-12850.

Alberti, A., P. Davoli and G. Z. Vezzalini. 1986. The crystal-structure refinement of a natural mordenite. **Kristallography** 175(3-4): 249-256.

Aquino, A.J.A., D. Tunega, M.H. Gerzabek and H. Lischka. 2001. Modeling catalytic effects of clay mineral surfaces of peptide bond formation. **J. Phys. Chem. B** 108(28): 10120-10130.

Babitz, S.M., B.A. Williams, J.T. Miller, R.Q. Snurr, W.O. Haag and H.H. Kung, 1999. Monomolecular cracking of n-hexane on Y, MOR, and ZSM-5 zeolite. **Appl. Catal. A** 179(1-2): 71-86.

Bhan, A. and E. Iglesia, 2008. A Link between Reactivity and Local Structure in Acid Catalysis on Zeolites. **Acc. Chem. Res.** 41: 559-567.

Barich, D.H., J.B. Nicholas, T. Xu and J.F. Haw. 1998. Theoretical and experimental study of the ^{13}C chemical shift tensors of acetone complexes with Brönsted and Lewis Acids. **J. Am. Chem. Soc**. 120: 12342-12350.

Barlow, S.M., K.J. Kitching, S. Haq and N.V. Richardson. 1998. A study of glycine adsorption on a Cu{110} surface using reflection absorption infrared spectroscopy. **Surf. Sci.** 401(3): 322-335.

Basiuk, V.A. 2001. Quantum chemical calculations of infrared spectra for the identification of unknown compounds by GC/FTIR/MS in exobiological simulation experiments**. Adv. Space Res**. 27(2): 255-260.

Basiuk, V.A. 2002. **Adsorption of Biomolecules at Silica. In Encyclopedia of Surface and Colloid Science**, Hubbard, A., Ed., Marcel Dekker: New York.

Basiuk, V.A., T.Y. Gromovoy, V.G. Golovaty and A.M. Glukhoy. 1991. Mechanisms of amino-acid polycondensation on silica and alumina surfaces. **Origins Life Evol. B** 20 (6):483-498.

Biaglow, A.I., R.J. Gorte, G.T. Kokotailo and D. White. 1994. A probe of Brönsted site acidity in zeolites: ^{13}C chemical shift of acetone. **J. Catal.** 148: 779-786.

_____, J. Šepa, R.J. Gorte and D. White. 1995. A ^{13}C NMR study of the condensation chemistry of acetone and acetaldehyde adsorbed at the Brönsted acid sites in H-ZSM-5. **J. Catal.** 151: 373-384.

Bobuatong, K. and J. Limtrakul. 2003. Effects of the zeolite framework on the adsorption of ethylene and benzene on alkali-exchanged zeolites: an ONIOM study. **Appl. Catal. A-Gen.** 253(1): 49-64.

Bordiga, S., G. T. Palomino, C. Paze, A. Zecchina. 2000. Vibrational spectroscopy of H2, N2, CO and NO adsorbed on H, Li, Na, K-exchanged ferrierite. **Micro. Meso. Mater.** 34(1): 67-80.

Boronat, M., C.M. Zicovich-Wilson, P. Viruela and A. Corma. 2001. Influence of the local geometry of zeolite active sites and olefin size on the stability of alkoxide intermediates. **J. Phys. Chem. B** 105(45): 11169-11177.

Brand, H. V., L. A. Curtiss, I. E. Iton. 1993. Ab initio molecular orbital cluster studies of the zeolite ZSM-5. 1. Proton affinities. **J. Phys. Chem.** 97 (49): 12773-82.

Brändle, M. and J. Sauer. 1998. Acidity differences between inorganic solids induced by their framework structure. A combined quantum mechanics molecular mechanics ab initio study on zeolites. **J. Am. Chem. Soc.** 120(7): 1556-1570.

Cant, N.W. and W. K. Hall. 1972. Studies of hydrogen held by solids .21. interaction between ethylene and hydroxyl groups of a Y-zeolite at elevated-temperatures. **J. Catal.** 25(1): 161-172.

Carlos, D.C.D., S. Locatalli and E.E. Gonzo. 1992. Acetaldehyde adsorption on HZSM-5 studied by infrared spectroscopy. **Zeolites.** 12:851.

Chiang, Y., A. J. Kresge, Y. S. Tang, J. Wirz. 1984. The pKa and keto-enol equilibrium constant of acetone in aqueous solution. **J Am Chem Soc.** 106 (2): 460-2.

_____,_____, N. P. Schepp. 1989. Temperature coefficients of the rates of acid-catalyzed enolization of acetone and ketonization of its enol in aqueous and acetonitrile solutions. Comparison of thermodynamic parameters for the keto-enol equilibrium in solution with those in the gas phase. **J Am Chem Soc.** 111 (11): 3977-80.

Choi, S.H., B.R., Wood, J.A., Ryder, and A.T. Bell. 2003. X-ray adsorption fine structure characterization of the local structure of Fe in Fe-ZSM-5. **J. Phys. Chem. B** 107(43): 11843-11851.

Chudasama, C.D., J. Sebastian and R.V. Jasra. 2005. Pore-size engineering of zeolite A for the size/shape selective molecular separation. **Ind. Eng. Chem. Res.** 44(6): 1780-1786.

Coker, E.N., J., Chunjuan, and H.G., Karge. 2000. Adsorption of Benzene and Benzene Derivatives onto Zeolite H-Y Studied by Microcalorimetry, **Langmuir**, 16: 1205-1210

Corma, A. 2003. State of the art and future challenges of zeolites as catalysts**, J. Catalysis.** 216: 298-312.

Corma, A and H. García. 2002. Lewis Acids as Catalysts in Oxidation Reactions: From Homogeneous to Heterogeneous Systems. **Chem. Rev.** 102: 3837-3892.

_____,_____, G. Sastre and P.M. Viruela. 1997. Activation of molecules in confined spaces: An approach to zeolite-guest supramolecular systems. **J. Phys. Chem. B** 101(23): 4575-4582.

_____, M.J. Diaz-Cabanas, J. Martinez-Triguero, F. Rey and J. Rius. 2002. A large-cavity zeolite with wide pore windows and potential as an oil refining catalyst. **Nature** 418: 514-517.

Cosimo J.I.D. and G. Torres. 2002. C.R. Apesteguía, One-Step MIBK Synthesis: A New Process from 2-Propanol, J. Catal. 208:114.

Cucinotta, C. S., A. Ruini, A. Catellani, A. Stirling. 2006. Ab initio molecular dynamics study of the keto-enol tautomerism of acetone in solution. **ChemPhysChem** 7 (6): 1229-1234.

Cui, Y., Q. Wei, H. Park and C.M. Lieber. 2001. Nanowire nanosensors for highly sensitive and selective detection of biological and chemical species. **Science** 293(5533): 1289-1292.

Dapprich, S., I. Komiromi, K.S. Byun, K. Morokuma. and M. J. Frisch. 1999. A new ONIOM implementation inGaussian98. Part I. The calculation of energies, gradients, vibrational frequencies and electric field derivatives. **Theochem**. 461-462: 1-21.

Davis, M. E. and R.F. Lobo. 1992. Zeolite and molecular sieve synthesis. **Chem. Mater.** 4: 756-768.

Demontis, P. and G.B. Suffritti. 1997. Structure and dynamics of zeolites investigated by molecular dynamics. **Chem. Rev.** 97: 2845-2878.

Derouane E.G., J.M. Andre and A.A. Lucus. 1988. Surface curvature effects in physisortion and catalysis by microporous solids and molecular-sieves. **J. Catal.** 110(1): 58-73.

Derouane E.G. 1986. Shape selectivity in catalysis by zeolites – The nest effect. **J. Catal.** 100(2): 541-544.

_____ and C.D. Chang. 2000. Confinement effects in the adsorption of simple bases by zeolite. **Microporous Mesoporous Mater.** 35-36: 425-433.

_____, J.M. Andre and A.A. Lucas. 1988. Surface curvature effects in physisorption and catalysis by microporous solids and molecular-sieves. **J. Catal.** 110(1): 58-73.

Derouane E.G. 1998. Zeolite as solid solvents. **J. Mol. Catal. A: Chem.** 134(1-3): 29-45.

Dolg, M., U., Wedig, H., Stoll, and H., Preuss. 1987. Energy-adjusted abinitio pseudopotentials for the 1st –row transition-elements. **J. Chem. Phys.** 86(2): 866-872.

Dubbeldam, D., S. Calero, T.L.M. Maesen and B. Smit. 2003. Understanding the window effect in zeolite catalysis. **Angew. Chem., Int. Ed.** 42(31): 3624-3626.

Dubkov, K.A., V.I., Sobolev, and G.I., Panov. 1998. Low-temperature oxidation of methane to methanol on FeZSM-5 zeolite. **Kint. Catal.** 39(1): 72-79.

Eder, F. and J.A. Lercher. 1983. Alkane sorption in molecular sieves: The contribution of ordering, intermolecular interactions, and sorption on Brønsted acid sites. **Zeolites** 18(1): 75-81.

_____, M. Stockenhuber and J.A. Lercher. 1997. Brønsted acid site and pore controlled siting of alkane sorption in acidic molecular sieves. **J. Phys. Chem. B** 101(27): 5414-5419.

Ernst, S. and J. Weitkamp. 1991. Zeolite ZSM-57: synthesis, characterization and shape selective properties. **Studies in Surface Science and Catalysis**, 65: 645-52.

Farneth, W.E. and R.J. Gorte. 1995. Methods for Characterizing zeolite acidity. **Chem. Rev.** 95:615-635.

Flego, C., C. Perego. 2000. Acetone condensation as a model reaction for the catalytic behavior of acidic molecular sieves: a UV-Vis study. **Applied Catalysis, A: General**, 192(2): 317-329.

Fowkes, A.J., R.M., Ibberson, and M.J., Rosseinsky. 2002. Structural characterization of the redox behavior in copper-exchanged sodium zeolite Y by high-resolution powder neutron diffraction. **Chem. Mater.** 14(2): 590-602.

Ghandi, K., B. Addison-Jones, J.-C. Brodovitch, B. M. McCollum, I. McKenzie, P. W. Percival. 2003. Enolization of Acetone in Superheated Water Detected via Radical Formation. **J Am Chem Soc.** 125 (32): 9594-9595.

Gray, J.J. 2004. The interaction of proteins with solid surfaces. **Curr. Opin. Struct. Biol.** 14(1): 110-115.

Greatbanks, S.P., I.H. Hillier, N.A. Burton and P. Sherwood. 1996. Adsorption of water and methanol on zeolite Bronsted acid sites: An ab initio, embedded cluster study including electron correlation. **J. Chem. Phys.** 105(9): 3770-3776.

Gutmann, V. 1978. **The donor-Acceptor Approach to Molecular Interaction**, Plenum Press, New York.

Hartmann, M. 2005. Ordered mesoporous materials for bioadsorption and biocatalysis. **Chem. Mater.** 17(18): 4577-4593.

Heyden, A., B., Peters, A.T., Bell, and F.J., Keil. 2005. Comprehensive DFT study of nitrous oxide decomposition over Fe-ZSM-5. **J. Phys. Chem. B** 109(5): 1857-1873.

Hillier, I.H. 1999. Chemical reactivity studied by hybrid QM/MM methods. **Theochem**. 463(1-2): 45-52.

Hiroshige, M., K. Yasui and Y. Morita. 1968. Catalytic activity of the zeolite-hydrogen chloride system. **J. Catal.** 12: 84-9.

Hunger, M. 2005. Applications of in situ spectroscopy in zeolite catalysts. **Microporous and Mesoporous Materials.** 82: 241-255.

Injan, N., N. Pannorad, M. Probst and J. Limtrakul. 2005. Pyridine adsorbed on H-Faujasite zeolite: Electrostatic effect to the infinite crystal lattice calculated from a point charge representation. **Int. J. Quantum Chem.** 105(6): 898-905.

Jansang, B., T., Nanok, and J. Limtrakul. 2006. Structures and reaction mechanisms of cumene formation via benzene alkylation with propylene in a newly synthesized ITQ-24 zeolite: An embedded ONIOM study. **J. Phys. Chem. B** 110(25): 12626-12631.

Jensen, J.H. and M.S. Gordon. 1995. On the number of water-molecules necessary to stabilize the glycine zwitterions. **J. Am. Chem. Soc.** 117(31): 8159-8170.

Jia, J., Q., Sun, B., Wen, L.X., Chen and W.M.H. Sachtler. 2002. Identification of highly active iron sites in N2O-activated Fe/MFI. **Catal. Lett.** 82(1-2): 7-11.

Joyner, R. and M. Stockenhuber. 1999. Preparation, characterization, and performance of Fe-ZSM-5 catalysts. **J. Phys. Chem. B** 103(29): 5963-5976.

Kasuriya, S., S. Namuangruk, P. Treesukol, M. Tirtowidjojo and J. Limtrakul. 2003. Adsorption of ethylene, benzene, and ethylbenzene over faujasite zeolites invertigated by the ONIOM method. **J. Catal.** 219(2): 320-328.

Khaliullin, R.Z., A.T. Bell and V.B. Kazansky. 2001. An experimental and density functional theory study of the interactions of CH4 with H-ZSM-5. **J. Phys. Chem. A** 105(45): 10454-10461.

Klinowski, J. 1991. Solid State NMR Studies of Molecular Sieve Catalysts, **Chem. Rev**. 1991: 1459-1479.

Kondo, J.N. and K. Domen. 2003. IR observation of adsorption and reactions of olefins on H-form zeolites. **J. Mol. Catal. A: Chem.** 199(1-2): 27-38.

Kong, J., N.R. Franklin, C. Zhou, M.G. Chapline, S. Peng, K. Cho and H. Dailt. 2000. Nanotube molecular wires as chemical sensors. **Science** 287(5453): 622-625.

Krohn J.E. and M. Tsapatsis. 2005. Amino acid adsorption on zeolite beta. **Langmuir** 21(19): 8743-8750.

_____. and _____. 2006. Phenylalanine and arginine adsorption in zeolites X, Y, and beta. **Langmuir** 22(22): 9350-9356.

Lanewala, M.A, A.P. Bolton. 1969. Isomerization of the xylenes using zeolite catalysts. **J. Org Chem.** 34 (10): 3107-3112.

Lee, D., C. K. Kim, B.-S. Lee, I. Lee, B. C. Lee. 1997. A theoretical study of keto-enol tautomerization involving simple carbonyl derivatives. **J. Comp. Chem.** 18 (1): 56-69.

Limtrakul, J., S. Jungsuttiwong and P. Khongpracha. 2000. Adsorption of carbon monoxide in H-FAU and Li-FAU zeolites: an embedded cluster approach. **J. Mol. Struct.** 525: 153-162.

Lomratsiri, J., M. Probst and J. Limtrakul. 2006. Structure and adsorption of a basic probe molecule on H-ZSM-5 nanostructured zeolite: An embedded ONIOM study. **J. Mol. Graph. Mol.** 25(2): 219-225.

Maesen, T.L.M., E. Beerdsen, S. Calero, D. Dubbeldam and B. Smit. 2006. Understanding cage effects in the n-alkane conversion on zeolites. **J. Catal.** 237(2): 278-290.

Mayorga, G.D. and D.L. Peterson. 1972. Adsorption in mordenite.2. Gas-chromatographic measurement of limiting heats of adsorption on nonpolar molecules. **J. Phys. Chem.** 76(11): 1647-1650.

Meng, M., L. Stievano and J.-F. Lambert. 2004. Adsorption and thermal condensation mechanisms of amino acids on oxide supports. 1. Glycine on silica. **Langmuir** 20(3): 914-923.

Morris, R.E., S.J., Weigel, N.J., Henson, L.M., Bull, M.T., Janicke, B.F., Chmelka, and A.K. Cheetham. 1994. A synchrotron X-Ray-Diffraction, Neutron-Diffraction, Si-29 MAS-NMR, and computational study of the siliceous form of zeolite ferrierite. **J. Am. Chem. Soc.** 116(26): 11849-11855.

Munsch, S., M. Hartmann and S. Ernst. 2001. Adsorption and separation of amino acids from aqueous solutions on zeolites. **Chem. Commun.** (19): 1978-1979.

Namuangruk, S., D. Tantanak and J. Limtrakul. 2006. Application of ONIOM calculations in the study of effect of the zeolite framework on the adsorption of alkenes to ZSM-5**. J. Mol. Catal. A-Chem**. 256(1-2): 113-121.

_____, P. Khongpracha, P. Pantu and J. Limtrakul. 2006. Structure and reaction mechanism of propene oxide isomerization on H-ZSM-5: An ONIOM study. **J. Phys. Chem. B** 110(51): 25950-25957.

_____, P. Pantu and J. Limtrakul. 2004. Alkylation of benzene with ethylene over faujasite zeolite investigated by the ONIOM method. **J. Catal.** 225(2): 523-530.

_____, _____and _____. 2005. Investigation of ethylene dimerization over faujasite zeoliteby the ONIOM mothod. **ChemPhysChem** 6 (7): 1333-1339.

Newsam, J.M., M.M.J., Treacy, W.T., Koetsier, and C.B., de Gruyter. 1988. Structure characterization of zeolite-Beta. **Proc. R. Soc. Lond. A** 420(1859): 375.

Olson, D. H. and E., Dempsey. 1969. Crystal structure of zeolite hydrogen faujasite. **J. Catal.** 13(2): 221-231.

Onyestyak, G., G. Pal-Borbely, H.K. Beyer. 2002. Cyclohexane conversion over H-zeolite supported platinum. **App. Cat. A-Gen.** 229 (1-2): 65-74.

Øygarden, A. H. and J., Pérez-Ramírez. 2006. Activity of commercial zeolites with iron impurities in direct NO2 decomposition. **Appl. Catal. B-Environ.** 65(1-2): 163-167.

Parrilloa, D.J., C., Leea and R.J., Gorte. 1994. Heats of adsorption for ammonia and pyridine in H-ZSM-5: evidence for identical Brønsted-acid sites, **Applied Catalysis A: General**. 110: 67-74.

Panjan W. and J. Limtrakul. 2003. The influence of the framework on adsorption properties of ethylene/H-ZSM-5 system: an ONIOM study. **J. Mol. Struct.** 654(1-3): 35-45.

Panov A.G. and J.J. Fripiat. 1998. Acetone Condensation Reaction on Acid Catalysts. J. Catal. 178, 188-197.

Panov, G.I., V.I., Sobolev, and A.S., Kharitonov. 1990. The role of iron in N2O decomposition on ZSM-5 zeolite and reactivity of the surface oxygen formed. **J. Mol. Catal.** 61(1): 85-97.

_____, _____, K.A., Dubkov, V.N., Parmon, N.S., Ovanesyan, A.E. Shilov, and A.A., Shteinman. 1997. Iron complexes in zeolites as a new model of methane monooxygenase. **React. Kinet. Catal. L.** 61(2): 251-258.

Panyaburapa, W., T., Nanok and J. Limtrakul. 2007. Epoxidation reaction of unsaturated hydrocarbons with H2O2 over defect TS-1 investigated by ONIOM method: Formation of active sites and reaction mechanisms. **J. Phys. Chem.** C 111(8): 3433-3441.

Parsons, I., M.R. Lee and J.V. Smith. 1998. Biochemical evolution II: Origin of life in tubular microstructures on weathered feldspar surfaces. **Proc. Natl. Acad. Sci. U. S. A.** 95(26): 15173-15176.

Peng, L., Y. Liu, N. Kim, J.E. Readman and C.P. Grey. 2005. Detection of Brønsted acid sites in zeolite HY with high-field 17O-MAS-NMR techniques. **Nat. Mat.** 4: 216-219.

Pieterse, J.A.Z., S. Veefkind-Reyes, K. Seshan and J.A. Lercher. 2000. Sorption and ordering of dibranched alkanes on medium-pore zeolites ferrierite and TON. **J. Phys. Chem. B** 104(24): 5715-5723.

Pirngruber, G.D., P.K., Roy and R. Prins. 2006. On determining the nuclearity of iron sites in Fe-ZSM-5 a critical evaluation. **Phys. Chem. Chem. Phys.** 8(34): 3939-3950.

Rappe, A.K., C.J. Casewit, K.S. Colwell, W.A. Goddard and W.M. Skiff. 1992. UFF, A full periodic-table force-field for molecular mechanics and molecular-dynamics simulations. **J. Am. Chem. Soc.** 114(25): 10024.

Rimola, A., M. Sodupe, S. Tosoni, B. Civalleri and P. Ugliengo. 2006. Interaction of glycine with isolated hydroxyl groups at the silica surface: First principles B3LYP periodic simulation. **Langmuir** 22(15): 6593-6604.

_____, S. Tosoni, M. Sodupe and P. Ugliengo. 2006. Does silica surface catalyse peptide bond formation? New insights from first-principles calculations. **ChemPhysChem**. 7 (1): 157-163.

Rodriguez-Santiago L., A. Vendrell, I. Tejero, M. Sodupe and J. Bertran. 2001. Solvent-assisted catalysis in the enolization of acetaldehyde radical cation, Chem. Phys. Lett., 334: 112.

Rosseinsky, M.J. 2004. Recent developments in metal-organic framework chemistry: design, discovery, permanent porosity and flexibility. **Microporous Mesoporous Mater.** 73(1-2): 15-40.

Ryder, J.A., A.K., Chakraborty, and A.T., Bell. 2002. Density functional theory study of nitrous oxide decomposition over Fe- and Co-ZSM-5. **J. Phys. Chem. B** 106(28): 7059-7064.

Sahoo SK, N. Viswanadham, N. Ray, J.K. Gupta, I.D. Singh. 2001. Studies on acidity, activity and coke deactivation of ZSM-5 during n-heptane aromatization. **App. Cat. A-Gen.** 205 (1-2):1-10.

Sauer, J., P. Ugliengo, E. Garrone and V.R. Saunders. 1994. Theoretical Study of van der Waals Complexes at Surface Sites in Comparison with the Experiment. **Chem. Rev.** 94: 20095.

Šepa J., C. Lee, R.J. Gorte, D. White, E. Kassab, E.M. Evleth, H. Jessri and M. Allavena. 1996. Carbonyl 13C Shielding Tensors and Heats of Adsorption of Acetone Adsorbed in Silicalite and the 1:1 Stoichiometric Complex in H-ZSM-5**, J. Phys. Chem.** 100: 18515.

Schuring, D., A.O. Koriabkina, A.M. de Jong, B. Smit and R.A. van Santen. 2001. Adsorption and diffusion of n-hexane/2-methylpentane mixtures in zeolite silicalite: Experiments and modeling. **J. Phys. Chem. B** 105(32): 7690-7698.

Sridevi, U., B.K.B. Rao, N.C. Prahan, S.S. Tambe, C.V. Satyanarayana, B.S. Rao. 2001. Kinetics of isopropylation of benzene over HBeta catalyst. **Ind. Eng. Chem. Res.** 40 (14) 3133-3138.

Sillar, K. and P. Burk. 2002. Calculation of the properties of acid sites of the zeolite ZSM-5 using ONIOM method. **Theochem**. 589: 281-290.

Simperler, A.; R. G. Bell, M. D. Foster, A. E. Gray, D. W. Lewis, M. W. Anderson, 2004. Probing the Acid Strength of Bronsted Acidic Zeolites with Acetonitrile: An Atomistic and Quantum Chemical Study. **J. Phys. Chem. B** 108 (22): 7152-7161.

Sinclair, P.E., A. de Vries, P. Sherwood, C.R.A. Catlow and R.A. van Santen. 1998. Quantum-chemical studies of alkene chemisorption in chabasize: A comparison of cluster and embedded-cluster models. **J. Chem. Soc., Faraday T.** 94(22): 3401-3408.

Shelef, M. 1995. Selective Catalytic Reduction of NOx with N-Free Reductants. **Chem. Rev.** 95(1): 209-225.

Smit, B. and T. L. M. Maesen. 2008. Towards a molecular understanding of shape selectivity, **Nature.** 451: 671-678.

Smith, J.V. 1998. Biochemical evolution. I. Polymerization on internal, organophilic silica surfaces of dealuminated zeolites and feldspars. **Proc. Natl. Acad. Sci. U S A.** 95(7): 3370-3375.

Solans-Monfort X., J. Bertan, V. Branchadell, M. Sodupe. 2002. Keto-Enol Isomerization of Acetaldehyde in HZSM5. A Theoretical Study Using the ONIOM2 Method, **J. Phys. Chem. B**, 106: 10220-10226.

Solans-Monfort X., M. Sodupe, V. Branchadell, J. Sauer, R. Orlando and P. Ugliengo. 2005. Adsorption of NH3 and H2O in acidic chabazite. Comparison of ONIOM approach with periodic calculaions. **J. Phys. Chem. B** 109(41): 3539-3545.

Spoto, G., S. Bordiga, G. Ricchiardi, D. Scarano, A. Zecchina and E. Borello. 1994. IR study of ethene and propene oligomerization on H-ZSM-5 – hydrogen-bonded precursor formation, initiation and propagation mechanims and structure of the entrapped oligomers. **J. Chem. Soc., Faraday Trans.** 90(18): 2827-2835.

Stach, H., U. Lohse, H. Thamm and W. Schirmer. 1986. Adsorption equilibria of hydrocarbons on highly dealuminated zeolites. **Zeolites** 6(2): 74-90.

Svensson, M., S. Humbel, R.D.J. Froese, T. Matsubara, S. Sieber and K. Morokuma, 1996. ONIOM: A multilayered integrated MO+MM method for geometry optimizations and single point energy predictions. A test for Diels-Alder reactions and Pt(P(t-Bu)(3))(2)+H-2 oxidative addition. **J. Phys. Chem.** 100 (50): 19357-19363.

Tielens, F., J.F.M. Denayer, I. Daems, G.V. Baron, W.J. Mortier and P. Geerlings. 2003. Adsorption of the butane isomers in faujasite: A combined ab-initio theoretical and experimental study. **J. Phys. Chem. B** 107(40) 11065-11071.

Treesukol, P., J.P. Lewis, J. Limtrakul and T.N. Truong. 2001. A full quantum embedded cluster study of proton siting in chabazite. **Chem. Phys. Lett.** 350 (1-2): 128-134.

Tsai, T., A. Chang, L. Chin and I. Wang. 1991. Cumene disproportionation over zeolite b. I. Comparison of catalytic performances and reaction mechanisms of zeolites. **Appl. Cat.** 77(2): 199-207.

Tzvetkov, G., G. Koller, Y. Zubavichus, O. Fuchs, M.B. Casu, C. Heske, E. Umbach, M. Grunze, M.G. Ramsey and F.P. Netzer. 2004. Bonding and structure of glycine on ordered Al2O3 film surfaces. **Langmuir** 20(24): 10551-10559.

van Bokhoven, J.A., B.A. Williams, W. Ji, D.C. Koningsberger, H. H. Kung and J.T. Miller. 2004. Observation of a compensation relation for monomolecular alkane cracking by zeolites: the dominant role of reactant sorption. **J. Catal.** 224(1): 50-59.

van Koningsveld, H., H., van Bekkum and J.C., Jansen. 1987. On the location and disorder of the tetrapropylammonium (TPA) ion in zeolite ZSM-5 with improved framework accuracy. **Acta Crystallogr. B** 43(2): 127-132.

Van Santen, R.A. and G. J. Kramer. 1995. Reactivity theory of zeolitic Brønsted acidic sites. **Chem. Rev.** 95: 637-660.

Venuto, P. B. 1994. Organic catalysis over zeolites: a perspective on reaction paths within micropore. **Mircoporous Materials** 2: 297-411.

Wei, J. 1994. Nonlinear phenomena in zeolite diffusion and reaction. **Ind. Eng. Chem. Res.** 33(10): 2467-2472.

Xing, G.W., X.-W. Li, G.-L. Tian and Y.-H. Ye. 2000. **Tetrahedron** 56 (22): 3517-3522.

Xu, F., Y. Wang, X. Wang, Y. Zhang, Y. Tang and P. Yang. 2003. A novel hierarchical nanozeolite composite as sorbent for protein separation in immobilized metal-ion affinity chromatography. **Adv. Mater**. 15(20): 1751-1753.

Xu, T., E.J. Munson, J.F. Haw. 1994. Toward a Systematic Chemistry of Organic Reactions in Zeolites: In Situ NMR Studies of Ketones, **J. Am. Chem. Soc.** 116: 1962.

Yang, L., K. Trafford, O. Kresnawahjuesa, J. Sepa, R.J. Gorte and D. White. 2001. An examination of confinement effects on high-silica zeolite. **J. Phys. Chem. B** 105(10): 1935-1942.

Yoda, E., J.N. Kondo and K. Domen. 2005. Detalied process of adsorption of alkanes and alkenes on zeolites. **J. Phys. Chem. B** 109(4): 1464-1472.

Yonsel, A., W. Schaefer-Treffenfeldt, A. Kiss, E. Sextl and H. Naujok. 1993. **Separation of amino acids from aqueous solutions by adsorption to zeolites**. Degussa A.-G., Germany., Application: DE.

Zakharov, M., A. E. Masunov, A. Dreuw. 2008. Catalytic Role of Calix[4]hydroquinone in Acetone-Water Proton Exchange: A Quantum Chemical Study of Proton Transfer via Keto-Enol Tautomerism. **J. Phys. Chem. A** 112 (41): 10405-10412.

Zecchina, A., G. Spoto and S. Bordiga. 2005. Probing the acid sites in confined spaces of microporous materials by vibrational spectroscopy. **Phys. Chem. Chem. Phys.** 7(8): 1627-1642.

Zicovich-Wilson, C.M., A. Corma and P. Viruela. 1994. Electronic confinement of molecules in microscopic pores – A new concept which contributes to explain the catalytic activity of zeolite. **J. Phys. Chem.** 98(42): 10863-10870.

CURRICULUM VITAE

NAME	:	Mr. Bundet Boekfa
BIRTH DATE	:	September 9, 1980
EDUCATION	:	YEAR,INSTITUTION, DEGREE
		2002, Thaksin University, B.S.(Chemistry)
		2004, Kasetsart University, M.S.(Chemistry)

PUBLICATIONS

1. Boekfa, B., J. Sirijareansre, P. Piboon and J. Limtrakul. 2004. A Quantum Chemical Study of the Interaction of Carbonyls with H-ZSM5 Zeolite. **Stud. Surf. Sci. Cat**. 154:1582-1588.
2. Boekfa, B., J. Sirijareansre, P. Limtrakul, P. Piboon and J. Limtrakul. 2007. Adsorption of Glycine Amino Acid in Zeolite: An Embedded QM/MM Study. **NSTI-Nanotech**. 1:454-457.
3. Pantu, P., B. Boekfa and J. Limtrakul. 2007. The adsorption of saturated and unsaturated hydrocarbon on nanostructured zeolite (H-MOR and H-FAU): An ONIOM study. **J. Mol. Cat. A** 277:171-179.
4. Pantu, P., B. Boekfa, S. Sunpetch and J. Limtrakul. 2008. Nanocavity effects on N2O decomposition on different types of Fe-zeolites (Fe-FER, Fe-BEA, Fe-ZSM-5 and Fe-FAU). **ChemEngComm**. 195:1477-1485.
5. Boekfa, B., S. Choomwattana, C. Wattanakit, P. Limtrakul, P. Pantu, P. Khongpracha and J. Limtrakul. 2008. Effects of the framework on the adsorption of methane on IRMOF-1, IRMOF-2 and IRMOF-6 Metal-Organic Frameworks: A combined QM and MM study. **Nanoporous Materials – V**, 431-438.
6. Boekfa, B., P. Pantu and J. Limtrakul. 2008. Interaction of Amino Acids with H-ZSM-5 Zeolite: an Embedded ONIOM Study. **J Mol Struct**, 889:81-88.

7. Maihom, T., B. Boekfa, J. Sirijaraensre, T. Nanok, M. Probst and J. Limtrakul. 2009. Reaction Mechanisms of the Methylation of Ethylene with Methanol and Dimethyl Ether over H-ZSM-5: An ONIOM Study, **J. Phys. Chem**, In press.

CONFERENCES

1. Boekfa, B. and J. Limtrakul. 2004. The ONIOM study of the surface species present in acetone condensation on H-ZSM-5 catalyst. **The proceeding of 30th Congress on Science and Technology of Thailand**, October 19-21, Bangkok, Thailand.
2. Boekfa, B. and J. Limtrakul. 2006. The adsorption and diffusion of 1-butene and cis-2-butene on H-FER: combined Quantum Mechanics/ Molecular Mechanics and Molecular Dynamics Simulation. **The proceeding of 32th Congress on Science and Technology of Thailand**, October 10-12, Bangkok, Thailand.
3. Boekfa, B., J. Sirijareansre, P. Limtrakul, P. Piboon and J. Limtrakul. 2007. Adsorption of Glycine Amino Acid in Zeolite: An Embedded QM/MM Study. **NSTI-Nanotech**, May 20-23, Santa Clara, CA, USA.
4. Boekfa, B., S. Choomwattana, C. Wattanakit, P. Limtrakul, P. Pantu, P. Khongpracha and J. Limtrakul. 2008. Effects of the framework on the adsorption of methane on IRMOF-1, IRMOF-2 and IRMOF-6 Metal-Organic Frameworks: A combined QM and MM study. **Nanoporous Materials – V**, May 25-28, Vancouver, BC, Canada.
5. Boekfa, B., S. Choomwattana, P. Maitarad, P. Limtrakul and J. Limtrakul. 2009. The Quantum Confinement Effect on the Adsorption and Reaction of Aliphatic and Aromatic Hydrocarbons on 'Nano Reactor' ZSM-5 Zeolite: A Newly Developed Density Functional Theory (DFT) Investigation, **NSTI-Nanotech,** Houston, USA.